EPA-600/2-76-247a
September 1976

Environmental Protection Technology Series

INFLUENCE OF AERODYNAMIC PHENOMENA ON POLLUTANT FORMATION IN COMBUSTION (Phase I Gaseous Fuels)

Industrial Environmental Research Laboratory
Office of Research and Development
U.S. Environmental Protection Agency
Research Triangle Park, North Carolina 27711

RESEARCH REPORTING SERIES

Research reports of the Office of Research and Development, U.S. Environmental Protection Agency, have been grouped into five series. These five broad categories were established to facilitate further development and application of environmental technology. Elimination of traditional grouping was consciously planned to foster technology transfer and a maximum interface in related fields. The five series are:

1. Environmental Health Effects Research
2. Environmental Protection Technology
3. Ecological Research
4. Environmental Monitoring
5. Socioeconomic Environmental Studies

This report has been assigned to the ENVIRONMENTAL PROTECTION TECHNOLOGY series. This series describes research performed to develop and demonstrate instrumentation, equipment, and methodology to repair or prevent environmental degradation from point and non-point sources of pollution. This work provides the new or improved technology required for the control and treatment of pollution sources to meet environmental quality standards.

EPA REVIEW NOTICE

This report has been reviewed by the U.S. Environmental Protection Agency, and approved for publication. Approval does not signify that the contents necessarily reflect the views and policy of the Agency, nor does mention of trade names or commercial products constitute endorsement or recommendation for use.

This document is available to the public through the National Technical Information Service, Springfield, Virginia 22161.

EPA-600/2-76-247a
September 1976

INFLUENCE OF AERODYNAMIC PHENOMENA ON POLLUTANT FORMATION IN COMBUSTION

(Phase I. Gaseous Fuels)

by

Louis J. Spadaccini, F. Kevin Owen, and Craig T. Bowman

United Technology Research Center
400 Main Street
East Hartford, Connecticut 06108

Contract No. 68-02-1873
ROAP No. 21BCC-014
Program Element No. 1AB014

EPA Project Officer: W. Steven Lanier

Industrial Environmental Research Laboratory
Office of Energy, Minerals, and Industry
Research Triangle Park, NC 27711

Prepared for

U.S. ENVIRONMENTAL PROTECTION AGENCY
Office of Research and Development
Washington, DC 20460

TABLE OF CONTENTS

TABLE OF CONTENTS (Cont'd.)

ABSTRACT

An experimental investigation of the effects of the interaction between fluid dynamics and chemistry on pollutant formation and destruction in a natural gas fired turbulent diffusion flame burner has been carried out. In this investigation, the effects of inlet air swirl, combustor pressure and air/fuel velocity ratio on the time-mean and fluctuating flow field have been determined using probing and optical techniques, and the changes in flow field structure have been correlated with changes in pollutant emissions from the burner. The results of this investigation show that variation of these inlet parameters produces major changes in the time-mean flow field within the burner which significantly influence pollutant formation. In addition, it was found that there are substantial large-scale contributions to the total rms turbulent velocity field. These large-scale fluctuations results in significant departures from Gaussian turbulence and isotropy in the initial mixing regions of the burner and have pronounced effects on mixing, chemical reaction and pollutant formation.

This report was submitted in partial fulfillment of Contract 68-02-1873 by United Technologies Research Center under the sponsorship of the Environmental Protection Agency. Work was completed as of April 30, 1976.

LIST OF FIGURES

LIST OF FIGURES (Continued)

LIST OF FIGURES (Continued)

LIST OF TABLES

LIST OF TABLES (Cont'd)

ACKNOWLEDGMENTS

A number of individuals at UTRC made significant contributions to the experimental investigation. Dr. M. F. Zabielski and Mr. G. L. Dodge designed the sampling system used in the investigation and developed the calibration procedures employed in the gas sampling portion of the experiments. Mr. T. A. Murrin assisted throughout the experimental program and was responsible for operation of the combustor and for reduction of much of the experimental data. The high-speed motion pictures of the reacting flows were made by Mr. R. J. Haas. Mrs. P. A. Rose and Mrs. B. B. Johnson assisted in reduction and compilation of the experimental data and in the preparation of the final report.

This research program was carried out under the sponsorship of the Environmental Protection Agency, EPA Contract 68-02-1873, Research Triangle Park, North Carolina, under the direction of Mr. W. S. Lanier, Project Officer.

SECTION I

INTRODUCTION

Recent investigations of factors affecting pollutant emissions from furnaces (Refs. 1-4) and gas turbines (Refs. 5,6) indicate that changes in operating conditions, which alter mean flow patterns in the combustion chamber, can have a substantial effect on pollutant formation and destruction. Experiments carried out on a laboratory-scale turbulent diffusion flame burner (Ref. 7) under EPA Contract 68-02-1092 confirmed these observations and demonstrated that the interaction between fluid dynamics and chemistry is a major factor governing pollutant emissions. At the present time, our understanding of the nature of this coupling is insufficient to permit quantitative prediction of the effects of changes in operating conditions on pollutant emissions. Analytical studies of turbulent reacting flows (Refs. 8-12) have provided some insight into the effects of mixing and turbulence on flow field structure and pollutant formation. However, it is uncertain whether existing analytical models can provide accurate descriptions of turbulent reacting flows of practical interest. Furthermore, it is difficult to assess the limitations of these models because of inadequate local flow field measurements in practical combustor geometries to serve as test cases and because of a lack of information on the turbulent structure of reacting flows which can be used to assess the validity of present turbulence models.

In a previous study (Ref. 7), fluid dynamic and chemical phenomena in the regions near the injection plane were found to influence flame stabilization, energy release and pollutant formation. If these significant phenomena and their interaction with the pollutant formation process are to be understood, then detailed information on the velocity, temperature and species concentrations in the near-injector region is necessary. Of particular importance are measurements of the location and size of the flame-stabilizing recirculation zones and characterization of the turbulent structure of the flow. To permit meaningful comparison of the experimental data with predictions of combustor flow

model, careful determination of the combustor inlet conditions is required.

The present report documents the results of an experimental investigation, sponsored by EPA Contract 68-02-1873, of the effects of several operating parameters on the flow field structure near the injection plane in a turbulent diffusion flame burner and the subsequent effects on pollutant formation and destruction. The investigation is a logical extension of the previous contract effort (Ref. 7) in that it addresses many of the questions outlined above and provides an expanded data base on the effect of combustor inlet conditions on flow field structure and pollutant formation. The principal objectives of the program were -- (1) to obtain detailed maps of the combustor flow field, including recirculation zones, as operating conditions were varied and (2) to correlate changes in flow field structure with changes in pollutant formation and energy release. The results will be used to evaluate a combustor flow analysis being developed in the theoretical portion of this program. Results from the analytical study will be documented in a subsequent report (Ref. 12).

SECTION II

EXPERIMENTAL APPARATUS AND INSTRUMENTATION

COMBUSTOR FACILITY

The experimental configuration and approach utilized in the present investigation are similar to those employed in the previous effort carried out under EPA Contract 68-02-1092 (Ref. 7). Tests were conducted in the instrumented, water-cooled combustion system shown schematically in Fig. 1. The facility design was modified slightly from that employed in the previous contract effort (Ref. 7). Particular emphasis was placed on acquisition of species concentration, temperature and velocity data throughout the initial regions of the reacting flow for comparison with results obtained in the analytical study (Ref. 12).

Air from a 30-atm supply, at flow rates up to 0.65 kg/sec, may be heated in an electrical heater section to provide inlet air temperature up to 1000°K. Within the heater, the air flows through and around four 6 m long stainless steel tubes which may be supplied with as much as 720 kW of electrical power. The heated air enters the combustor through a circular annulus formed by a replaceable axisymmetric fuel injector and a 12.23 cm diameter entry section. Natural gas (~ 96 percent CH_4) fuel, introduced through three (air foil shaped) struts into the center deliver duct, is brought into contact with the annular airstream at the exit of the injector. Thereafter, mixing and chemical reaction proceed at constant area in the remainder of the injection section and into the instrumented combustor and extender sections. Flame stabilization in the high velocity flows investigated was achieved by producing a recirculation zone(s) in the initial region of the combustor by imparting a swirl component to the air flow and/or by reducing the fuel/air velocity ratio. For the present investigation, porous-metal discs installed in the fuel injector and air entry sections serve to provide uniform inlet flows. (The uniformity of the inlet flow was verified by laser velocimeter and pitot probe measurements.) In order to impart swirl to the airflow, straight swirl vanes are inserted into the annular passage of the injector. In the previous contract effort,

FIG. 1

SCHEMATIC DIAGRAM OF AXISYMMETRIC COMBUSTION FACILITY

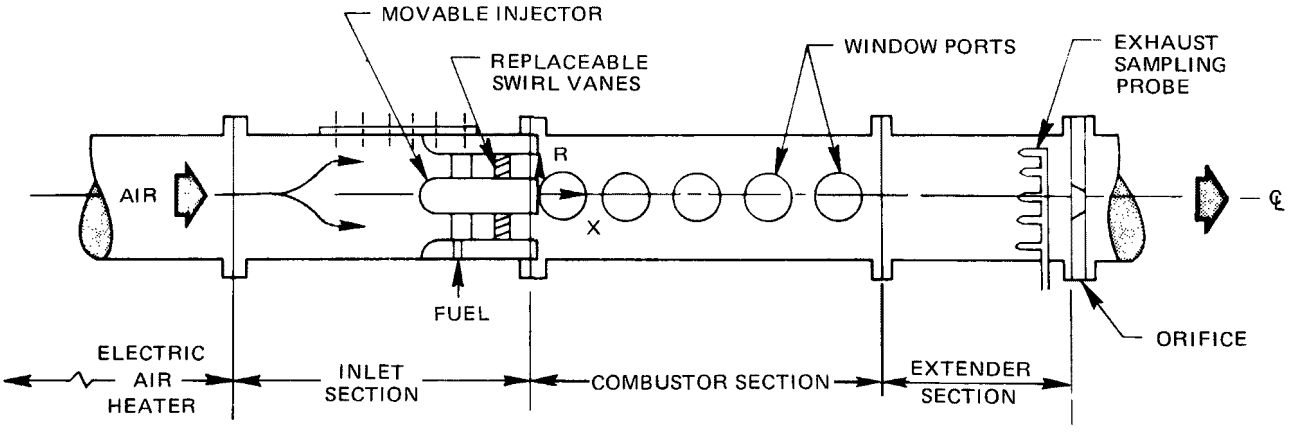

76-05-198-1

these swirl vanes were located at the exit of the injector section. In the present study, the swirl vanes are located upstream of the injector exit plane to permit measurement of the characteristics of the airflow entering the combustor. These measurements together with measurements made within the fuel injector should provide the inlet conditions needed in the analytical modeling effort (Ref. 12). The two injectors utilized in the study are described in Fig. 2 in terms of the ratio of the inner and outer diameters of the air annulus, $Z \equiv d_h/d$, and the nominal air/fuel velocity ratio, $m = V_a/V_f$, associated with air and natural gas coaxial jets having a nominal overall fuel/air equivalence ratio, Φ, of 0.9. With the exception of the porous plug insert, these injectors are identical to those used in the previous contract effort (Ref. 7). Swirl vane designs are identical to those employed in the previous effort and are shown in Fig. 2, where the swirl number, S, has been computed from the injector geometry, Z, and the angle of the swirl vanes, η, according to the following expression (Ref. 13):

$$S = \frac{1}{3} \frac{(1-Z^3)}{(1-Z^2)^{1.5}} \tan\eta \qquad (1)$$

The swirl number is simply the ratio of the angular momentum flux to the axial momentum flux multipled by an effective nozzle diameter. A swirl number of 0.3 connotes relatively low swirl, while S = 0.6 results in a moderately high swirl situation. A practical upper limit of S = 0.8 exists for straight blades from the standpoint of packaging the vanes.

Observation of the combusting flow may be made through the 6.4-cm diameter quartz window ports in the combustor section (Fig. 1). A pair of window ports 180 deg apart are present at each location and permit the use of optical measurement techniques (e.g., laser velocimetry and laser holography). The location of a port directly downstream of the injector exit plane allows an unhindered view of the flame in the vicinity of the fuel delivery duct and permits acquistion of flow field data close to the injector exit. The combustor probing devices used to make temperature and species concentration measurements are compatible with all window ports and may replace a window or water-cooled plug in any given port. In addition, the entry section was redesigned to permit axial relocation of the fuel injector between tests, thereby greatly increasing the number of axial locations at which radial traverses can be made.

The 12.23 cm diameter, 100 cm long instrumented combustor is divided into five water-cooled zones of approximately equal length. Water flow can be set independently in each zone, as needed, to keep

INJECTOR AND SWIRL VANE GEOMETRIES

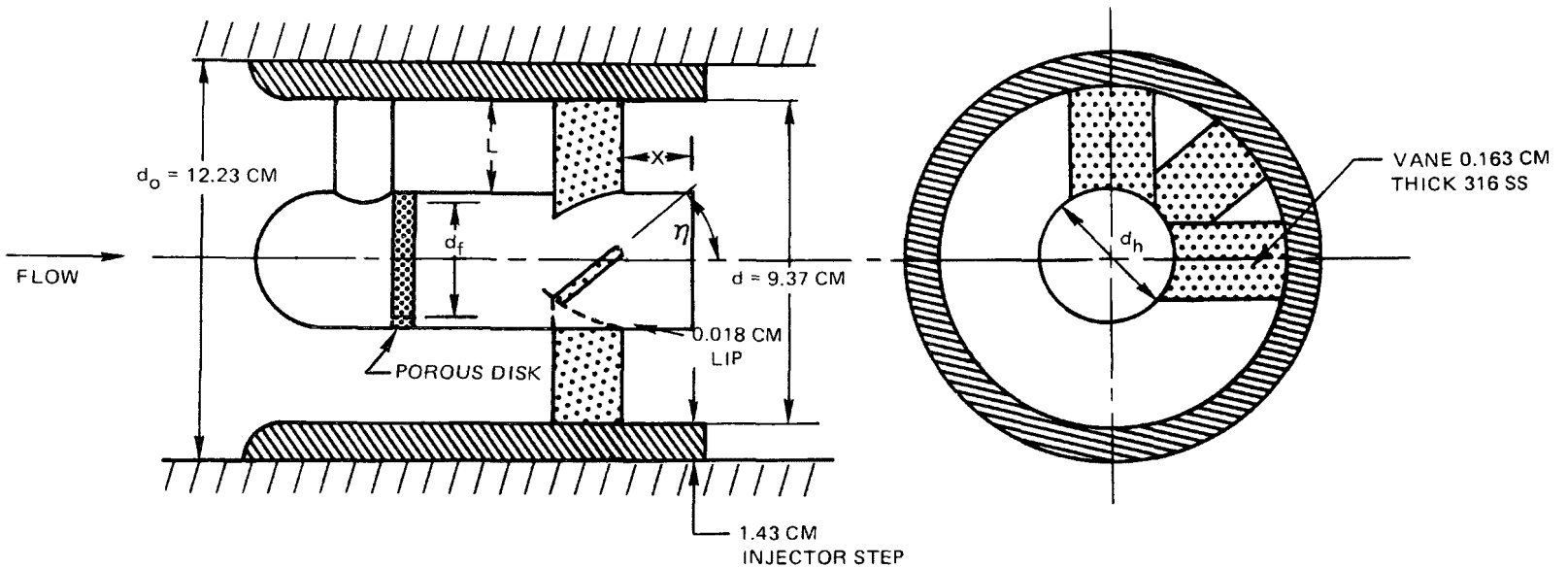

INJECTOR DESIGNATION	m, VELOCITY RATIO*	d_f (CM)	$Z = d_h/d$	L(CM)	S	η (DEG)	NO. OF VANES	X (CM)
I	21:1	6.314	0.677	1.499	0.3 0.6	28 47	18 12	7.37
III	0.2:1	0.757	0.084	4.290	0.6	60	8	1.59

*BASED ON NATURAL GAS AND $\Phi = 0.9$

R05-58-1

FIG. 2

wall temperature (~ 500°K) roughly constant along the entire length of the combustor. Wall temperatures are set and monitored using thermocouples installed on the outer surface and at various depths in the combustor wall and cooling passages. Static pressure taps are also installed at several locations along the combustor. Flow exhausts from the combustor and extender sections to the facility exhaust stack. Combustor extender pieces, 33.4 cm in length, are inserted when required to fully contain the flame; the extender section consisted of two extender pieces during all of the current experimental effort. Water-cooled orifices can be installed downstream of the extender section to raise the pressure in the combustor. A photograph of the combustion facility is given in Fig. 3.

PROBES

Species concentration distributions within the combustor were measured using a traversing gas sampling probe and an exhaust gas sampling rake. Composition information is determined on-line by aspirating flow through the cooled probes and analyzing the gas sample using a Scott Model 119 Exhaust Gas Analyzer. Pressurized hot water at 400°K was used as the probe coolant to minimize wall-catalyzed reactions and to prevent water condensation and loss of species within the sampling lines.

The exhaust probe rake, located at the exit of the extender section, consists of five identical probes centered on equal area annuli (Fig. 4). The individual probes are manifolded downstream and a single mixed sample is transferred to the gas analyzer. Radial traverses are made at selected axial locations within the instrumented combustor section using a single gas sampling probe of similar design (Fig. 5). The inlet flow into both sampling probes was maintain choked, resulting in aerodynamic cooling of the sample by means of a rapid internal expansion. This expansion combined with the wall cooling effect served to quench chemical reactions involving stable species. Errors associated with sampling probe measurements in turbulent flames are discussed in Refs. 14 and 15.

Temperature profiles at the exhaust plane and within the combustor were measured by traversing a calibrated-heat-loss thermocouple probe across a combustor diameter. Although conventional thermocouple materials limit application of these sensors to temperatures below about 2000°K, cooling the exposed junction by conduction heat transfer extends the range of thermocouple utilization above the melting point of the material to the 2000-2500°K range. In order to obtain the local stream temperature, the measured stream thermocouple temperature must be corrected for

COMBUSTOR FACILITY

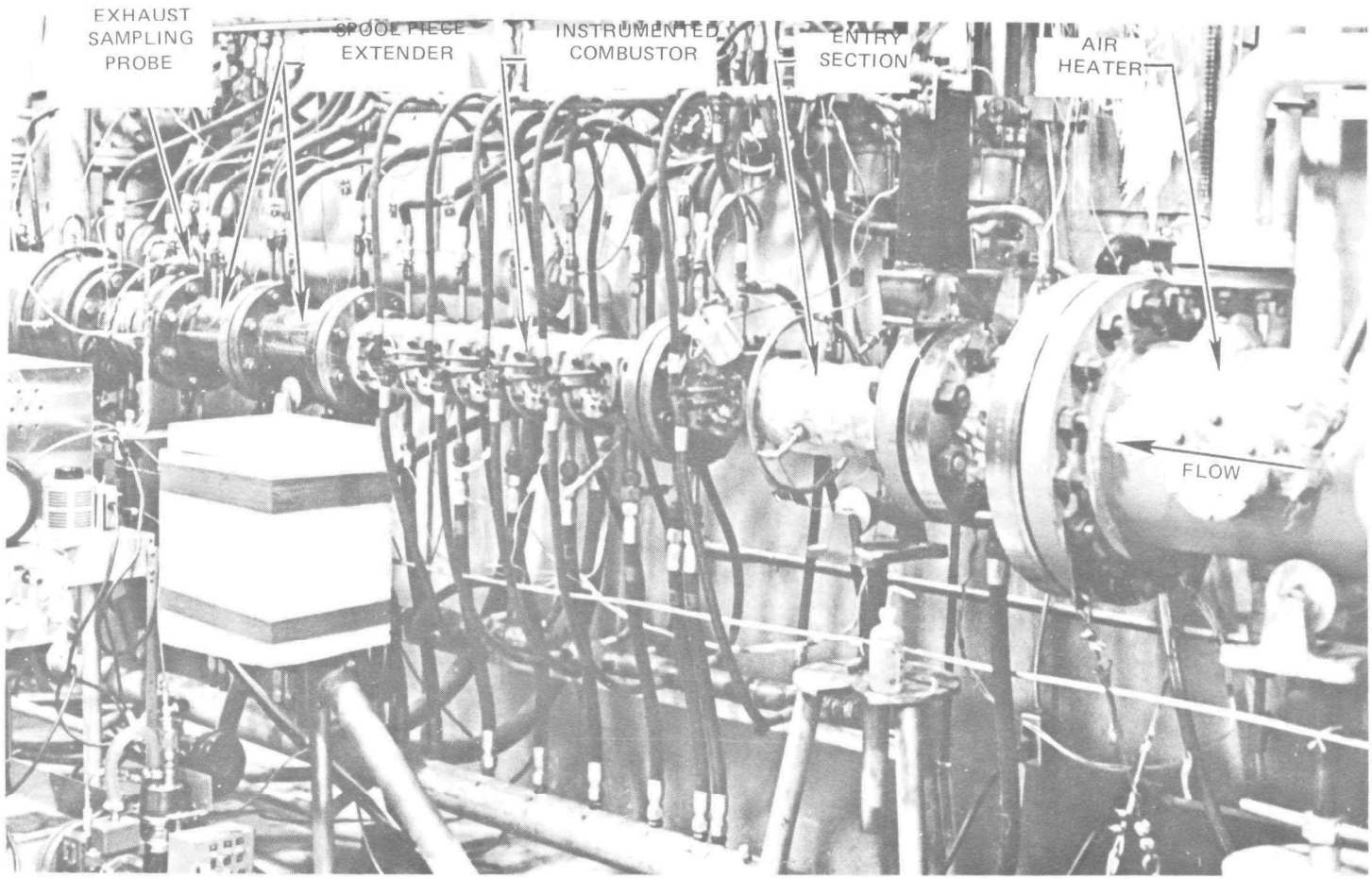

FIG. 3

EXHAUST SAMPLING PROBE RAKE

- PROBES CENTERED ON EQUAL AREAS
- FLOW FROM ALL PROBES MIXED BEFORE ON–LINE ANALYSIS

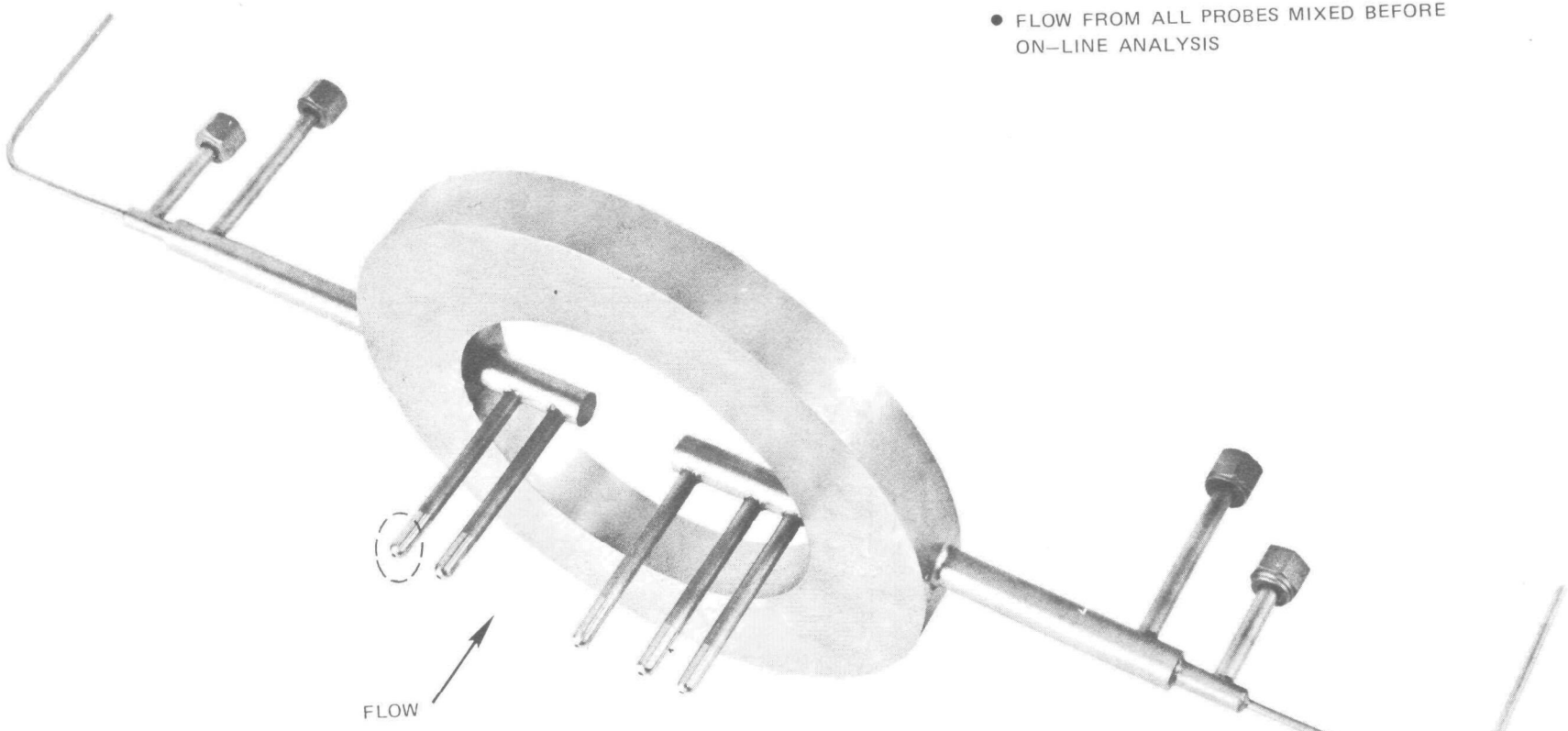

ALL DIMENSIONS IN CM
NOT TO SCALE

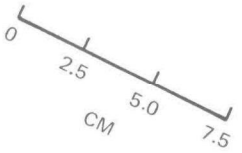

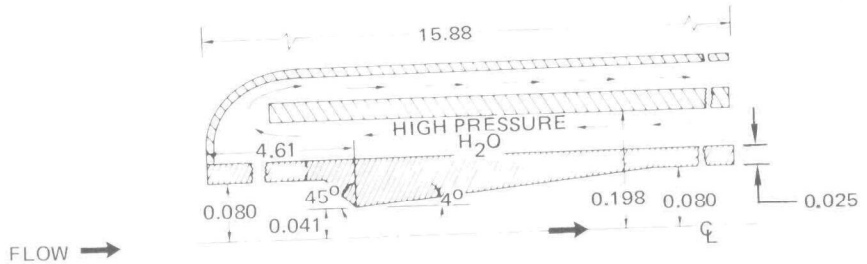

TIP DETAILS

76–05–79–4

FIG. 4

TRAVERSING GAS SAMPLING PROBE

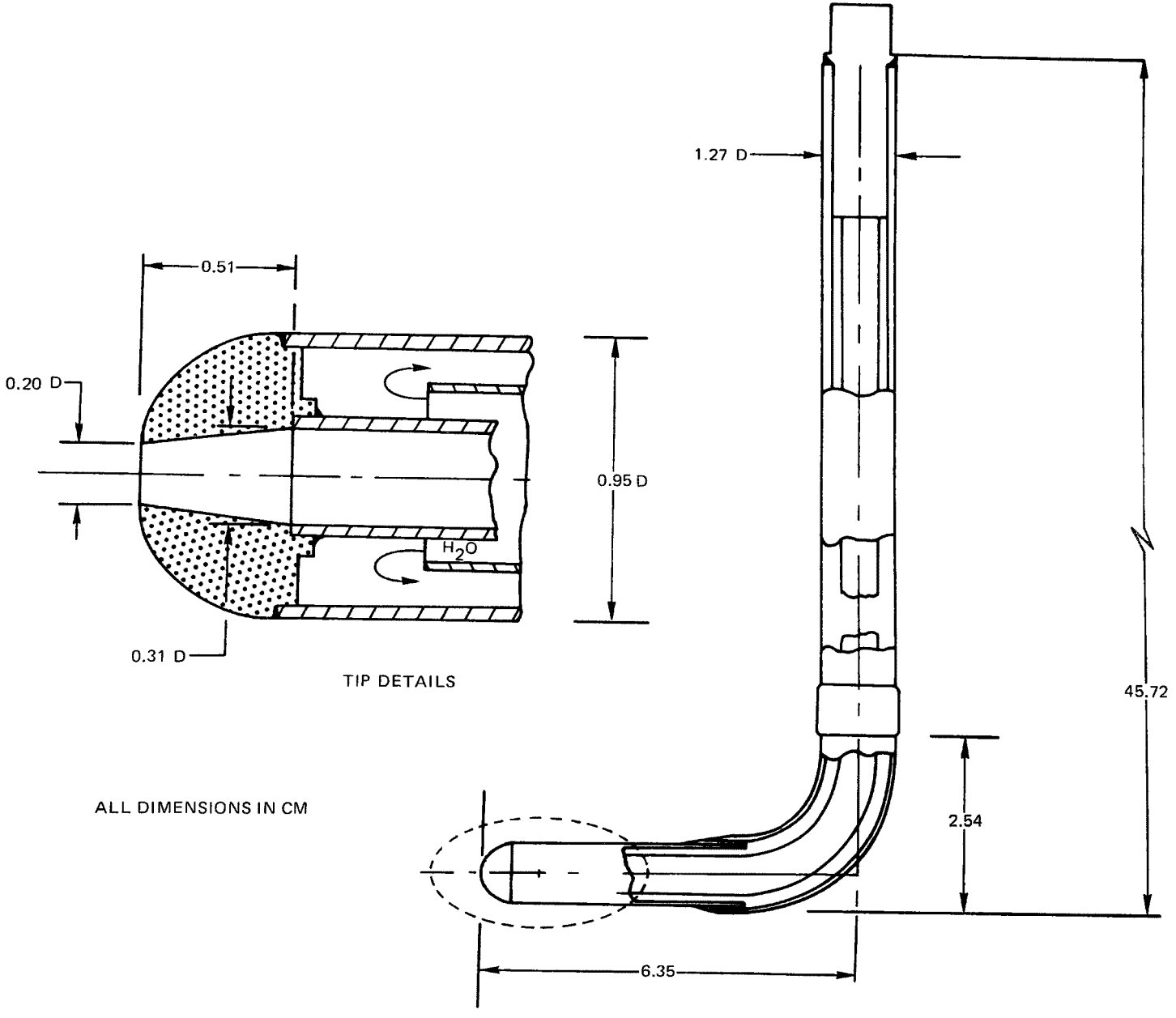

ALL DIMENSIONS IN CM

FIG. 5

conduction and radiation heat losses; therefore, calibration information is acquired simultaneously with the required temperature measurement. The probe consists of three thermocouples including, an iridium - 60 percent rhodium/iridium thermocouple which protrudes from a water-cooled copper base into the reacting flow, and two platinum - 10 percent rhodium/platinum thermocouples installed on the ends of the iridium wire to record the base temperature and thereby permit calculation of the conduction heat loss (Fig. 6). A thermocouple probe of this type was applied without difficulty in the natural gas-air combustion environment. Confidence in the accuracy of the temperature measurements was established during the previous contract effort (Ref. 7) by measurements made at identical test conditions using a conventional thermocouple probe and a double-sonic-orifice probe. Potential errors in the use of thermocouple probes to measure temperatures in turbulent flames are discussed in Refs. 14 and 15.

An uncooled five-hole, hemispherical-nose pitot probe (Fig. 7) was used to measure the radial distribution of the time-mean velocity of the fuel jet by traversing within the fuel injector. A pitot tap is located at the center of the probe and four static taps are symmetrically-located on a centerline circle 40 deg from the tip. Flow velocity and direction are determined from the differential pressures measured between various static locations and the pitot pressure. The probe is calibrated in pitch and yaw to measure flow angles of up to $\pm$ 40 deg.

SAMPLING SYSTEM

The gas samples withdrawn through the five-probe exhaust rake or the traversing probe are analyzed on-line to determine the time-averaged concentrations of carbon dioxide (CO_2), carbon monoxide (CO), oxygen (O_2), nitrogen oxides (NO, NO_2) and unburned hydrocarbons (THC). The samples are transferred to the analytical instruments through a teflon-coated, flexible line which is heated ($\sim$ 400°K) electrically to prevent water condensation. The sample is then directed through a condensate trap ($\sim$ 277°K), where most of the water is removed, and it is pumped through an unheated, teflon coated, aluminum line to a Scott Model 119 Exhaust Analyzer. A schematic diagram of the sampling system is shown in Fig. 8. Because natural gas was the only fuel considered in this phase of the investigation, it was unnecessary to heat the sample lines for THC measurements. A stainless steel bellows pump increased the sample pressure from subatmospheric levels present downstream from the probes to 1 atm as required by the Exhaust Analyzer. The Analyzer, located in the combustion facility control room, approximately 10 m from the combustor, was used to measure the molar concentrations of CO, CO_2, O_2, NO, NO_2 and THC.

CALIBRATED–HEAT–LOSS THERMOCOUPLE PROBE

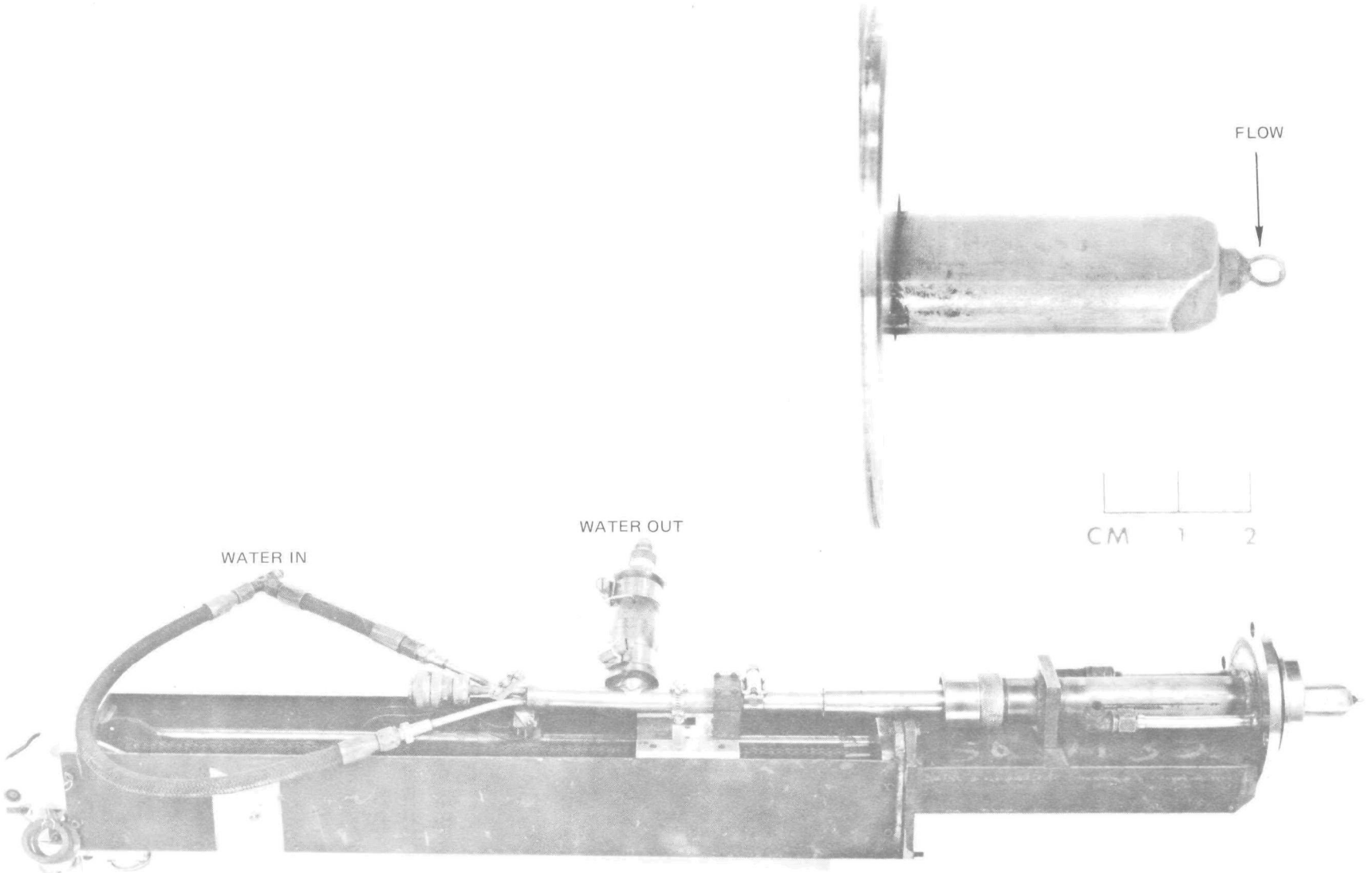

FIG. 6

76–05–127–1

UNCOOLED FIVE HOLE HEMISPHERICAL PITOT PROBE

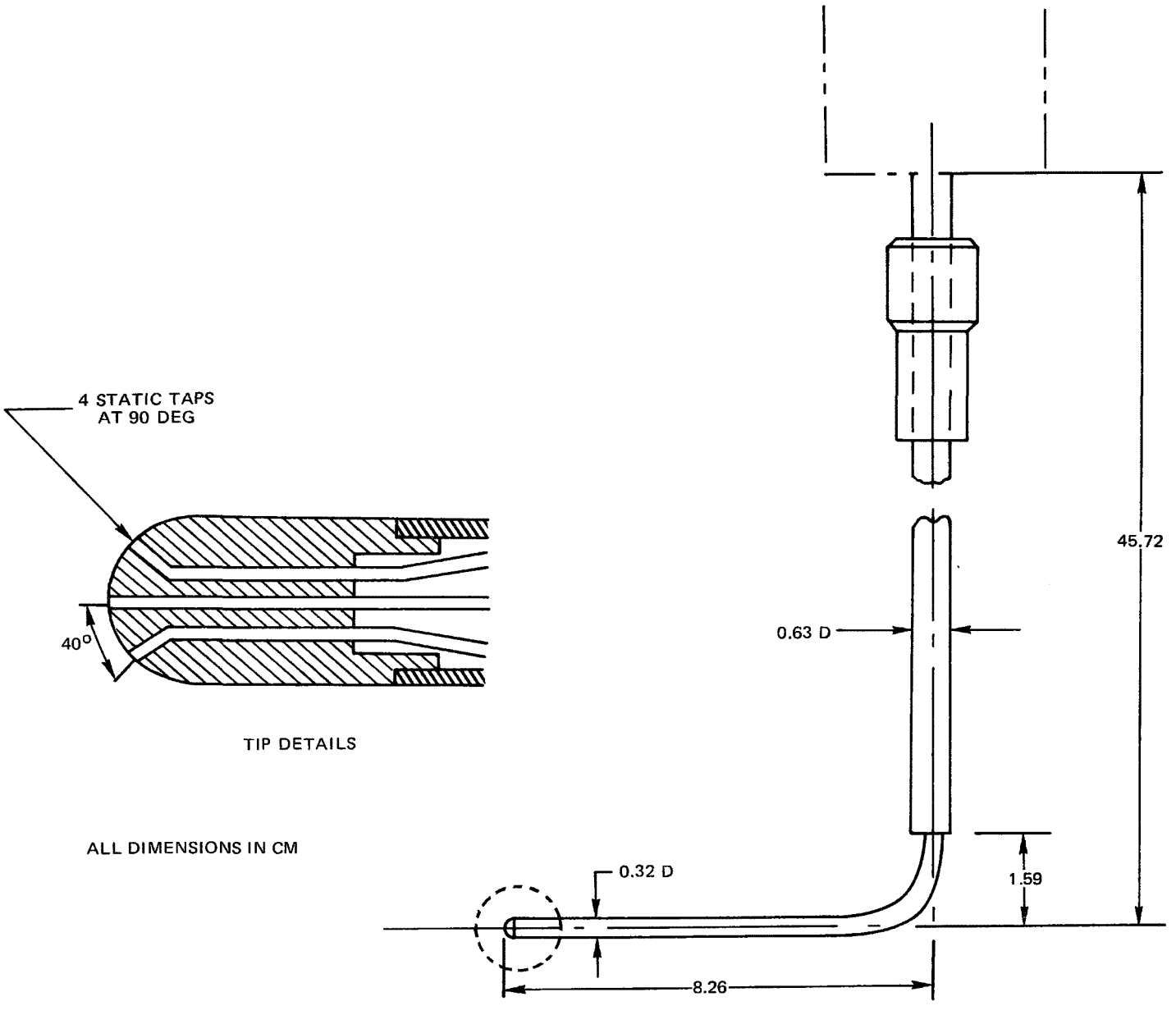

FIG. 7

SCHEMATIC DIAGRAM OF ON–LINE GAS ANALYSIS SYSTEM

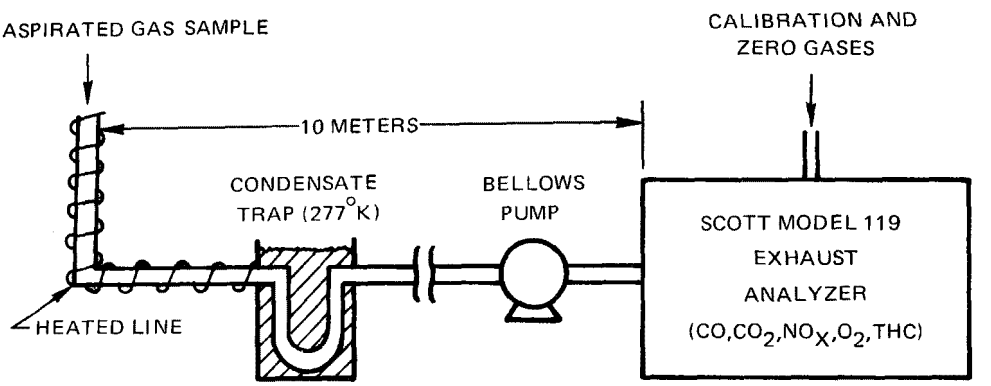

N12–161–1

The Scott Model 119 Exhaust Analyzer (Fig. 9), is an integrated analytical system, with flow controls for sample, zero and calibration gases conveniently located on the control panel. The incoming gas sample passes through a refrigeration condenser (~ 275°K), to remove residual water vapor. As the sample passes from the condenser, it is filtered to remove particulate matter. The Exhaust Analyzer is comprised of five different pieces of analytical instrumentation. Beckman Model 315B Nondispersive Infrared (NDIR) Analyzers were used to measure the CO and CO_2 concentrations (mole fractions) in the gas sample. Concentration ranges available on the CO analyzer were from 0-200 ppm to 0-15 percent on several scales. Concentration ranges available on the CO_2 analyzer were 0-4 percent and 0-16 percent. The accuracy of the NDIR analyzers is nominally ± 1 percent of full scale. A Scott Model 125 Chemiluminescence Analyzer was used to measure the NO and NO_2 concentrations in the gas sample. Concentration ranges available with this instrument were from 0-1 ppm to 0-10,000 ppm on several scales, with a nominal ± 1 percent of full scale accuracy. The thermal converter used in the chemiluminescent analyzer was stainless steel, and was operated at a temperature of approximately 1030°K. The converter efficiency (i.e., the percent NO_2 dissociated) was determined using the method outlined in Ref. 16. In this method, an NO/N_2 span gas is diluted with O_2 which flows through an ozonator. Measurements with the ozonator off and on are made both going through and bypassing the converter to determine converter efficiency. In the present study, a converter efficiency of 99 percent, was measured, with an uncertainty in the measurement of 4 percent. During the course of the calibration tests, a loss of NO was noted when calibration mixtures were flowed through the converter. The observed loss never exceeded 2 percent of the NO in the stream entering the converter. A Scott Model 150 Paramagnetic Analyzer was used to measure the O_2 concentration in the gas sample. Concentration ranges available with this instrument were from 0-1 percent to 0-25 percent on several scales, with a nominal accuracy of ± 1 percent of full scale. A Scott Model 116 Total Hydrocarbon Analyzer was used to measure the hydrocarbon concentration in the gas sample. This analyzer utilizes an unheated flame ionization detection system to provide for measurement of hydrocarbons (as carbon) in concentration ranges from 0-1 ppm to 0-10 percent, with a nominal accuracy of ± 1 percent of full scale. Output signals from the various analyzers are displayed on chart recorders and on digital readouts. The Analyzer was calibrated prior to each test by flowing zero gases and calibration gas mixtures having compositions known to within two percent. Typically, at each test point, sampling data were acquired for a period of 2-4 min.

EXHAUST GAS ANALYTICAL SYSTEM

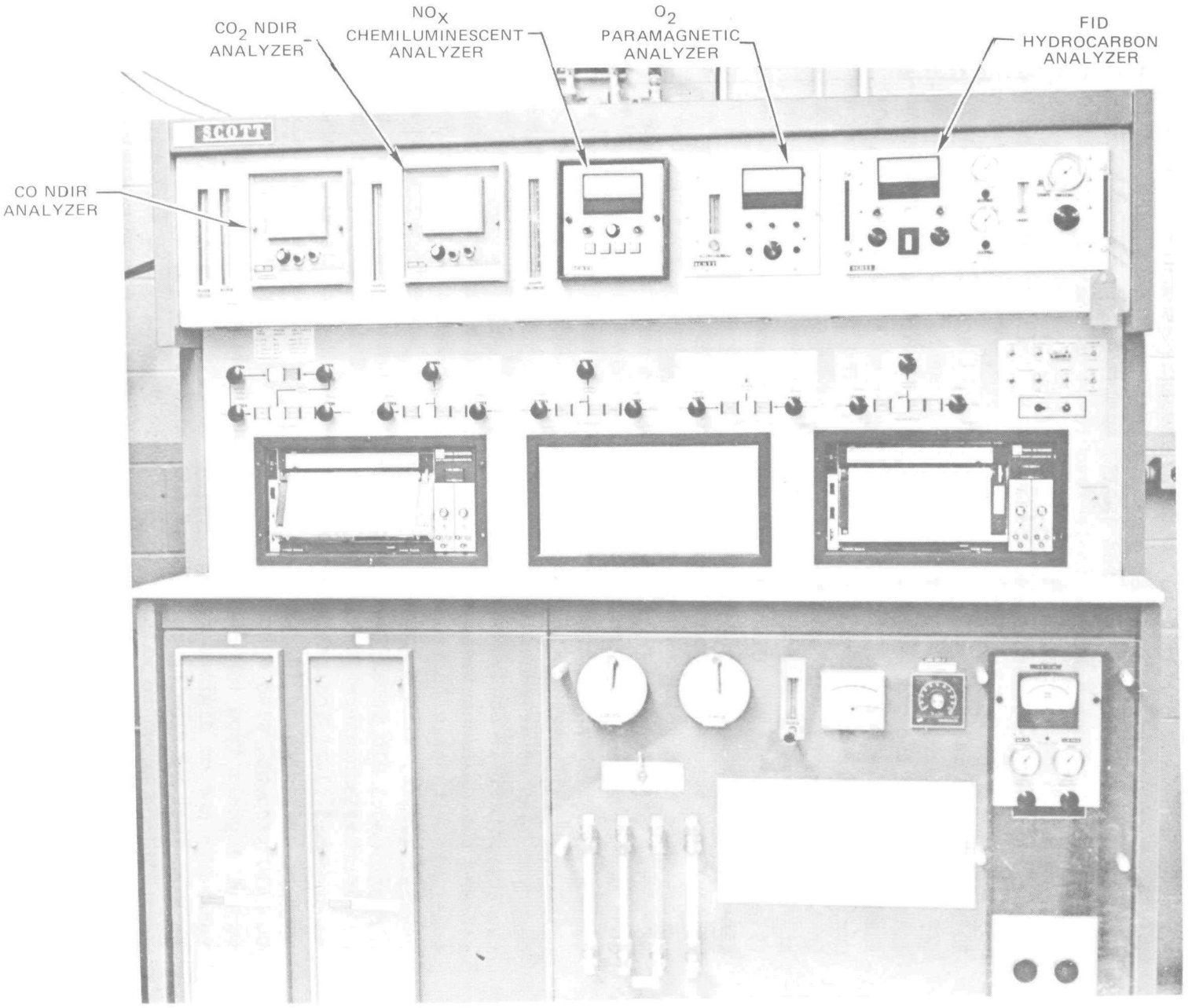

76-05-79-3

FIG. 9

LASER VELOCIMETER

The experimental examination of the interaction between fluid dynamic and chemical processes inside combustors is complicated by the fact that the mean flow fields and turbulence properties of combusting flows with recirculation are difficult to determine with any degree of reliability using conventional instrumentation. Flows with severe adverse pressure gradients, which normally give rise to separation and recirculation, are difficult to document as they are extremely sensitive to local geometry and probe interference (Ref. 14). In addition, streamline curvature and the associated static pressure variations make conventional mean flow instrumentation techniques unreliable.

Although precalibrated pneumatic and microphone probes can be used with acceptable accuracy in a wide variety of steady flow situations, significant errors can occur in highly turbulent or unsteady flows since large (> 20 percent) velocity fluctuations affect the response and subsequent interpretation of results (Ref. 15). Since most practical combustor designs involve extensive regions of highly turbulent recirculating flow these probes generally are inadequate for velocity measurement. Figure 10 shows a comparison between mean axial velocity measurements in a swirling natural gas-air flame with a cooled five-hole pitot probe and a laser velocimeter. In regions with relatively high mean flow velocities and relatively low turbulent intensities (as determined by the laser velocimeter), there is relatively good agreement between the two sets of data. However, in regions with low velocity and high turbulent intensity, the probe data are scattered and significantly different from the laser velocimeter results. Bennett (Ref. 17) has reviewed errors in pitot probe data resulting from turbulent fluctuations. Bilger (Ref. 15) has discussed the averaging characteristics of pitot probes in turbulent reacting flows and notes that proper interpretation of probe measurements requiresknowledge of the turbulent structure of the flow.

There are problems associated with turbulent structure measurements because linearized hot wire data interpretations are not accurate in highly turbulent flows (i.e., turbulent intensity > 20 percent) and because these probe cannot withstand the high temperatures encountered in combustors. With the advent of the laser velocimeter, linear nonperturbing fluid mechanical measurements of complex three-dimensional flow fields are possible provided light-scattering particles can be relied upon to follow the local fluid velocity.

COMPARISON OF PITOT PROBE AND LASER VELOCIMETER MEASUREMENTS OF VELOCITY

○ PROBE DATA

● LV DATA

SWIRL = 0.3, 1 ATM, $V_a/V_f = 21$

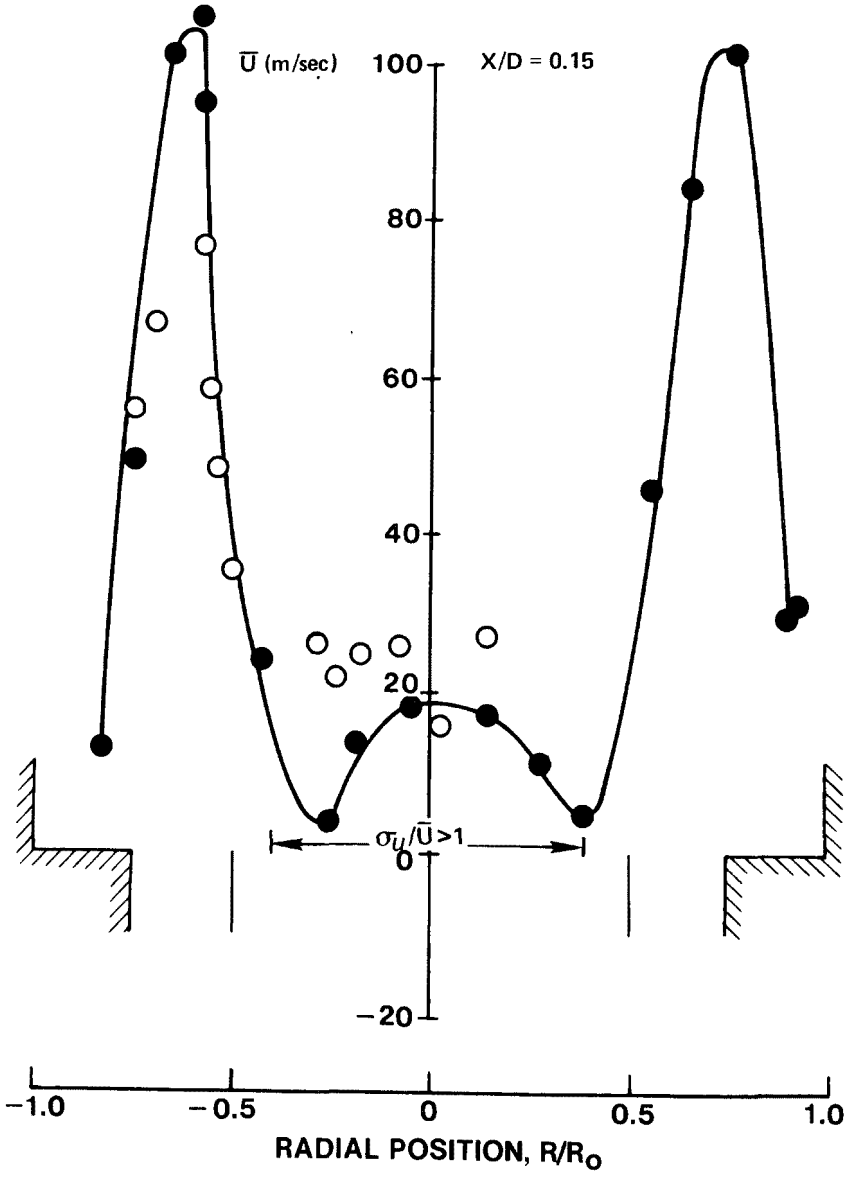

Since the flows to be investigated involved regions of flow reversal a laser velocimeter which could determine both the direction and magnitude of the instantaneous velocity was required. Such a system has been developed and used to obtain the detailed mean and turbulence measurements which are presented in this report.

The mean velocity and turbulence measurements were made with a dual-beam velocimeter utilizing a crystal Bragg cell which acted as a beam splitter and frequency shifted the first deflected beam. A schematic diagram of the optics and signal processing instrumentation is shown in Figs. 11 and 12. The sensing volume determined by beam crossover volume, off-axis collection and photomultiplier pin hole size resulted in an elliptic sampling volume with principal axes of 0.2 mm and 2.0 mm, respectively. The velocity component sensed with this optical arrangement lies in the plane of the two incident beams and is perpendicular to their bisector. Single-particle, time-domain signal processing was used to build-up the velocity probability density distributions from which both the mean velocities and rms velocity fluctuations were obtained using the following equations:

$$\bar{U} = \frac{1}{N}\left(\sum_{i=1}^{N} U_i\right) \tag{2}$$

$$\sigma_U = \sqrt{\overline{u'^2}} = \sqrt{\sum_{i=1}^{N} \frac{U_i^2}{N} - \bar{U}^2} \tag{3}$$

In the present experiments, a minimum of 1000 instantaneous velocity determinations were used to build-up the probability distribution functions. This number of determinations results in a maximum statistical error of less than 5 percent in the computed values of both the mean and variance with a confidence level of 95 percent (see Appendix A). Indeed, a mass balance computed for the case of zero swirl agreed to within 10 percent of the metered fuel and air supply.

The instantaneous axial and tangential velocities were measured by rotating the Bragg cell about an axis coincident with the laser beam. With the beams in the axial plane $\bar{U}$ and $\sqrt{\overline{u'^2}}$ are determined from Eqs. (2) and (3). With the beams oriented 90° to the axial plane tangential velocity provides ($\bar{W}$ and $\sqrt{\overline{w'^2}}$) were obtained by traversing of the optical system horizontally and radial velocity profiles ($\bar{V}$ and $\sqrt{\overline{v'^2}}$) were obtained by traversing the optical system vertically. With the beams orientated at ± 45 degrees to the axial plane the turbulent shear stress component $\overline{u'w'}$ was determined from the difference of the two variances.

SCHEMATIC DIAGRAM OF THE LASER VELOCIMETER

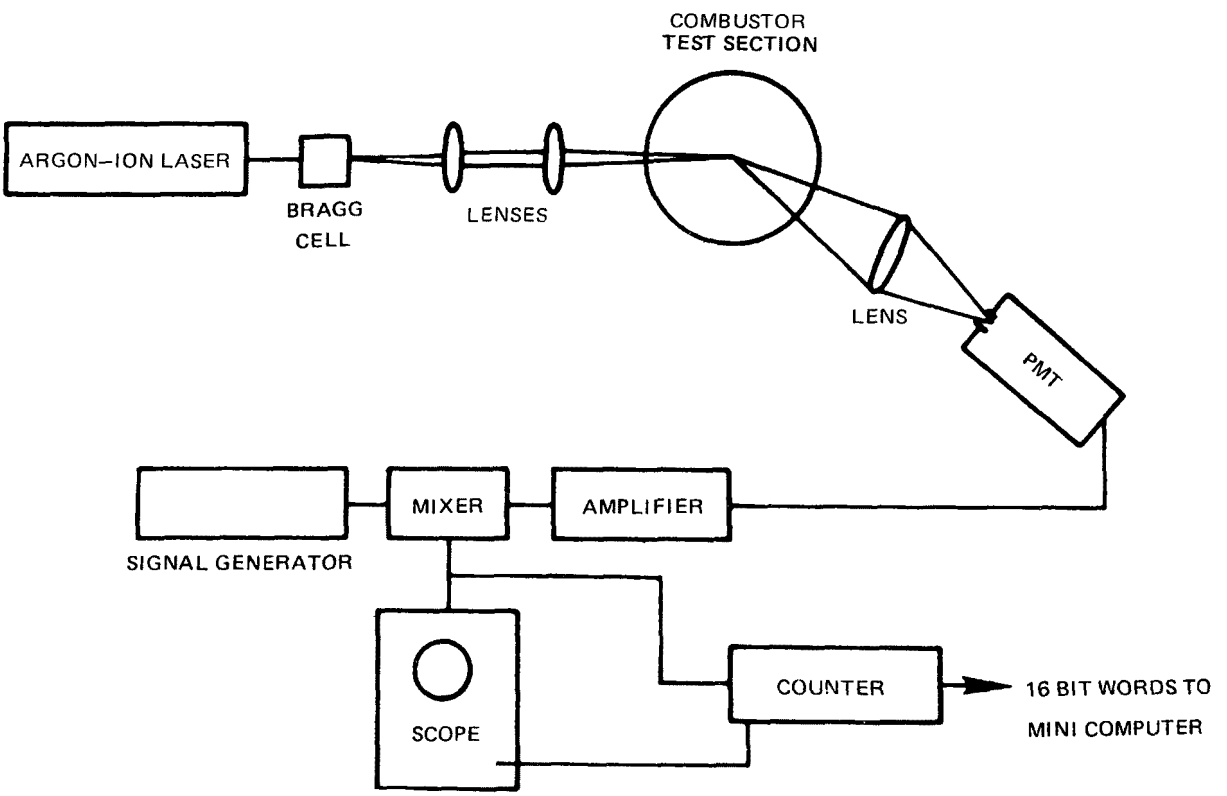

76–03–270–10

SCHEMATIC DIAGRAM OF THE LASER VELOCIMETER DATA PROCESSING EQUIPMENT

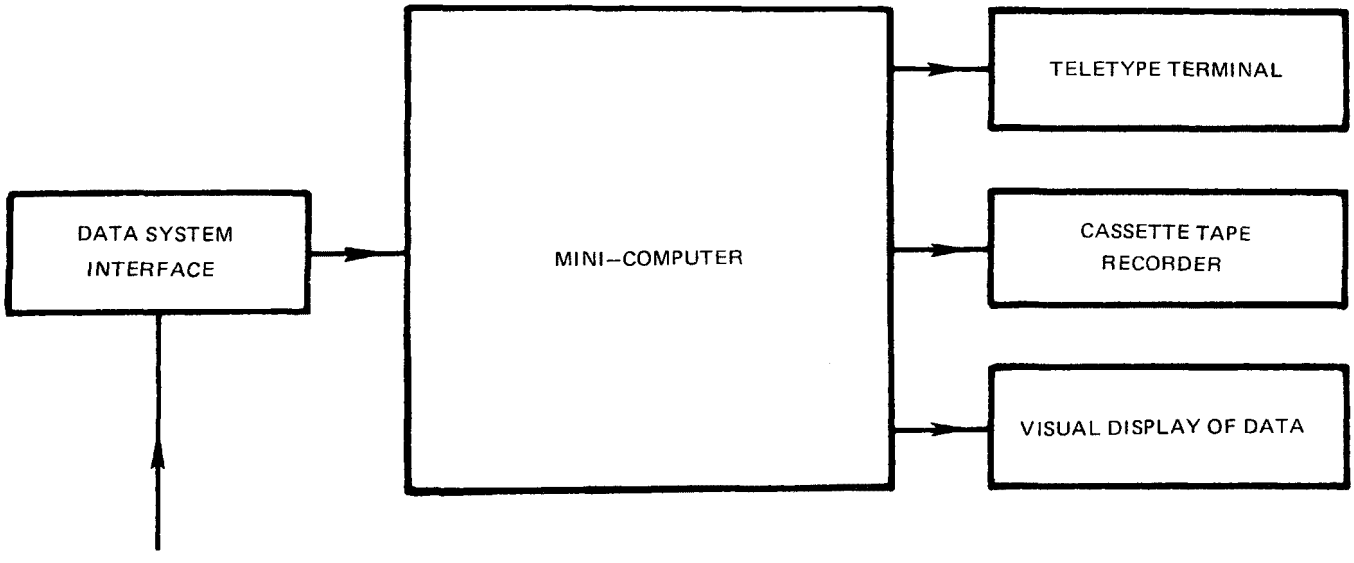

76–03–270–9

The optical sensitivity of the forward scatter system used in the investigation was such that naturally occurring submicron particles could be used for the velocity determinations. However, to increase the signal to noise ratio and thus increase the data acquisition rate the air flow was seeded with particles dispensed from a fluidized bed. A limited number of measurements were made with the fuel stream seeded and with both air and fuel streams seeded to evaluate biasing errors which can result from seeding only the air flow (Appendix A).

A number of materials which had previously been used to seed small open flames were tested but none proved suitable for the present experimental arrangement. Both Al_2O_3 and TiO_2 deposited on the combustor windows degrading the Doppler signals to an unacceptable extent, and silicone oil droplets dispensed from a Laskin nozzle evaporated on or before reaching the combustion zone. However, nominal 5 μm microballoons (hollow spheres) of bakelite phenolic resin were used successfully. Due to their low initial density (< 0.1 gm/cc) and to the fact that they charred to micron size in the combustion zone, these particles gave adequate turbulence response and excellent signal/noise ratio (> 10:1) without disturbing optical access.

For a spherical particle of diameter D_p suspended in a sinusoidally vibrated column of air and acted on by Stokes drag, the ratio of particle velocity to gas velocity can be expressed as (Ref. 18):

$$\frac{u_p}{u} = \left[1+\left(\frac{2\pi f}{a}\right)^2\right]^{-\frac{1}{2}} \tag{4}$$

where

$$a = \frac{18\mu}{\rho_p D_p^2}\left(1 + \frac{K\ell}{D_p}\right)^{-1} \tag{5}$$

where u_p and u are the rms velocities of the particle and the gas ρ_p is the particle density, f is the vibration frequency, ℓ is the molecular mean free path of the gas and K is the Cunningham constant (≈ 1.8 for air). Thus, a 5 μm phenolic resin microballoon in air at ambient conditions will follow velocity fluctuations up to 10 kHz within 10 percent. Power spectral density measurements in the shear layer of nonreacting jets (Ref. 18) indicate that for the reacting flows investigated in the present study more than 95 percent of the turbulence energy will be associated with Eulerian frequencies below 25 kHz. Hence, the scale of

the smallest energy containing eddy will be on the order of

$$\lambda = U/f \approx 100\,m/sec/25\,kHz = 4 \times 10^{-3} m$$

In the Lagrangian frame, this scale corresponds to the frequency on the order of

$$f = (U - U_c)/\lambda \approx 20\,m/sec/4 \times 10^{-3} m = 5\,kHz$$

so that errors due to particle response should be negligible.

Conventional laser velocimeters are subject to directional ambiguity which can result in data interpretation errors in highly turbulent and/or recirculating flows. This problem is illustrated in the insert of Fig. 13 where Gaussian probability density distributions of the instantaneous velocities corresponding to local turbulent intensities of 20 and 70 percent are presented. It can be seen that, with directional ambiguity, the negative velocities are assigned their equivalent positive values which leads to errors in the calculated mean value and standard deviation. These errors rise sharply for turbulence intensities above 40 percent.

To circumvent problems associated with directional ambiguity, zero velocity frequency offset was achieved by combining the primary and modulated beams at the detection volume where they generated moving fringes so that a stationary particle produced a Doppler frequency, f_o. Thus, in the flow field, moving particles generated Doppler frequencies of $f_o \pm f_D$ depending on their velocities normal to the moving fringes. Hence, the sign and the magnitude of the instantaneous velocities could be determined as follows:

$$U = \frac{(f_D - f_o)\lambda}{2 \sin \frac{\theta}{2}} \qquad (6)$$

where λ is the wavelength of the laser light and θ is the angle between the incident laser beams.

ERROR DUE TO DIRECTIONAL AMBIGUITY

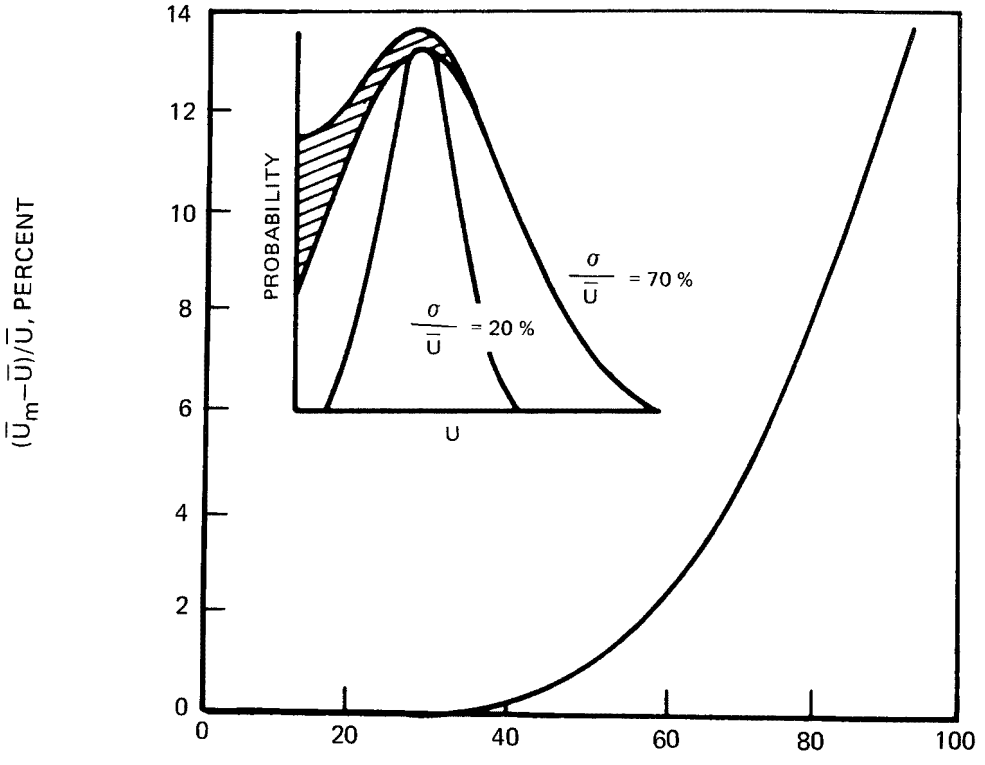

76–05–198–2

SECTION III

EXPERIMENTAL RESULTS

DESCRIPTION OF THE EXPERIMENTS

In a previous contract effort (Ref. 7) changes in combustor operating conditions which altered the mean flow field structure in the combustor were shown to influence pollutant emissions. The principal changes in the mean flow were found to occur in the initial regions of the combustor containing the recirculation zones. Furthermore, significant fluctuations in the flame structure were observed, and the nature of these fluctuations were found to depend on the operating conditions. The present experimental program was carried out to further investigate the effect of combustor operating conditions on flow field structure and pollutant formation. The principal objectives of the program were -- (1) to obtain detailed maps of the mean and fluctuating flow field in the vicinity of the injection plane, including recirculation zones, as operating conditions were varied and (2) to correlate changes in flow field structure with changes in pollutant formation and energy release. The results will be used to evaluate the combustor flow analysis (CRISTY code) being developed in the theoretical portion of this program (Ref. 12). Advanced optical and probing techniques were used to acquire detailed data describing the mean flow field properties, including velocity, temperature and species concentration, and to obtain information on the turbulence structure of the combustor flow field. The interaction of fluid dynamic and chemical processes was investigated for a range of test conditions using two different fuel injector geometries. Ultimately, it is intended that the information obtained from the experimental and theoretical studies will be utilized for evaluating potential emission control strategies.

The experimental program was comprised of two different types of tests: (1) input-output tests and (2) flow-field mapping tests. The input-ouput tests were conducted with the objective of determining the relationship of exhaust species concentrations and temperature to

selected combustor operating conditions. Measurements were made at the exit of the extender section (Fig. 1) using the exhaust probe rake and the traversing thermocouple probe. Previous test results (Ref. 7) demonstrated the importance of inlet air swirl, combustor pressure, and air/fuel velocity ratio on governing pollutant emissions and therefore, systematic variations of these parameters were performed in the present investigation. Exhaust species concentrations were shown in Ref. 7 to be less sensitive to variations in fuel-air equivalence ratio, inlet air temperature and airflow rate, and therefore, these parameters were maintained constant. The ranges of variation inlet conditions in the present input-output tests were selected generally to complement and expand the data base obtained during the previous contract effort.

Combustor mapping tests were carried out for the purpose of correlating changes in the fluid dynamic structure of the flow field, resulting from variation of operating conditions, with the formation and destruction of pollutant species. Detailed measurements were made within the combustor at a minimum of four axial locations to determine radial distributions of the time-mean and rms gas velocity, time-mean temperature and time-mean species concentrations for five different combustor operating conditions. The inlet conditions varied in these tests were those which had the greatest effect on pollutant emissions -- inlet air swirl, combustor pressure and air fuel velocity ratio. Measurements were made using the laser velocimeter and temperature and gas sampling probes described in Section II. Particular emphasis was placed on augmenting and expanding the data base compiled in Ref. 7; therefore, most measurements were made within the initial regions of the combustor (i.e., at axial distances less than five injector diameters) and in the recirculation zone(s). To assist in the interpretation of the test results, high-speed color motion pictures (500 frames per second) of the flame in the vicinity of the injector were obtained for each of the mapping tests. In addition, the frequency spectra and relative amplitudes of pressure fluctuations associated with the interaction of the combustion process with the acoustic or mechanical properties of the combustor were determined. Finally, mean velocity measurements were made within the fuel port, using a five-hole pitot probe, and near the exit of the fuel and air ports, using the laser velocimeter to determine the combustor inlet conditions.

TEST MATRIX

A matrix of combustor operating conditions for tests conducted using natural gas fuel is presented in Table 1. Eight input-output type tests and five flow-field mapping experiments were performed to evaluate the influence of air/fuel velocity ratio, pressure and inlet air swirl

Table 1. NOMINAL TEST CONDITIONS (NATURAL GAS-AIR)

Test No.	Swirl No.	Pressure (atm)	Air/Fuel Velocity Ratio	Φ	$\dot{M}_{air}$ (kg/sec)	T_{air} (^{o}K)	Input-Output	Mapping
1	0	3.8	21	0.9	0.137	750	X	X
2	0	7	21	0.9	0.137	750	X	-
3	0.3	1	21	0.9	0.137	750	X	X
4	0.3	3.8	21	0.9	0.137	750	X	X
5	0.3	7	21	0.9	0.137	750	X	-
6	0.6	1	21	0.9	0.137	750	X	X
7	0.6	1	0.2	0.9	0.137	750	X	X
8	0.6	3.8	0.2	0.9	0.137	750	X	-

on the temperature, velocity and species concentrations within the combustor. Selection of the parameters investigated was made with the objective of supplementing the existing experimental data of Ref. 7, with emphasis placed on studying those variables which had the greatest influence on the structure of the flow field and rates of pollutant formation. In each of the input-output tests the exhaust concentration of NO, NO_2, CO, CO_2, O_2 and THC were measured, while in the combustor mapping experiments detailed radial distributions of temperature, species concentration, and the mean and rms axial and tangential velocity were determined.

The natural gas fuel used for these tests was principally CH_4 (> 96 percent) with small amounts of other gaseous hydrocarbons, CO_2 and N_2 present. Fuel composition analyses are summarized in Appendix B. Tests were conducted at nominal combustor pressures of 1, 3.8 and 7 atm, and the overall fuel-air equivalence ratio was maintained constant at a nominal value of 0.9. The level of swirl of the inlet air was varied by changing the swirl vanes, and tests were conducted for zero, low (S = 0.3) and moderate (S = 0.6) swirls. Air/fuel velocity ratios of 21 and 0.2 were achieved by interchanging fuel injectors, shown previously in Fig. 2, and the inlet air flow rate and temperature were held constant at nominal values of 0.137 kg/sec and 750°K.

INPUT-OUTPUT TEST RESULTS

In the previous investigation, changes in inlet air swirl and pressure were found to have a significant influence on NO and hydrocarbon emissions. In the present study, the influence of inlet air swirl on exhaust species concentration levels was evaluated at combustor pressures of 1 (Tests 3 and 6) and 3.8 atm (Tests 1 and 4). The emissions data summarized in Table 2, indicate that imparting swirl (S = 0.3) to the airflow resulted in a significant increase in nitric oxide emissions and in large reductions in hydrocarbon emissions. However, with a further increase in the swirl intensity to S = 0.6 there was only a modest increase in NO and no significant change in THC emissions. The corresponding temperature distributions in the combustor exit plane, which are presented together with the flow-field mapping data in a later section of this report, indicated that flows with swirl resulted in higher peak temperatures while nonswirling flows resulted in temperature profiles with peaks of reduced magnitude.

Thermochemical considerations indicate that increased pressure will result in increased temperatures, resulting in more rapid chemical reaction. In addition, higher pressures result in reduced flow velocities and longer combustor residence times. Each of these effects

Table 2. EXHAUST SPECIES CONCENTRATIONS* (NATURAL GAS-AIR)

Test No.	Swirl No.	Pressure (atm)	Air/Fuel Velocity Ratio	Inlet Air Temperature (°K)	Φ
1	0	4.0	20.6	748	0.90
2	0	7.5	20.9	750	0.90
3	0.3	1.0	22.0	743	0.90
4	0.3	3.7	20.9	746	0.91
5	0.3	7.3	20.4	746	0.91
6	0.6	1.0	21.3	746	0.91
7	0.6	1.0	0.17	748	0.91
8	0.6	3.6	0.17	748	0.90

Test No.	O_2 (Mole %)	CO_2 (Mole %)	CO (Mole %)	NO ppm	NO_x** ppm	THC ppm, C	Carbon Balance*** (percent)
1	3.25	9.50	0.96	366	400	610	- 2.4
2	1.49	10.05	1.52	178	-	1914	+ 8.6
3	3.17	9.05	0.89	171	207	44	+ 5.5
4	1.67	9.80	1.00	429	476	65	+ 0.4
5	1.60	10.50	0.73	320	337	709	- 5.7
6	2.07	9.50	1.21	175	207	71	+ 1.3
7	5.60	8.05	0.68	117	154	184	+18.6
8	4.40	9.60	0.35	195	212	200	+ 8.4

* Expressed as measured on a dry basis.

** $NO_x = NO + NO_2$

*** (+) $C_{IN} > C_{OUT}$

(-) $C_{IN} < C_{OUT}$

favors increased NO formation, and the effect of an increase in combustor pressure from 1 to 3.8 atm for an inlet air swirl number of 0.3 (Tests 2 vs 4) was a significant increase in exhaust gas temperature levels and in NO emissions. However, a further increase in pressure to 7 atm (Tests 2 and 5) produced a decrease in NO emissions, substantially higher exhaust concentrations of unburned hydrocarbons and a modest increase in CO emissions (cf., Tests 1 and 2, and 3, 4, and 5), suggesting a significant change in flow field structure as the pressure is increased to this level.

A final series of input-output tests was conducted to evaluate the effect of air/fuel velocity ratio on pollutant emissions. Variation of this parameter was effected by replacing the large-diameter, low-velocity fuel injector with a smaller one (see Fig. 2), thereby increasing the fuel injection velocity and simultaneously decreasing the inlet air velocity. A change in air/fuel velocity from 21 to 0.2, for an inlet air swirl number of 0.6 and atmospheric pressure (Tests 6 vs 7), resulted in a reduction in NO and CO emissions and in increase in hydrocarbon emissions. Temperature measurements at the combustor exhaust indicated that at air/fuel velocity 0.2 the profile was significantly less uniform with large radial gradients.

A comparison of the emissions data obtained in the present investigation with observations previously reported in Ref. 7 indicates that there is general agreement with respect to trends resulting from variation of inlet air swirl, combustor pressure and air/fuel velocity ratio; however, exhaust concentrations of NO are lower, THC concentrations are higher and CO concentrations are generally higher in the present tests. This result suggests that the local temperature levels are lower than those measured in the corresponding tests of Ref. 7; a presumption that was confirmed by the mapping data. These differences may be due, in part, to modification of the previous combustion system which included (1) elimination of the uncooled portion of the combustor in the vicinity of the fuel injector and (2) relocation of the swirl vanes to a station upstream of the injector exit. These changes should increase the heat transfer to the combustor wall and reduce the temperature levels in the combustor.

The repeatability of the exhaust species concentration measurements was determined by obtaining several data points at each of the operating conditions listed in Table 1, and the accuracy of the gas sampling and analysis techniques was verified by performing a carbon balance between the reactant and product species. The overall repeatability of the measurements was approximately $\pm$ 5 percent for the species O_2, CO_2, CO, NO and NO_x, and approximately $\pm$ 25 percent for THC. These variations

are attributed primarily to small changes in input and combustor operating conditions and, to a lesser extent, to errors in the sampling and emissions measurement procedures. Normal acceptance criteria, specified in SAE ARP 1256 (Ref. 19) require that the carbon atom concentration determined from emission measurements agree to within 15 percent of the concentration determined from fuel analysis. Carbon balances were calculated for all of the exhaust emissions data and the results are tabulated in Table 2. Except for Test 7, in which large radial concentration gradients were observed throughout the combustor and at the exhaust station, the above acceptance criteria was satisfied and a balance to within nine percent was achieved.

FLOW FIELD MAPPING RESULTS

Detailed maps of the mean and fluctuating flow field were obtained for the five test conditions listed in Table 1. These test conditions were selected to encompass variations in combustor operating conditions which have the greatest influence on pollutant emissions.

High-Speed Motion Pictures

As an initial qualitative indication of flow field structure, high-speed (500 frames/sec) color motion pictures of the reacting flow in the vicinity of the injector were obtained for each of the five test conditions. These films showed that there were significant large-scale fluctuations in the flame luminosity for all test conditions. The nonswirling flow exhibited the largest unsteadiness, Fig. 14. The axial motions of the flame in this flow were sufficiently large so that the flame was observed to occasionally enter the fuel injector. Imparting swirl to the air stream reduced the fluctuations but even in swirling flows the flame is very unsteady in the vicinity of the injection plane. These visual observations of the flame structure support the conclusions drawn later from laser velocimeter data regarding the large-scale fluctuations of the flow in the initial mixing regions. Analysis of the transient pressure data, discussed below indicates that for most of the conditions investigated there are no significant resonant pressure fluctuations. Furthermore, similar large-scale fluctuations have been observed in the initial mixing regions of nonreacting jets (Ref. 20). Hence, the observed fluctuations are primarily fluid dynamic in origin and are not the result of coupling of the combustion process with the acoustic properties of the combustor or mechanical properties of the injector.

In addition to providing information on the time-dependent structure of the flame, the high-speed films also give qualitative information on

NO SWIRL
OVERALL EQUIVALENCE RATIO = 0.9
3.8 ATMOSPHERES

FRAMING RATE = 500/SEC
EXPOSURE TIME = 1 MSEC

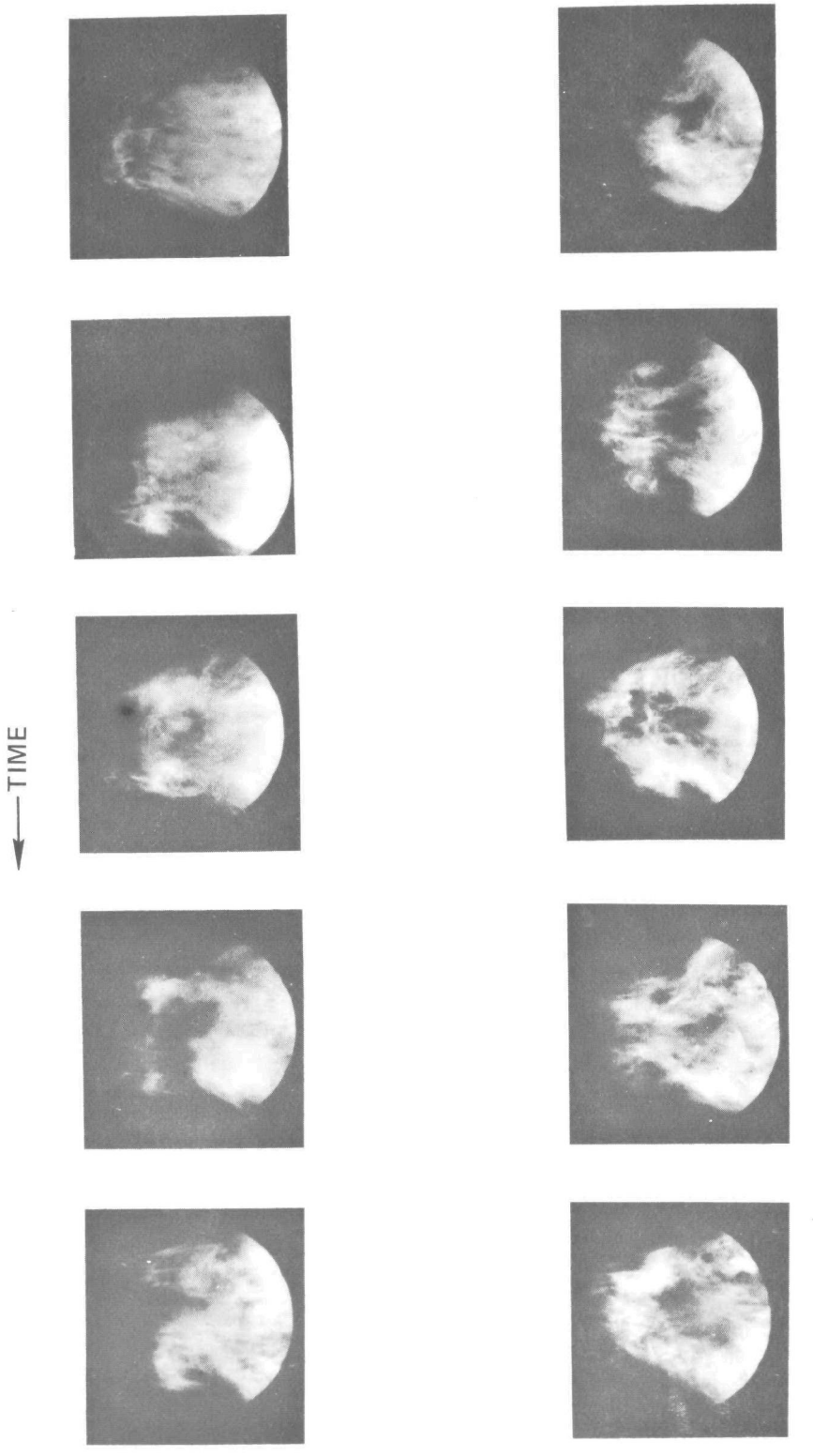

the spreading rate of the fuel jet. In all cases, the variations in spreading rate with changes in inlet conditions observed on the films are in agreement with the sampling data.

Transient Pressure Measurements

The high-speed motion pictures of the combustor flow field in Fig. 14 indicate a variation of the point of ignition from axial positions downstream of the injector to positions within the fuel injection port. Since the large-scale fluctuations will obviously complicate attempts to analytically model the combustor flow, a series of tests were conducted to evaluate the interaction of the combustion process with the acoustic or mechanical properties of the combustor and to thereby ensure that the configurations selected for detailed mapping were free of large-scale combustion instabilities.

The frequency spectra and the relative amplitudes of the pressure fluctuations occurring for each of the mapping experiments were determined by analyzing the output signal of a close-coupled high frequency pressure transducer installed in the combustor window port nearest the injector. A high-speed oscillograph was used to continuously record the signal and permit measurement of the amplitude of pressure fluctuation, and a spectrum analyzer was used to simultaneously determine the frequency of the temporal component. The results, summarized in Table 3, indicate that for operation at 1 atm and zero swirl a periodic pressure fluctuation occurs with a frequency of approximately 120 Hz and an amplitude of $\pm$ 6 percent. The measured frequency is in close agreement with a calculation of the fundamental harmonic for the combustor. Additional tests conducted at successively decreased fuel flow rates revealed that the magnitude of the fluctuations decreased rapidly and were less than $\pm$ 0.5 percent for $\phi = 0.6$.

When a swirl component was introduced on the inlet airflow at 1 atm, the frequency of the oscillation remained unchanged; however, the amplitude decreased steadily with increasing swirl and was less than $\pm$ 0.5 percent for $S = 0.6$. Also, the use of an orifice plate to increase the combustor pressure to 3.5 atm effectively changed the acoustic characteristics of the combustor and significantly reduced the natural frequency and the amplitude of the pressure fluctuations. The frequency spectra obtained for typical test conditions are presented in Fig. 15.

Temperature Data

The combustor mapping data have been reduced to isopleth form to permit visualization of the radial and axial variation of individual

Table 3. SUMMARY OF TRANSIENT PRESSURE MEASUREMENTS

Test No.	Swirl No.	Pressure (atm)	Air/Fuel Velocity Ratio	Φ	Frequency (Hz)	Amplitude Variation (%)
1	0	3.8	20	0.9	2	< ± 0.5
3	0.3	1.0	20	0.9	110	± 1.0
4	0.3	3.8	20	0.9	9	< ± 0.5
6	0.6	1.0	20	0.9	110	< ± 0.5
7	0.6	1.0	0.2	0.9	110	< ± 0.5
Ref. 7	0	1.0	20	0.9	120	± 6.0

FREQUENCY SPECTRA OF TRANSIENT PRESSURE FLUCTUATIONS

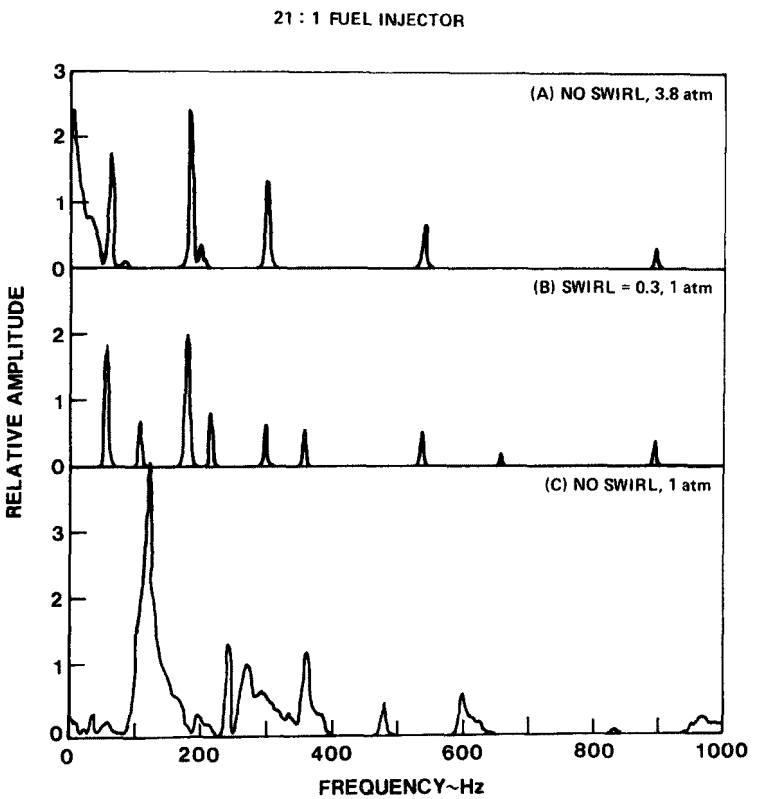

76-06-282-21

flow field parameters and to facilitate comparisons between these parameters in each of the flow configurations investigated. However, since the radial distributions of mean flow properties were determined at four to six axial locations within the combustor, interpolation between stations was necessary and, therefore, a certain amount of "artistic license" has been assumed in constructing these plots. In each of these isopleths the radial extent of the fuel delivery port and the air annulus is indicated to aid in visualization of the flow field structure. A complete tabulation of the experimental temperature data is presented in Appendix D.

Contours of constant temperature which show the time-mean temperature distributions obtained for all of the mapping test conditions are presented in Fig. 16. An initial examination of the data reveals the similarity of the flow field structure obtained for each of the test configurations and the temperature distributions characteristic of axisymmetric, turbulent diffusion flames, i.e., peak temperatures occurring in an annular region off the centerline. Specific trends in the temperature distributions resulting from variation of the inlet parameters are evident from a detailed examination of the isopleths. For example, imparting swirl = 0.3 to the airflow at 3.8 atm (Figs 16a and 16b) and increasing it from 0.3 to 0.6 at 1 atm (Figs. 16c and 16d) resulted in increased locally high temperatures developed off the centerline and increased radial temperature gradients. Furthermore, comparison of the axial temperature gradients indicate that increasing swirl also results in significantly higher temperatures in the vicinity of the fuel injector.

Increasing the combustor pressure from 1 atm to 3.8 atm, with all other inlet conditions remaining constant, results in longer combustor residence times, higher temperatures and more rapid chemical reaction. For the case of 0.3 swirl (Figs. 16b and 16c) the temperature distributions again exhibited the typical diffusion-flame-like structure; however, increasing pressure shifted the location of the peak temperature closer to the centerline and resulted in higher radial gradients. As expected, the temperature and heat release rate in the vicinity of the injector were increased, primarily due to reduced flow velocity.

The influence of air/fuel velocity ratio on the temperature distribution within the combustor is illustrated in Figs. 16d and 16e. For a combustor pressure of 1 atm and an inlet air swirl of 0.6 decreasing the air/fuel velocity (increased fuel velocity) from 21 to 0.2 resulted in a shift of the radial location of the peak temperatures away from the combustor centerline of the duct. The conspicuous change in the radial location of the maximum temperature suggests a significantly

TIME–AVERAGED TEMPERATURE DISTRIBUTIONS

(A) ZERO SWIRL, 3.8 ATM

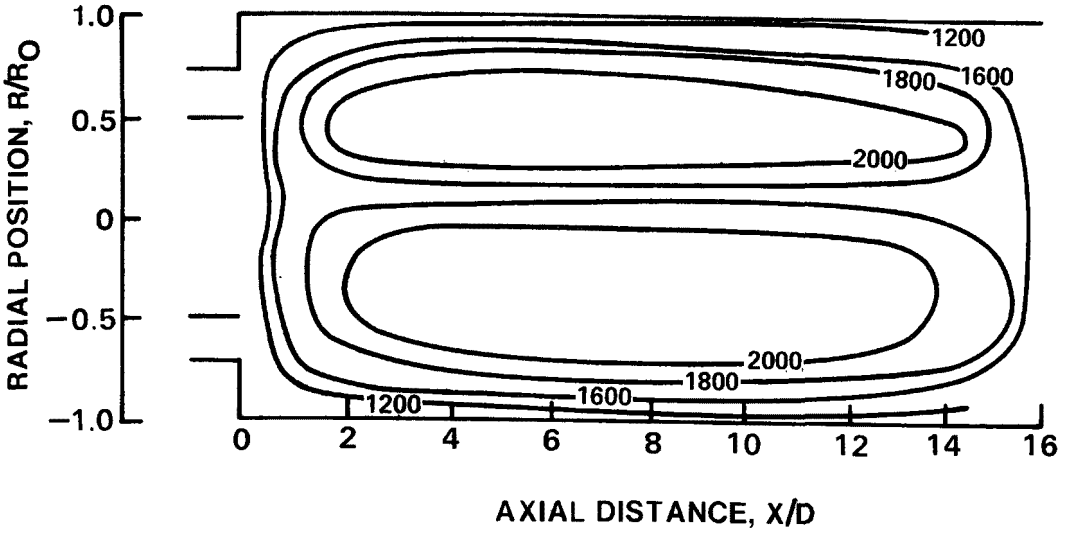

(B) SWIRL = 0.3, 3.8 ATM

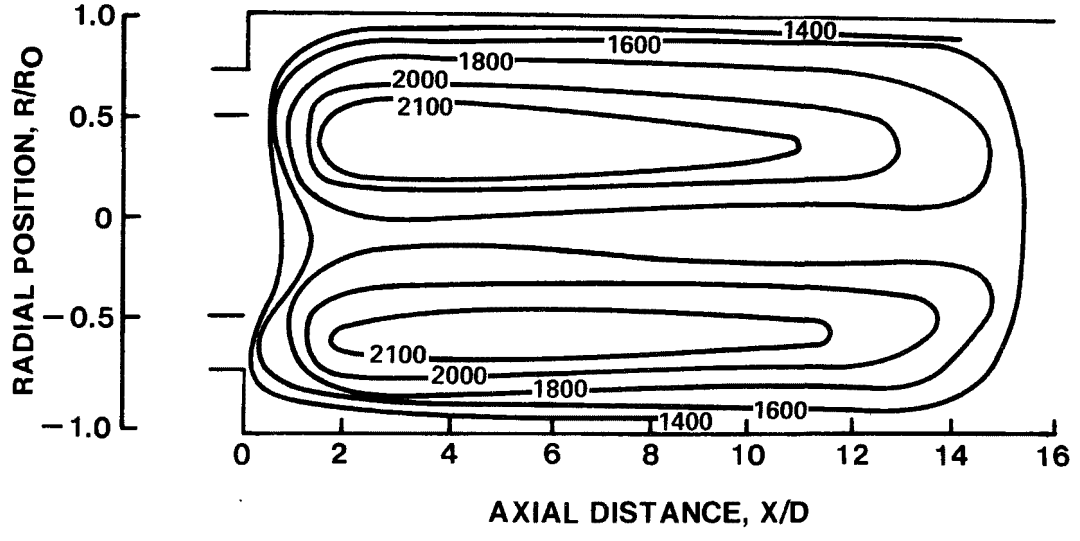

(C) SWIRL = 0.3, 1 ATM

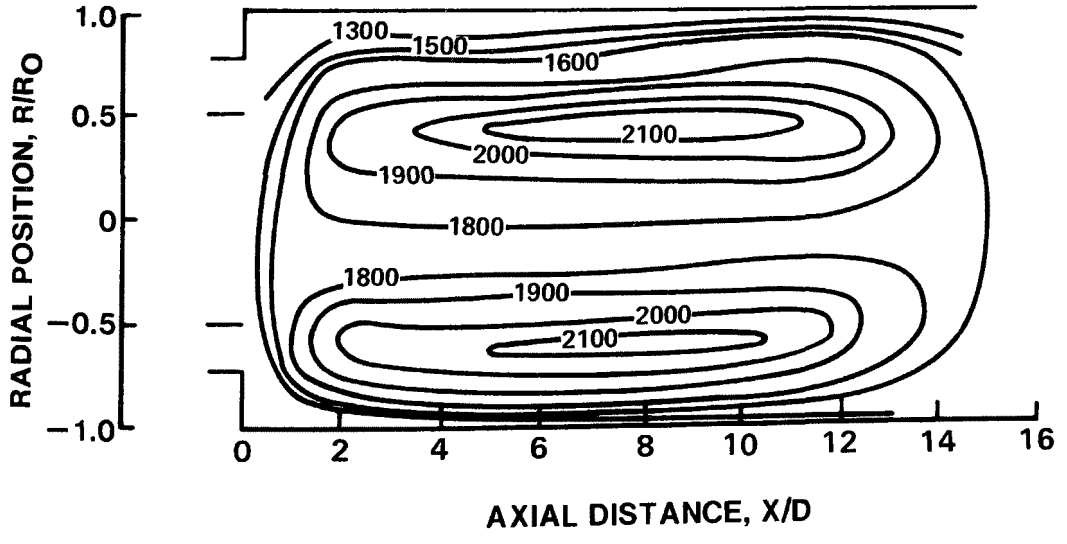

76–07–158–1

TIME–AVERAGED TEMPERATURE DISTRIBUTIONS

(D) SWIRL = 0.6, 1 ATM

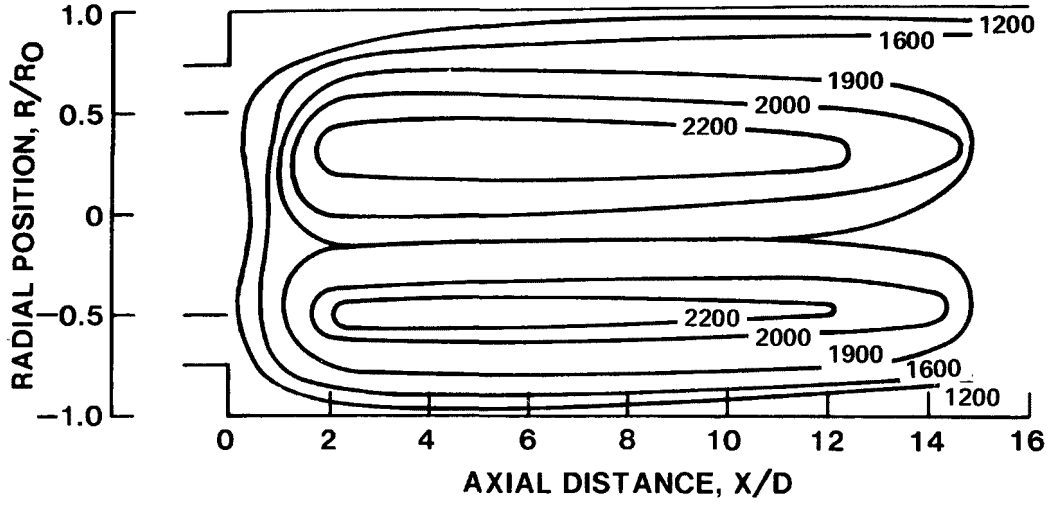

(E) SWIRL = 0.6, 1 ATM, 0.2 / 1 INJECTOR

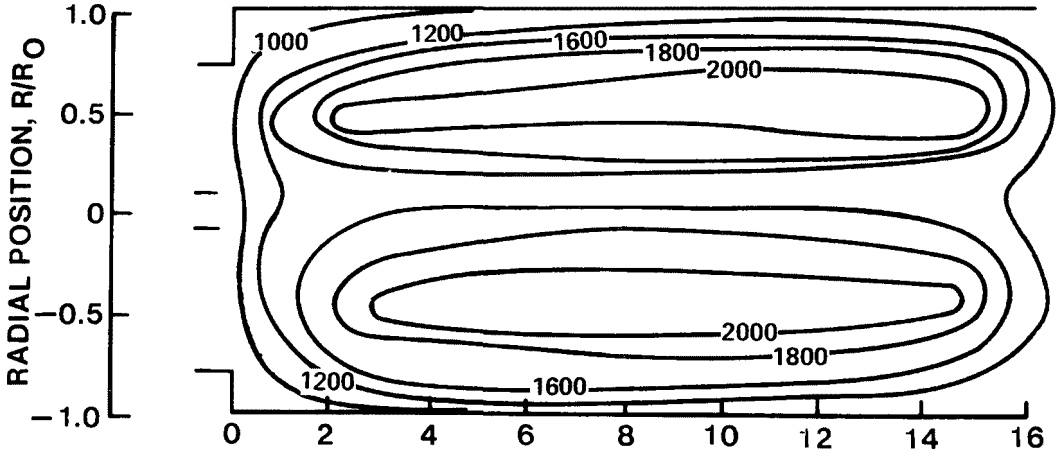

76–07–158–2

more rapid rate of spreading of the fuel jet for the high fuel injection velocity, an observation that was confirmed by measurements of the radial concentration gradients of unburned hydrocarbons. In addition, significantly lower temperatures were measured on the combustor centerline and, therefore, the radial temperature gradients also were increased.

Concentration Data

Because of the importance of the physical and chemical phenomena occurring in the region near the injector (e.g., formation of the recirculation zone(s) and initiation of mixing and chemical reaction) measurements of the species concentration profiles were made at four to six locations within an axial distance equivalent to four combustor diameters (X/D = 4). Detailed maps of the species concentration distributions are presented in Figs. 17 to 21. The concentration data are tabulated in Appendix E.

Examination of the species contours reveals significant changes in the mean species concentration distributions with variations in combustor operating conditions. For example, comparison of Figs. 17 and 18 (Tests 1 and 4) reveals that introduction of swirl at a combustor pressure of 3.8 atm greatly increases the rate of oxidation of the fuel to CO, as evidenced by the THC and CO concentration contours, accelerates the rate of NO formation, with a significant fraction of the exhaust NO concentration being formed within the first three combustor diameters, and increases the rate of oxidation of CO to CO_2. All of these observations point to a higher energy release rate in the swirling flow, which is consistent with the measured mean temperature contours. Introduction of swirl increases the spreading rate of the fuel jet, as evidenced by the THC contours, and the principal region of fuel-air mixing and reaction appears to be displaced radially outward. These observations also are consistent with the temperature data, which show an outward displacement of the temperature peaks upon imparting swirl.

Measurements of the species concentration distributions for the S = 0.3 and the S = 0.6 flows at 1 atm combustor pressure are presented in Figs. 19 and 20 (Tests 3 and 6). The THC concentration maps indicate that as the swirl number is increased the spreading rate of the fuel jet rapidly increases with a corresponding decrease in the concentration of unburned hydrocarbons along the centerline. Unlike the other flows investigated, moderately large fuel concentrations are measured near the combustor wall in the S = 0.6 test. As noted earlier, there appears to be significant large-scale fluctuations in all of the flows investigated. Transport of fuel radially outward in the swirling flows may be the

TIME–AVERAGED SPECIES DISTRIBUTIONS

NO SWIRL, 3.8 ATM, $V_a/V_f = 21$

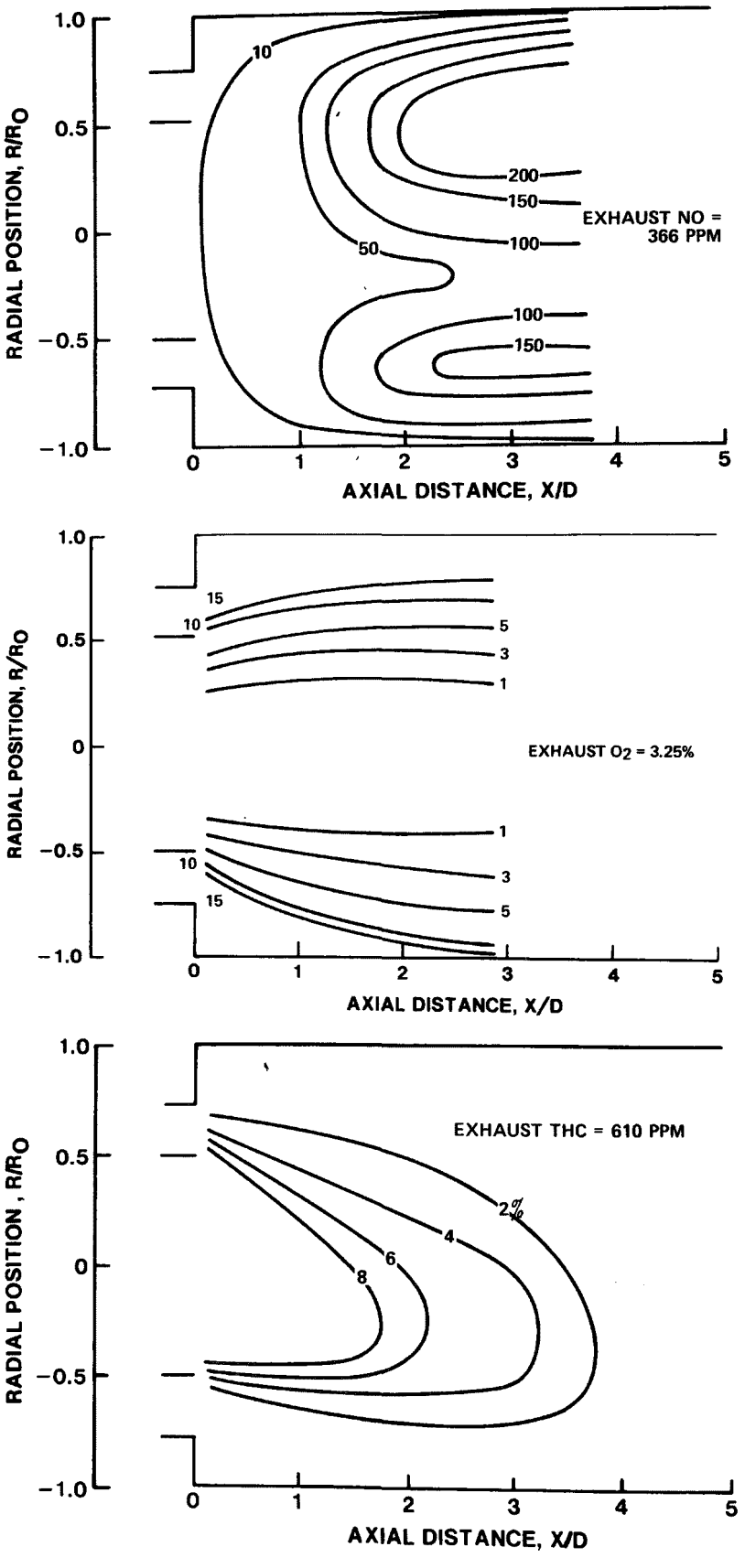

76–07–158–19

TIME–AVERAGED SPECIES DISTRIBUTIONS

NO SWIRL, 3.8 ATM, $V_a/V_f = 21$

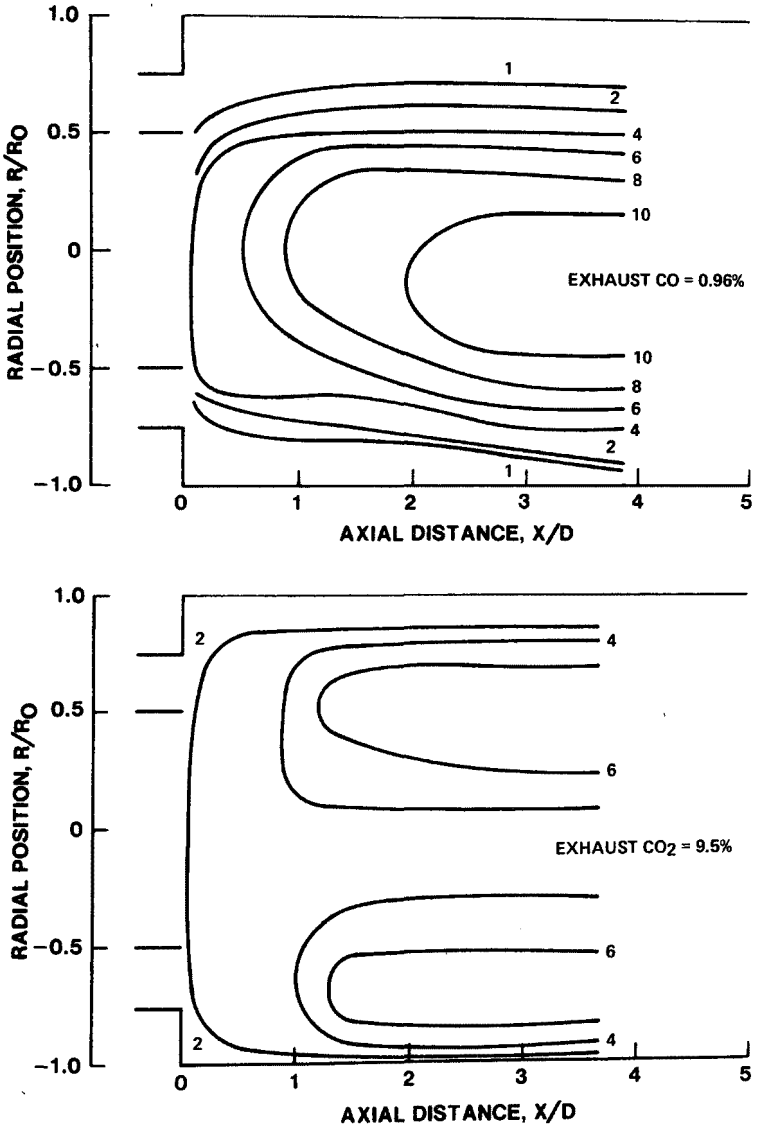

76–07–158–18

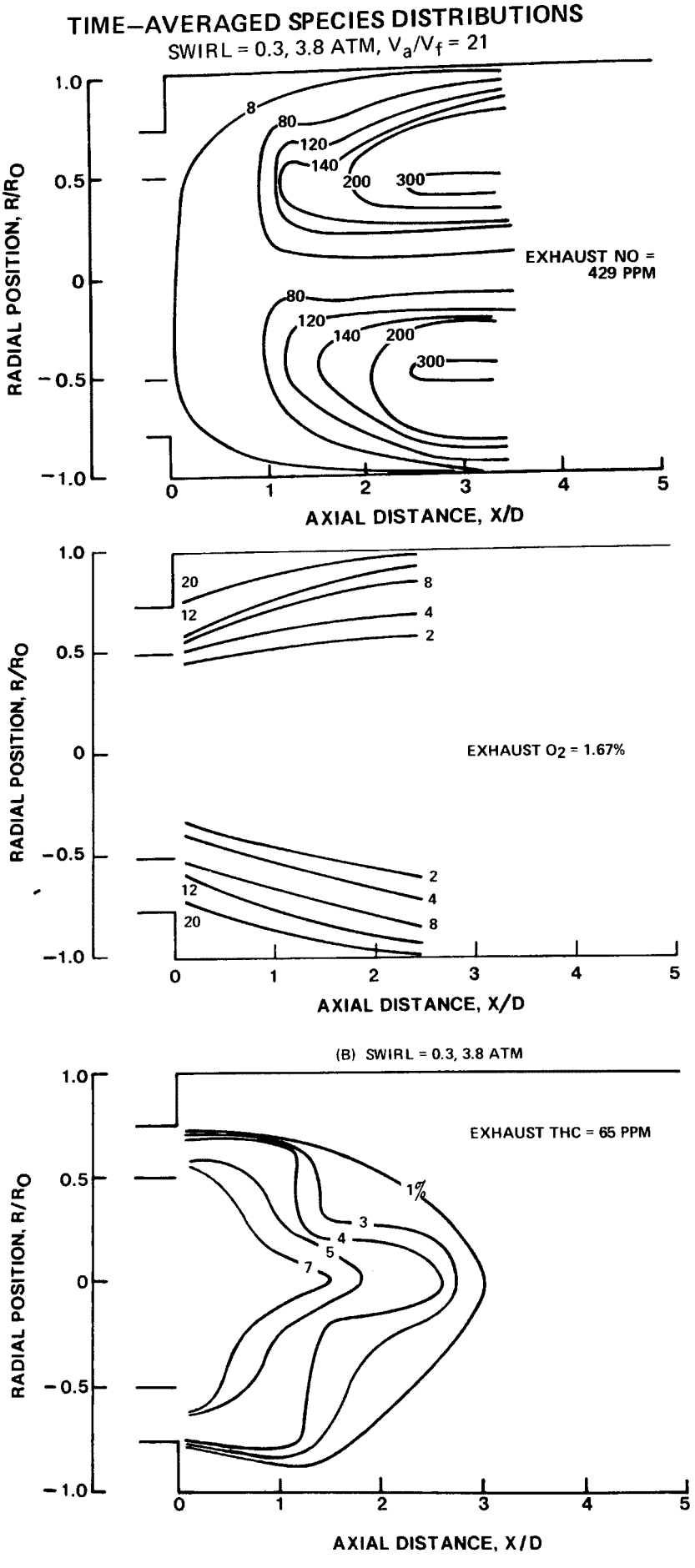
TIME–AVERAGED SPECIES DISTRIBUTIONS
SWIRL = 0.3, 3.8 ATM, V_a/V_f = 21
RADIAL POSITION, R/R$_O$
AXIAL DISTANCE, X/D
EXHAUST NO = 429 PPM
8
80
120
140
200
300
EXHAUST O_2 = 1.67%
20
12
4
2
(B) SWIRL = 0.3, 3.8 ATM
EXHAUST THC = 65 PPM
1%
3
4
5
7

76–07–158–4

TIME–AVERAGED SPECIES DISTRIBUTIONS

SWIRL = 0.3, 3.8 ATM, $V_a/V_f = 21$

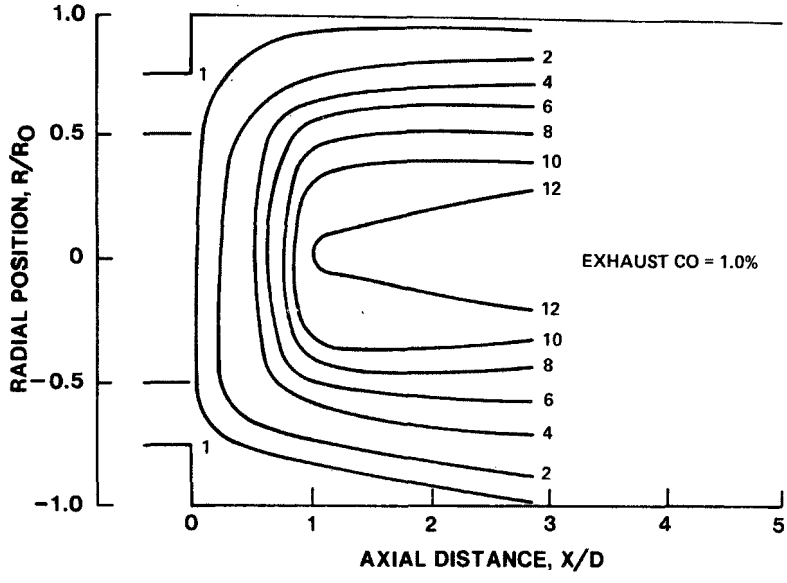

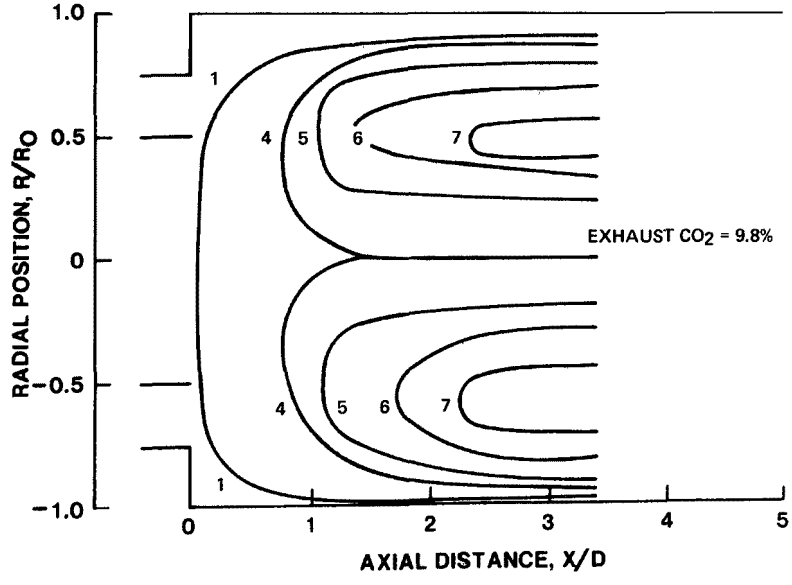

76–07–158–5

TIME–AVERAGED SPECIES DISTRIBUTIONS

SWIRL = 0.3, 1 ATM, V_a/V_f = 21

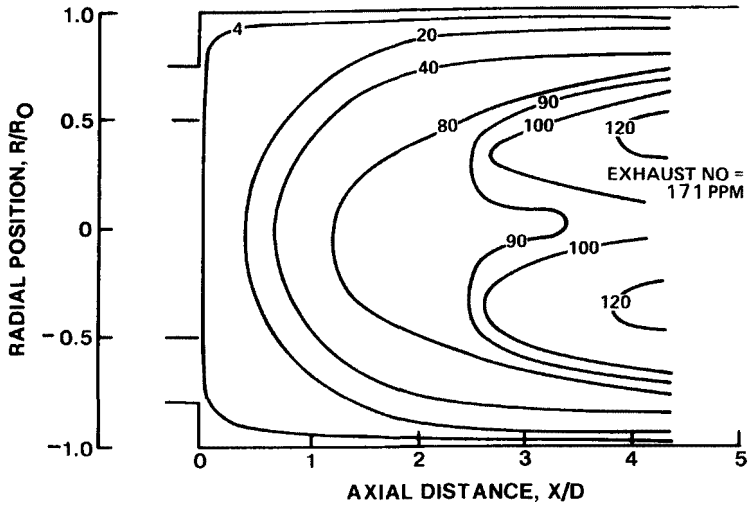

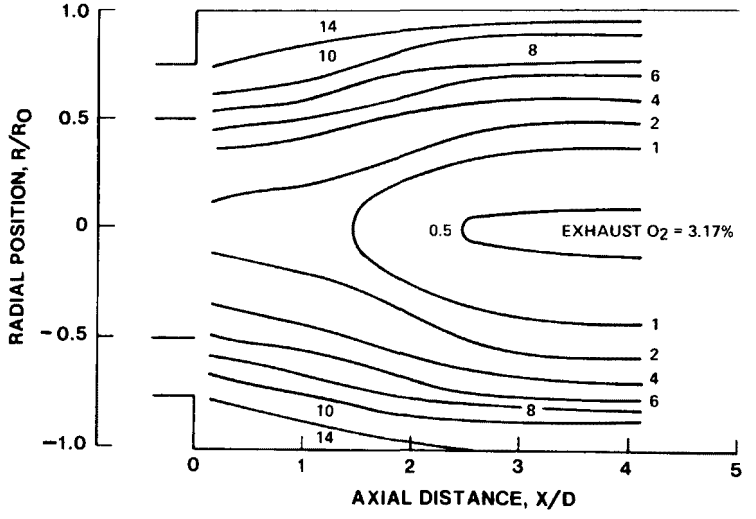

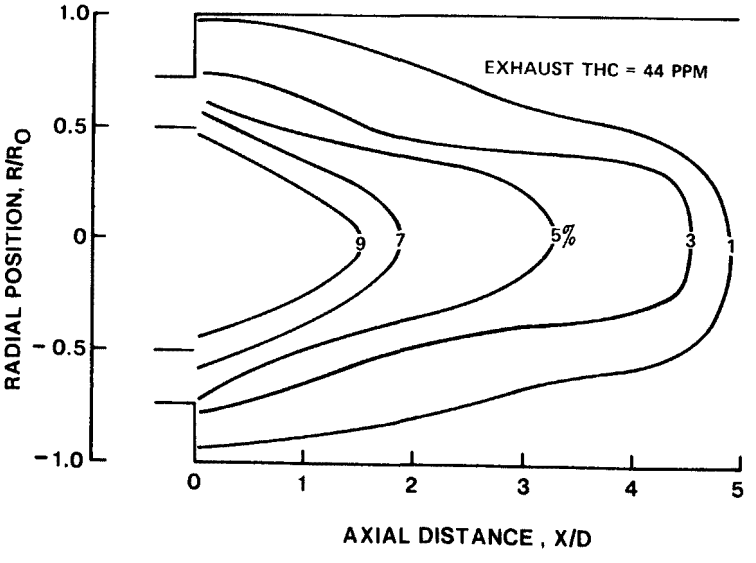

TIME–AVERAGED SPECIES DISTRIBUTIONS

SWIRL = 0.3, 1 ATM, $V_a/V_f = 21$

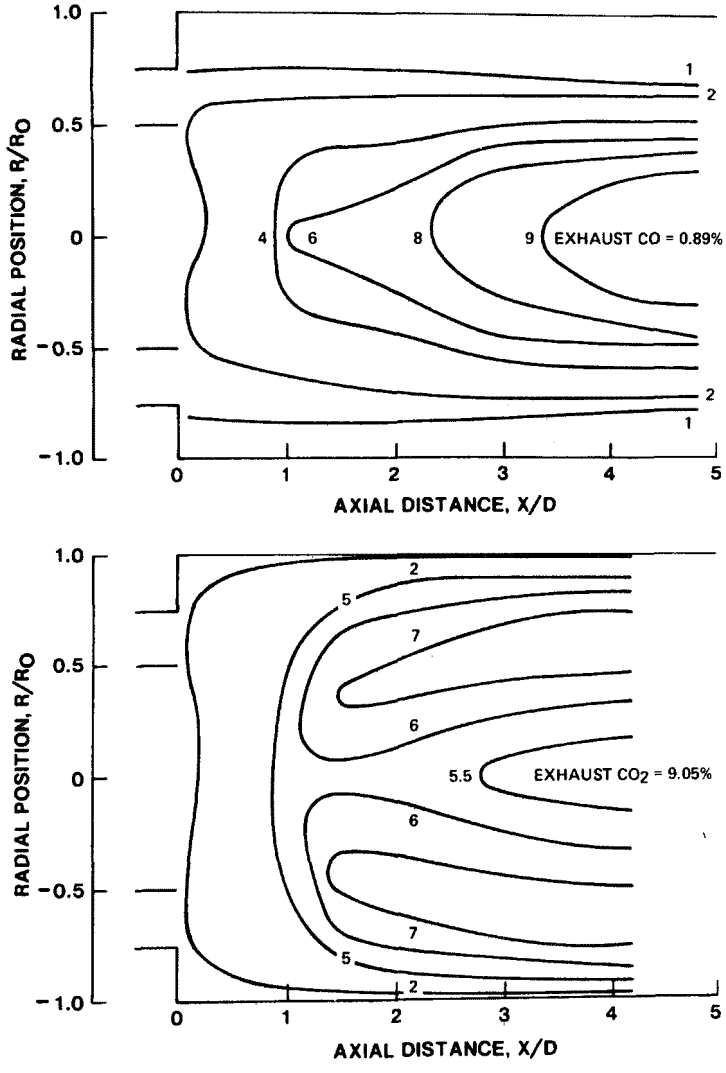

FIG. 20

TIME–AVERAGED SPECIES DISTRIBUTIONS

SWIRL = 0.6, 1 ATM, $V_a/V_f = 21$

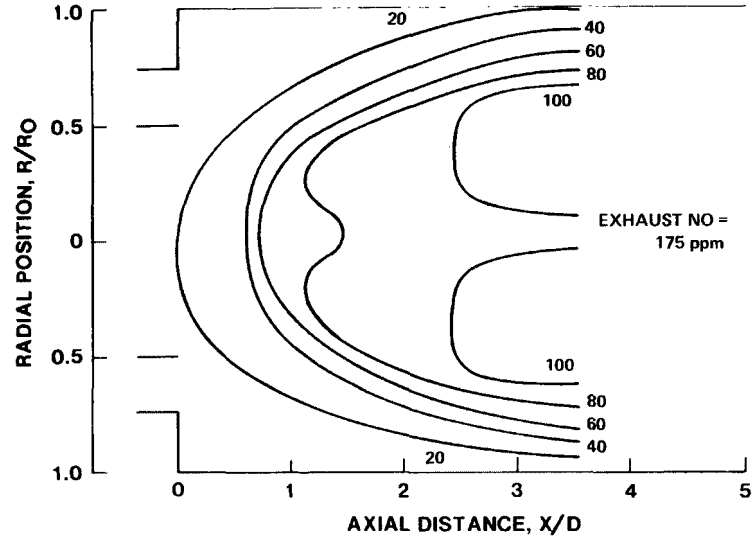

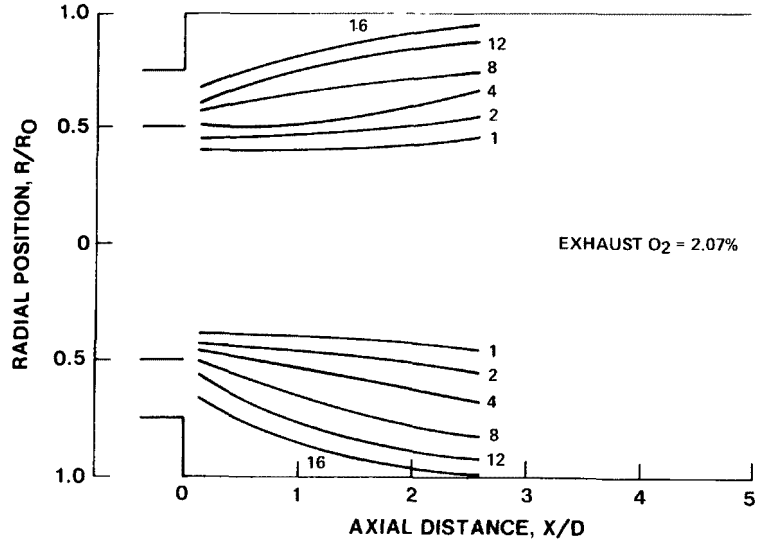

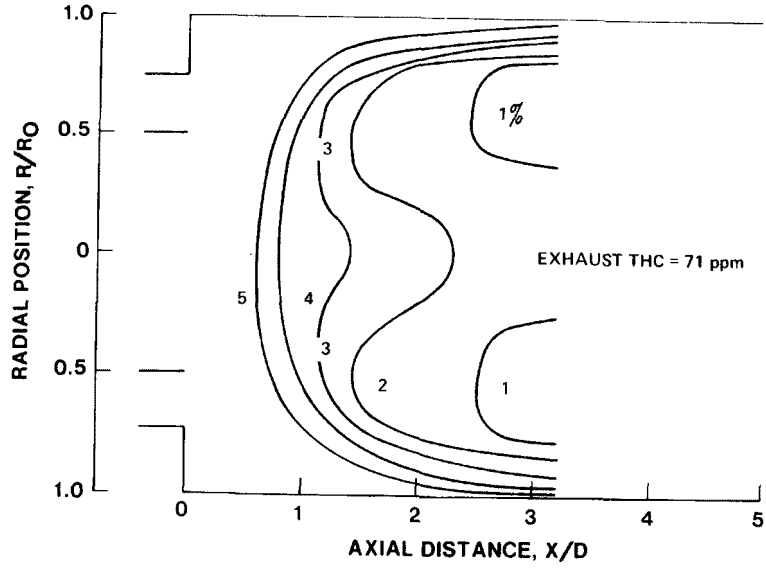

76–07–158–8

TIME–AVERAGED SPECIES DISTRIBUTIONS

SWIRL = 0.6,1 ATM, $V_a/V_f = 21$

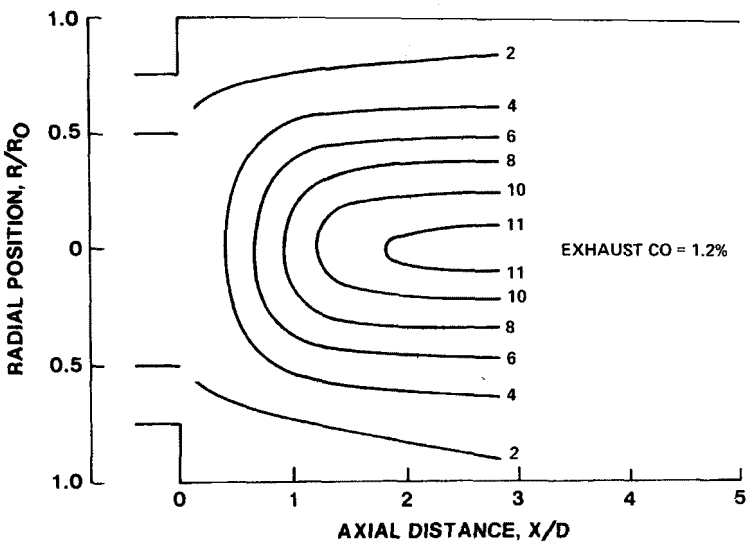

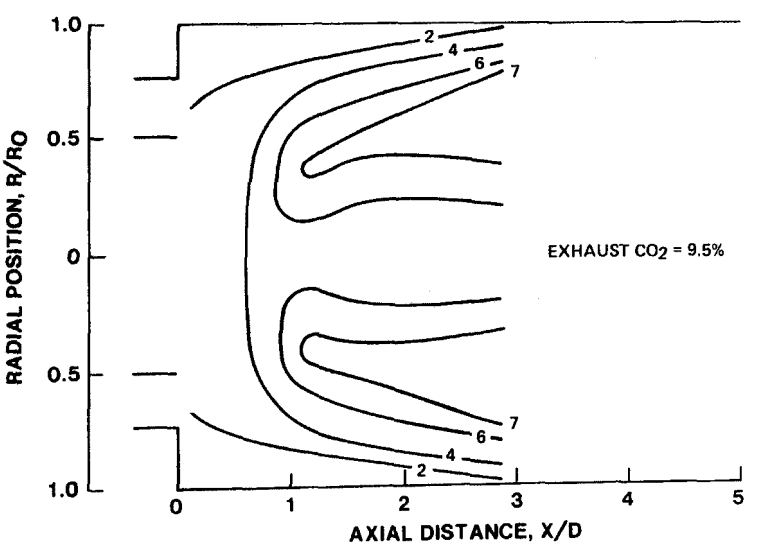

76–07–158–3

result of entrainment of large fuel eddies by the swirling air stream, with subsequent transport of the fuel toward the combustor wall due to the radial spreading of the air stream. With increased swirl, oxidation of the hydrocarbon fuel to CO is greatly accelerated with a lesser increase observed in the rate of oxidation of CO to CO_2. These observations suggest an increase in energy release rate with an increase in swirl from 0.3 to 0.6. This conclusion is supported by the measured temperature distributions. The higher temperature levels for the S = 0.6 flow result in a more rapid NO formation rate.

One of the principal effects of elevated pressure is a decrease in the flow velocity and increase in the time available for reaction. Analysis of the NO concentration data presented in Figs. 19 and 18 (Tests 4 and 3) indicates that an appreciable increase in the axial rate of NO formation occurred as a result of raising the combustor pressure from 1 to 3.8 atm. However, comparisons made on the basis of equivalent residence times (as opposed to equivalent axial distances) show a much smaller increase in NO concentrations and, therefore, demonstrate the residence time effect. At elevated pressure, radial spreading of the fuel jet was noticeably diminished as was the penetration of oxygen to the center of the flow. These trends are in agreement with the previously discussed shift of the temperature maxima toward the centerline. Also, at higher pressures, the oxidation of hydrocarbons to CO is accelerated, as is shown in Fig. 18, and significantly higher CO concentrations were measured along the centerline.

As indicated earlier, a significant alteration in the temperature distribution within the combustor was observed as a result of interchanging fuel injectors and operating at an air-fuel velocity ratio of 0.2 (Test 7). Qualitative evaluations suggested that rapid spreading of the fuel jet occurred. The O_2 and THC concentration contours for air-fuel velocity 0.2, Fig. 21, supports these observations and shows high concentrations of fuel extending well beyond the lip of the injector and low oxygen concentrations in the central portion of the flow. Low temperatures and near zero concentrations of NO were measured along the centerline. The appearance of the NO isopleth differs markedly from those obtained at low injection velocity and shows that high NO concentrations exist in a torroidal-shaped region close to the injector, approximately coincident with the recirculation zone. In this region, the local temperature is very high and there is rapid oxidation of the hydrocarbon fuel to form CO and ultimately CO_2. In contrast, low CO and CO_2 concentrations were measured near the centerline due to the slower rate of hydrocarbon reaction.

TIME–AVERAGED SPECIES DISTRIBUTIONS

SWIRL = 0.6, 1 ATM, V_a/V_f = 21

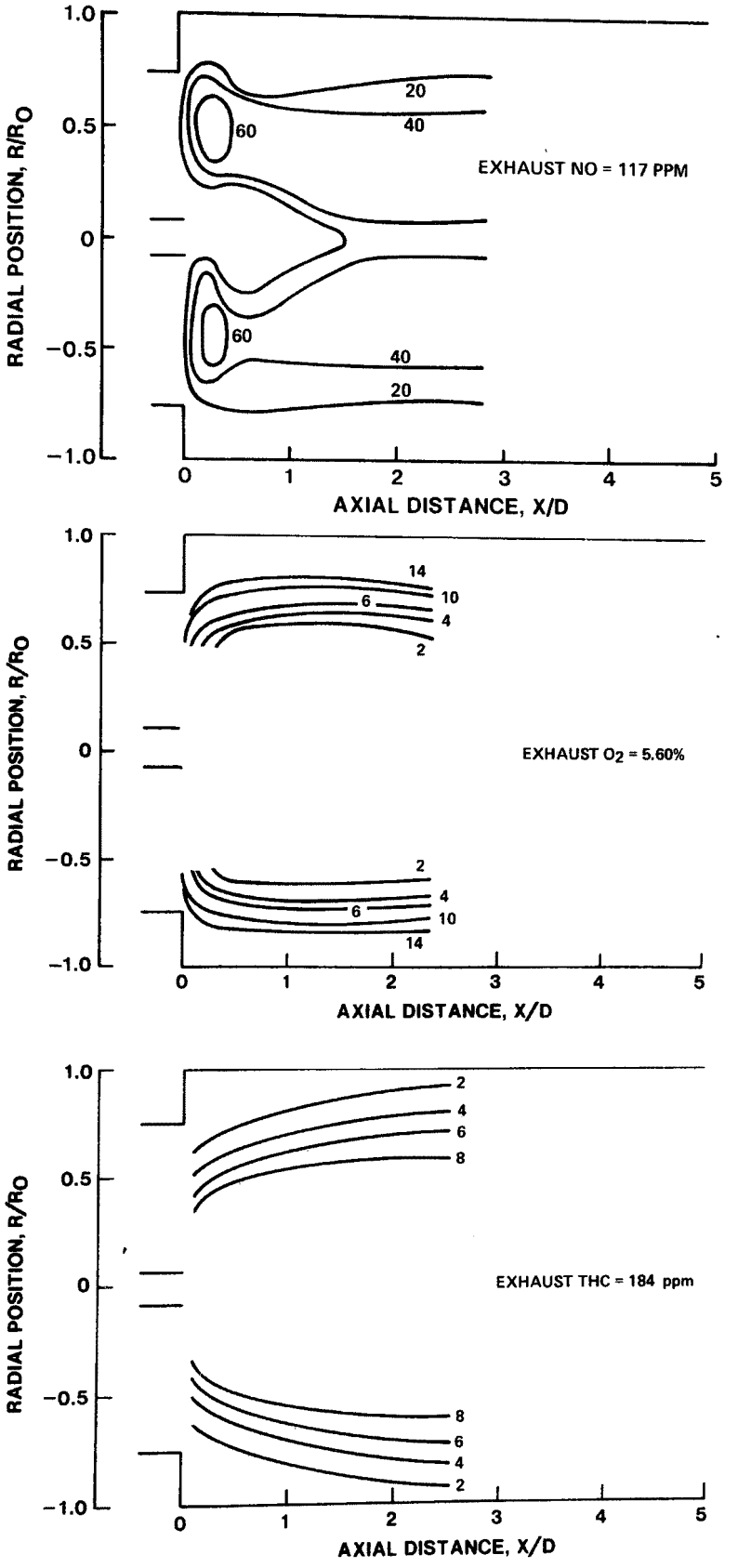

76–07–158–16

TIME–AVERAGED SPECIES DISTRIBUTIONS

SWIRL = 0.6, 1 ATM, $V_a/V_f = 21$

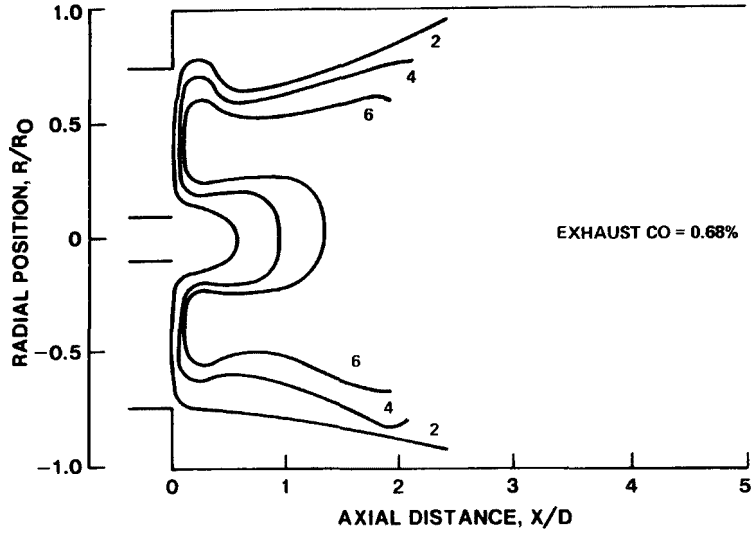

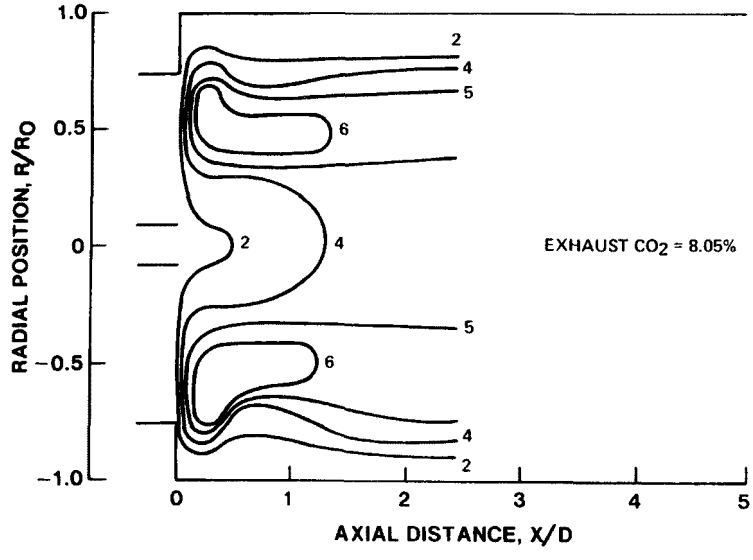

NO_2 Concentration Measurements

Evidence of significant nitrogen dioxide (NO_2) concentrations near the primary reaction zone of turbulent diffusion flames has been reported by several investigators (Refs. 21 and 22). In the present study NO_2 concentrations in excess of NO concentrations were measured along the mean flame boundaries in the vicinity of the fuel injector. Because of the difficulty in making quantitative measurements of NO_2 in strongly reducing atmospheres using the stainless-steel thermal converter of the chemiluminescence monitor (Ref. 16), NO_2 data could not be acquired as the probe was traversed into the fuel-rich regions of the combustor. Therefore, an NDUV analyzer was used to augment the chemiluminescence detector by measuring NO_2 emissions in selected tests. A typical profile, shown in Fig. 22, indicates that NO_2/NO ratios greater than unity were measured at the lean boundary of the flame zone, and NO_2 concentrations subsequently decreased to a low level in the fuel-rich central core region of the flow. As was stated in Ref. 7, significant NO_2 formation was observed within an axial distance equivalent to three combustor diameters downstream of the injector exit and thereafter the NO_2 concentration remained relatively constant with increasing axial distance. However, there remains considerable uncertainty in the observed NO_2 levels because of potential sources and sinks for NO_2 during transfer of the gas sample to the Exhaust Analyzer (Refs. 7 and 16).

Mean Velocity Measurements

The radial distributions of time-mean axial and tangential velocities were measured at a minimum of four and a maximum of six axial locations in the initial regions of the combustor ($X/D \leq 2$). In addition a limited number of measurements of the time-mean radial velocity were made. A typical set of mean axial velocity profiles is shown in Fig. 23. From profiles such as these, mean axial velocity contours were constructed, showing lines of constant velocity within the combustor. The mean axial velocity contours obtained for the five test conditions are presented in Fig. 24. These profiles show the location and shape of the time-averaged recirculation zones and indicate their approximate longitudinal and lateral extent. As was the case for the temperature and concentration isopleths, interpolation between data taken at various axial stations was required to develop the velocity contour plots. All the data show a consistent trend towards uniform velocity profiles with increasing distance from the injector, which would be expected for highly turbulent plug-like flows immediately downstream of the initial mixing region.

NITROGEN OXIDE DISTRIBUTIONS

SWIRL = 0.6, 1 ATM, V_a/V_f = 0.2

- ● NO MEASURED BY CLA
- ▲ NO_X = NO + NO_2 MEASURED BY CLA
- □ NO_2 MEASURED BY NDUV
- △ NO_X = NO (CLA) + NO_2 (NDUV)

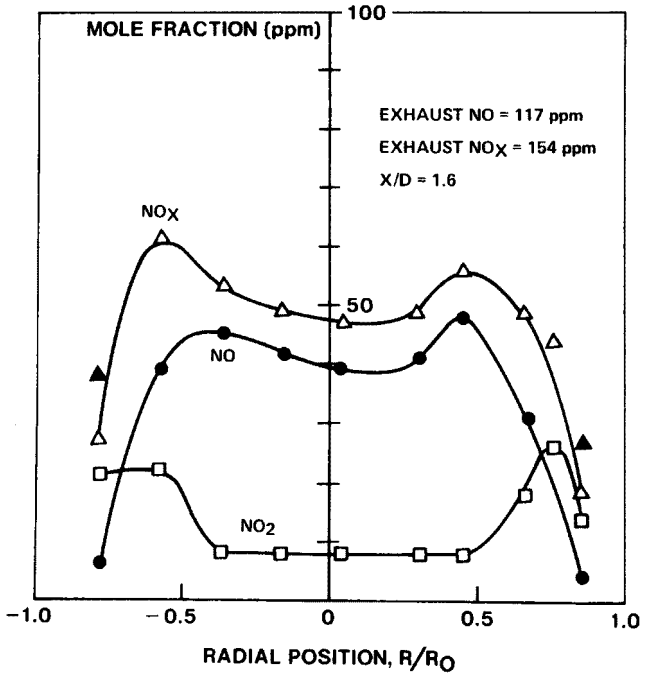

MEAN AXIAL VELOCITY PROFILES

SWIRL = 0.3, 1 ATM, $V_a/V_f = 21$

○ X/D = 0.13

□ X/D = 0.48

◇ X/D = 0.05

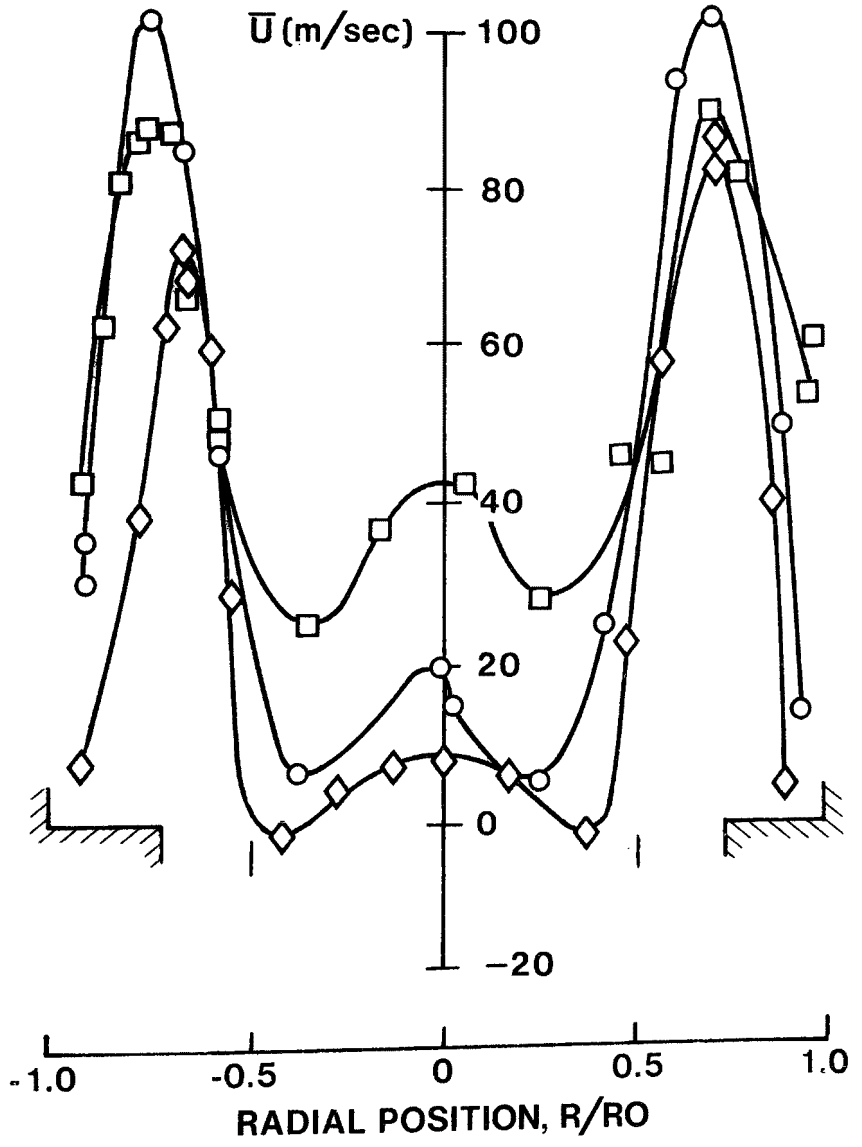

MEAN AXIAL VELOCITY DISTRIBUTIONS

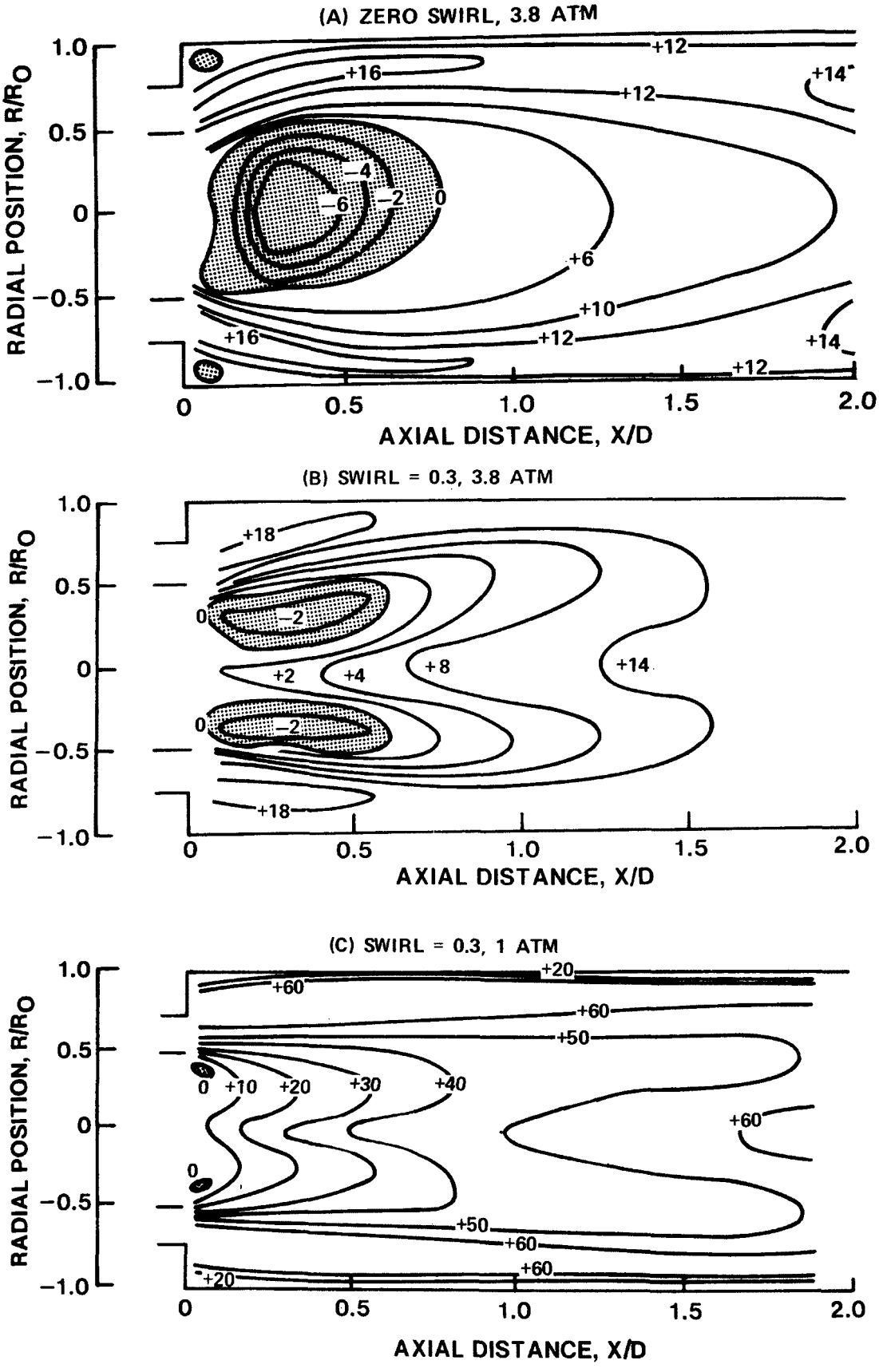

76−07−158−20

MEAN AXIAL VELOCITY DISTRIBUTIONS

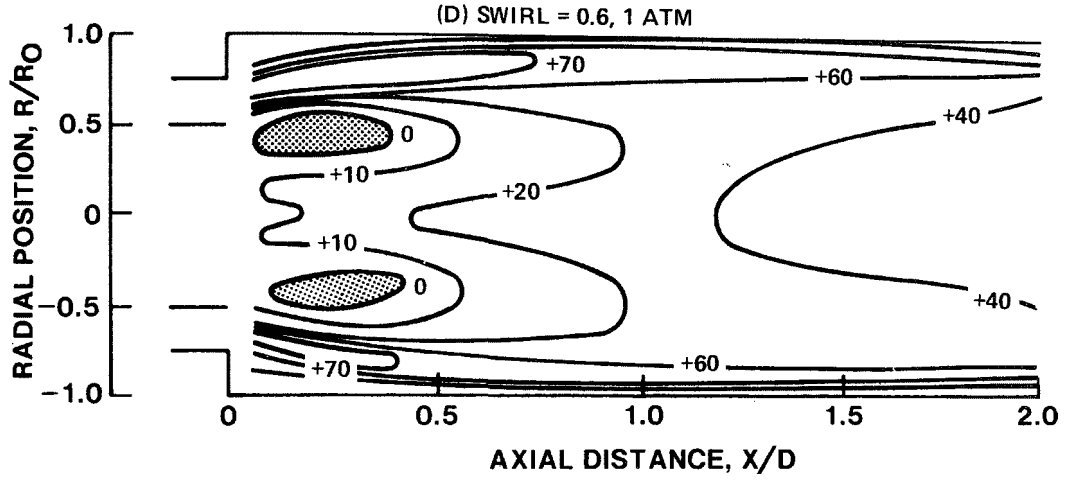

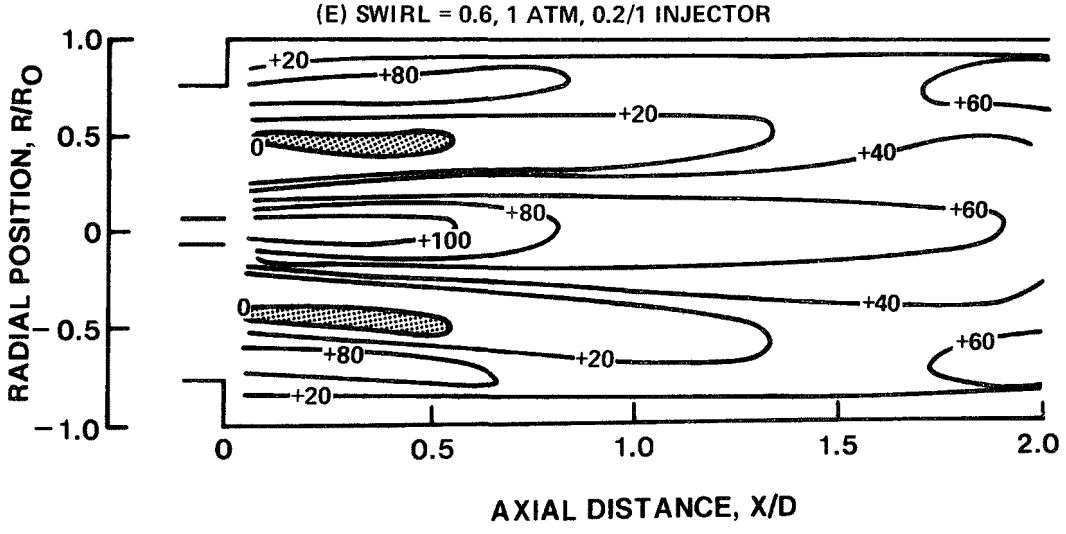

In the case of zero swirl at 3.5 atm a large spheroidal time-averaged recirculation zone is present immediately downstream from the center (fuel) jet with associated mean reverse velocities significantly larger than in any of the swirling flow cases. In addition to this central zone, there is a second recirculation zone behind the backward facing step at the nozzle exit plane.

The introduction of swirl brings about significant changes in the time-averaged flow field: a much smaller toroidal recirculation zone is present and the secondary recirculation zone is so reduced in size it cannot be detected. The primary results of increasing swirl from 0.3 to 0.6 at 1 atm are to produce a more pronounced initial radial mean flow and a somewhat larger, though still toroidal recirculation zone. However, in both these cases there is a much less rapid profile development than at 3.5 atm which can be primarily attributed to the decrease in combustor residence time.

For the small injector case there is extensive fuel jet coherence even though the annular air swirl induces a significant initial spreading rate.

The principal feature of each set of mean tangential velocity profiles (Fig. 25) is the change from solid body rotation (i.e., forced vortex flow) close to the injector towards a combined free/forced (i.e., Rankine) vortex flow downstream. Thus a region of irrotational flow develops and progresses towards the center of the duct as the flow proceeds downstream. As a result, the point of maximum tangential velocity moves radially inward. This trend from forced to Rankine vortex flow becomes more pronounced with both increased swirl and ambient combustor pressure (increased residence time). Such a transition from forced to Rankine vortex requires a sink, which in the present case is provided by the inward radial flow downstream of the time-averaged recirculation zones. This radial flow is evident from the increasing centerline axial velocities in Fig. 24, for example, and is more pronounced at 3.5 atm thereby enhancing the rate of vortex transition. Flow angle calculations based on the measured tangential velocity at the location of the peak axial velocity compare extremely well with the swirl vane blade angles at S = 0.3. For the 0.3 swirl cases, blade angle $\eta = 28^{\circ}$, the flow angles at 1 and 3.5 atm are 26°. At 0.6 swirl, $\eta = 47^{\circ}$, the calculated flow angle was 37°. However, in this latter case the number of blades was reduced from 18 to 12. Such a large change in solidity (chord/gap ratio), necessitated from a vane packaging standpoint, is the likely explanation for this reduced swirl efficiency.

MEAN TANGENTIAL VELOCITY PROFILES

SWIRL = 0.6, 1 ATM, $V_a/V_f = 21$

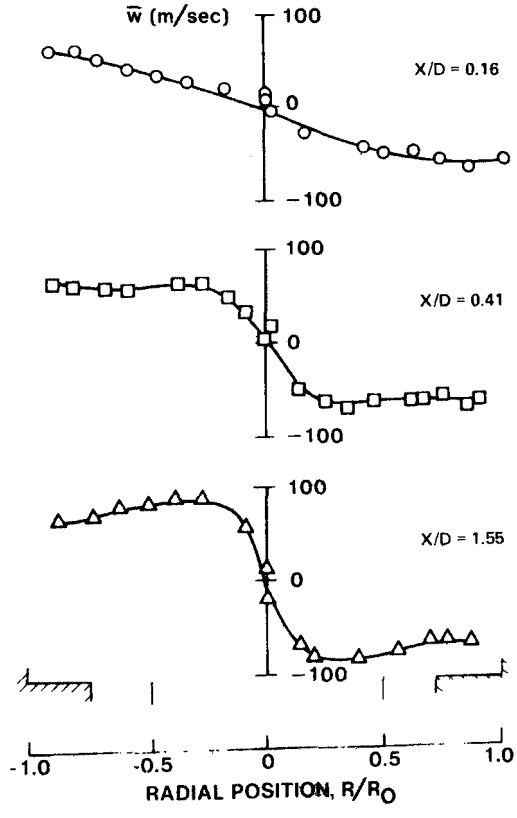

MEAN AND RMS TANGENTIAL VELOCITY DISTRIBUTIONS

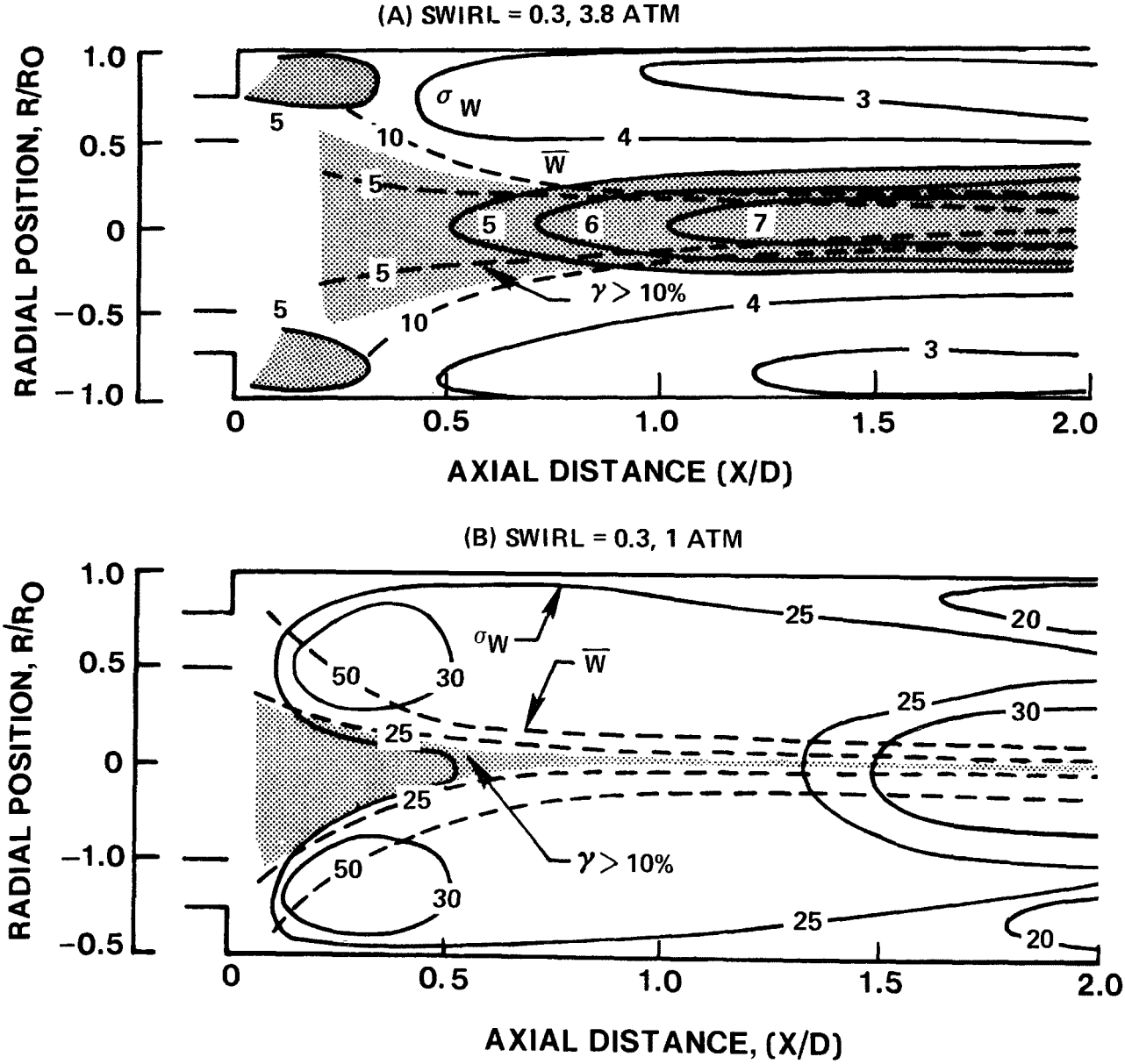

76-07-158-23

MEAN AND RMS TANGENTIAL VELOCITY DISTRIBUTIONS

(C) SWIRL = 0.6, 1 ATM

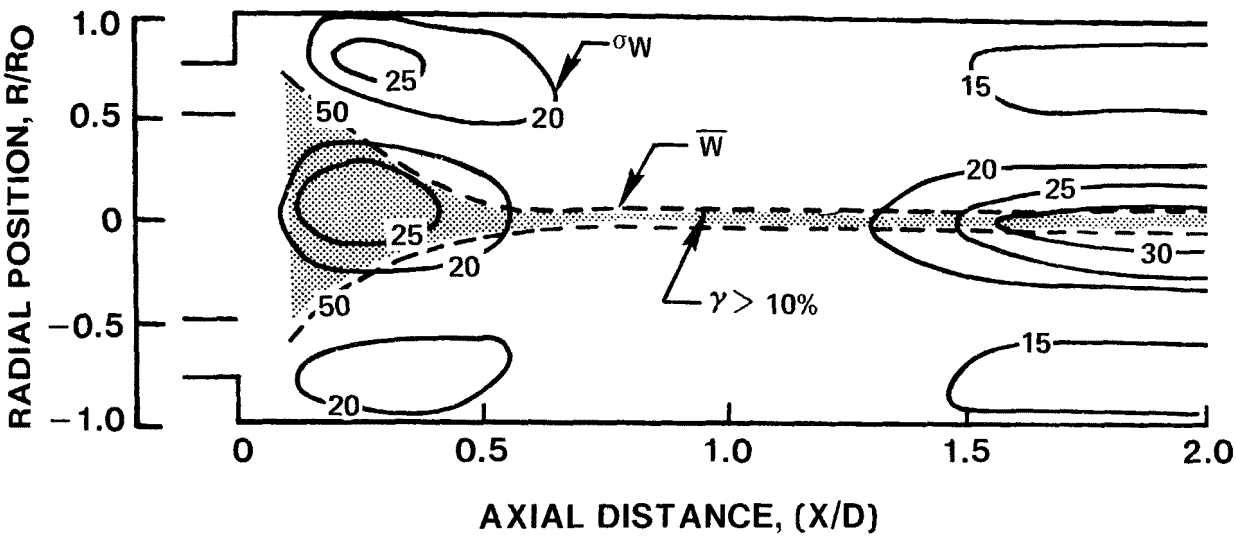

(D) SWIRL = 0.6, 1 ATM, 0.2/1 INJECTOR

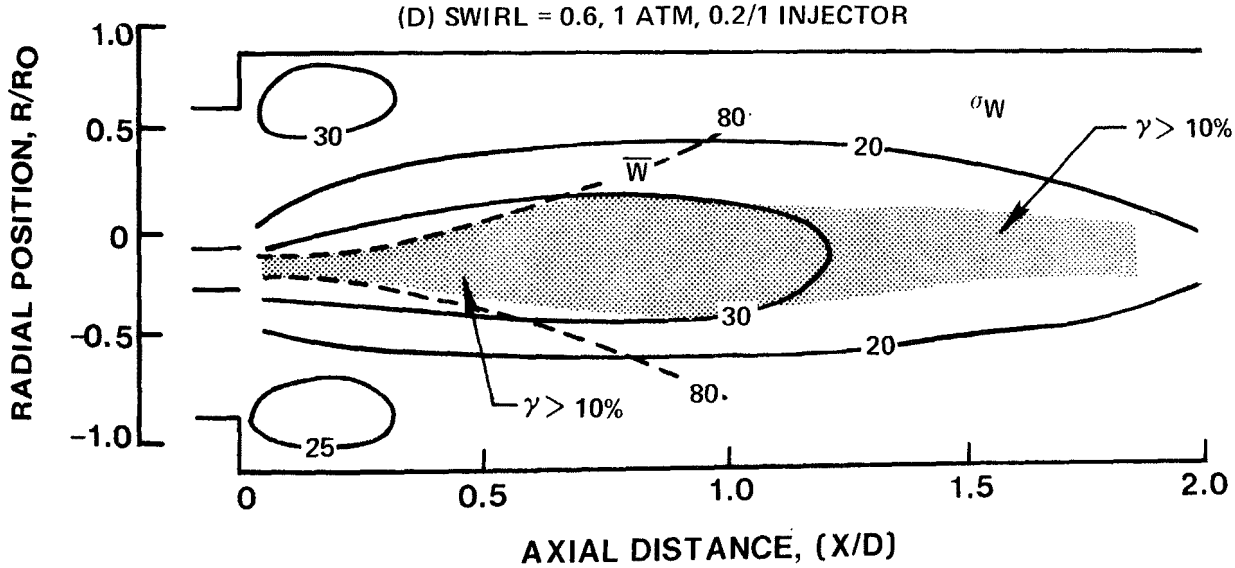

76-07-158-22

The presence of forced vortex flow immediately downstream of the injector has a pronounced effect on the flow field static pressure distribution since, neglecting viscous forces, there is a balance between pressure and inertial forces given by $dp/dr = -\rho W^2/r$. Since $W \propto r$ we obtain the well-known result that the static pressure increase in the core of a forced vortex is proportional to the square of the radius. This result significantly affects the mean axial velocity flow field because now the inviscid central fuel jet axial momentum is able to overcome the reduced static pressure gradient near the flow field centerline. This results in the formation of a smaller toroidal recirculation zone with reduced negative velocities made up primarily of lower momentum boundary layer fluid as indicated by their locations in Fig. 24.

To characterize the mean radial flow in the combustor, the mean radial velocity was measured at one axial location just downstream from the large fuel injector ($X/D = 0.34$) for a swirl number of 0.3 at atmospheric pressure, Fig. 27. The flow is directed radially inward toward the centerline in the central portion of the combustor, with peak mean radial velocities of approximately 10 m/sec. These observations are consistent with the description of the flow field determined from the axial and tangential velocity contours.

RMS Velocity Measurements

Measurements of the associated root-mean-square axial velocity fluctuations, presented in Fig. 28, indicate extremely high local fluctuation levels in the initial mixing regions. For the large-diameter injector, it was found that the normalized fluctuation levels decrease with both increasing swirl and ambient pressure. These data, when superimposed on the mean velocity contours, Fig. 29, show that the peak fluctuation levels coincide primarily with the locations of high mean shear, i.e., maximum local mean velocity gradient. However, measured rms velocity fluctuation levels provide no information on the turbulent scales involved. For instance, there are significant fluctuations associated with the time-averaged recirculation zones with local peak intensities occurring at points in the flow close to the time-averaged axial stagnation points. Since the mean velocity gradients are relatively low in these regions, the fluctuations must be due primarily to large-scale motion associated with recirculation zone entrainment and/or unsteadiness about its mean location. In the small diameter fuel injector case, the rms velocity contours are dramatically different and appear to be a result of fuel jet "flapping" about its mean location which was indicated by bi-modal probability density distributions

MEAN RADIAL VELOCITY PROFILE

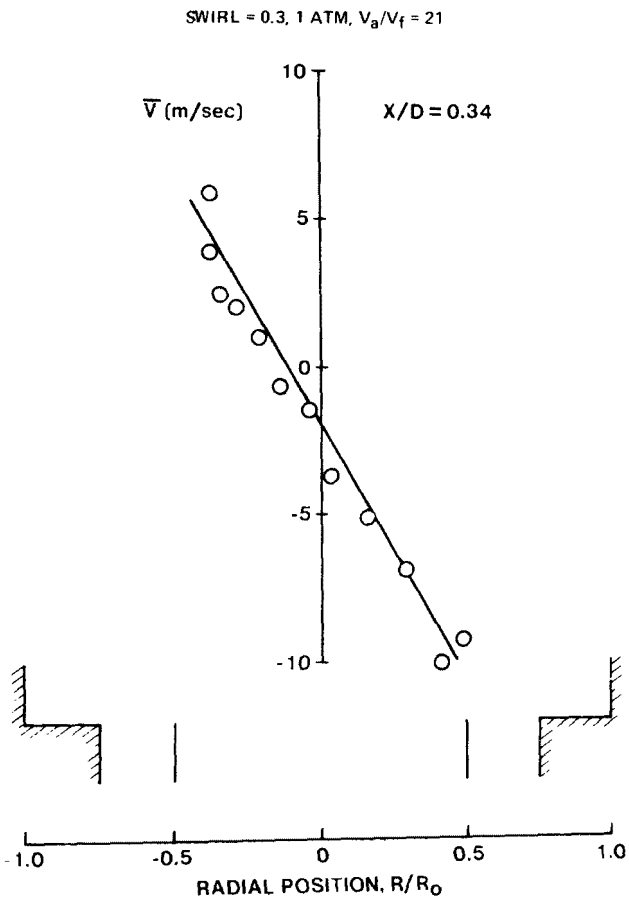

76-07-158-12

AXIAL RMS VELOCITY DISTRIBUTIONS

(A) ZERO SWIRL, 3.8 ATM

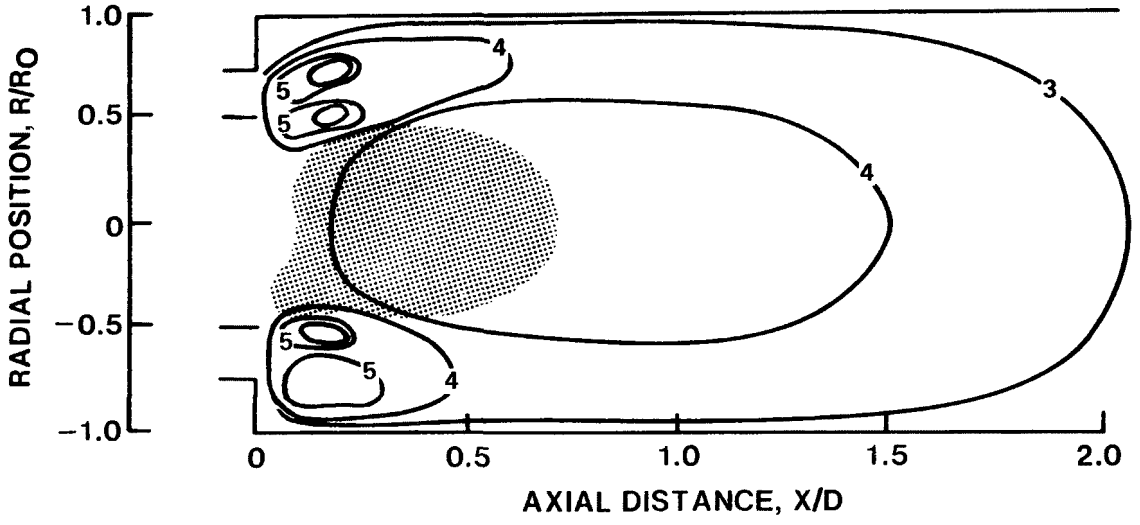

(B) SWIRL = 0.3, 3.8 ATM

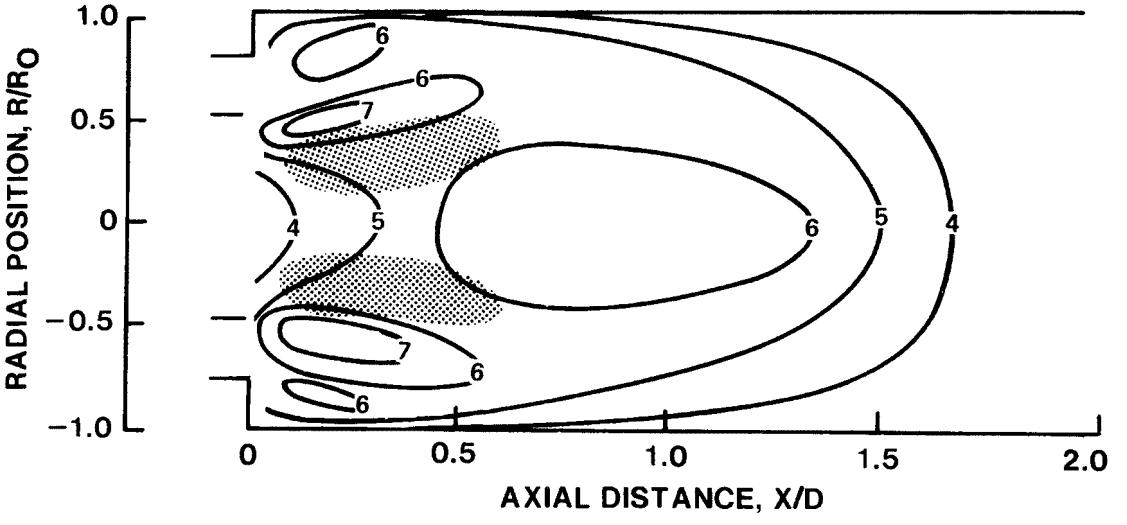

(C) SWIRL = 0.3, 1 ATM

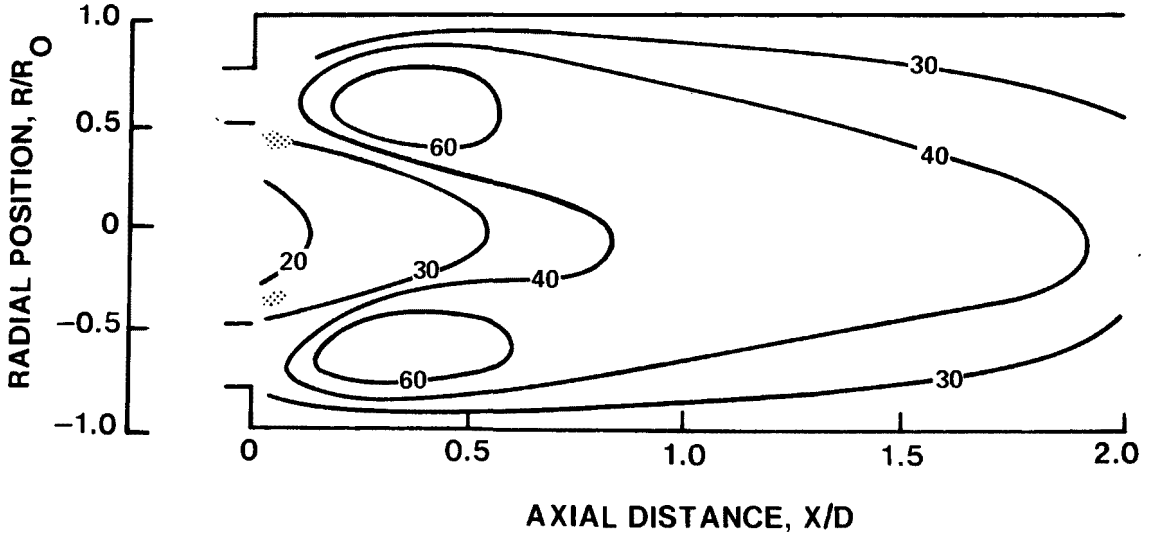

76-07-158-9

AXIAL RMS VELOCITY DISTRIBUTIONS

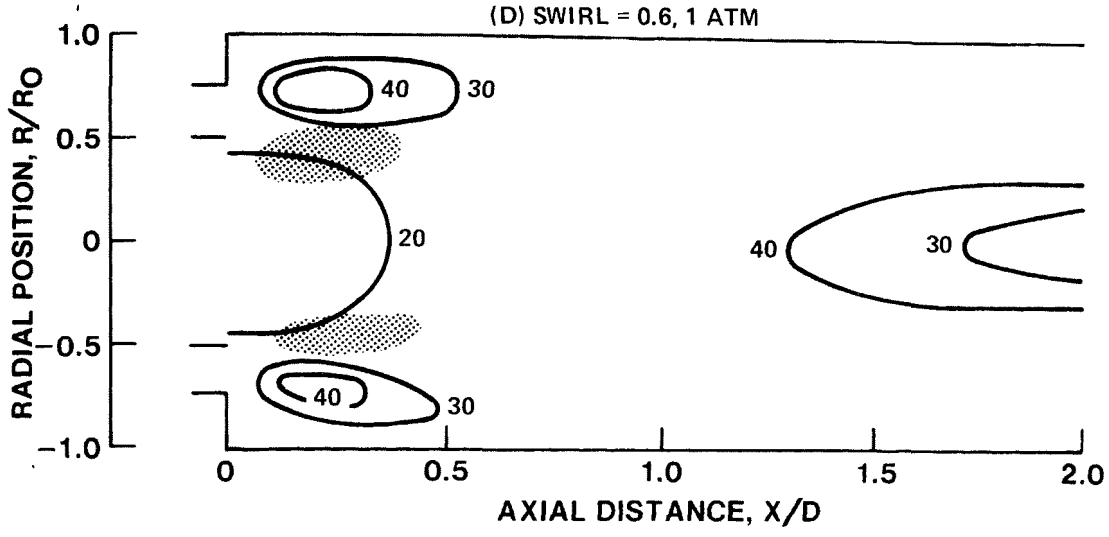

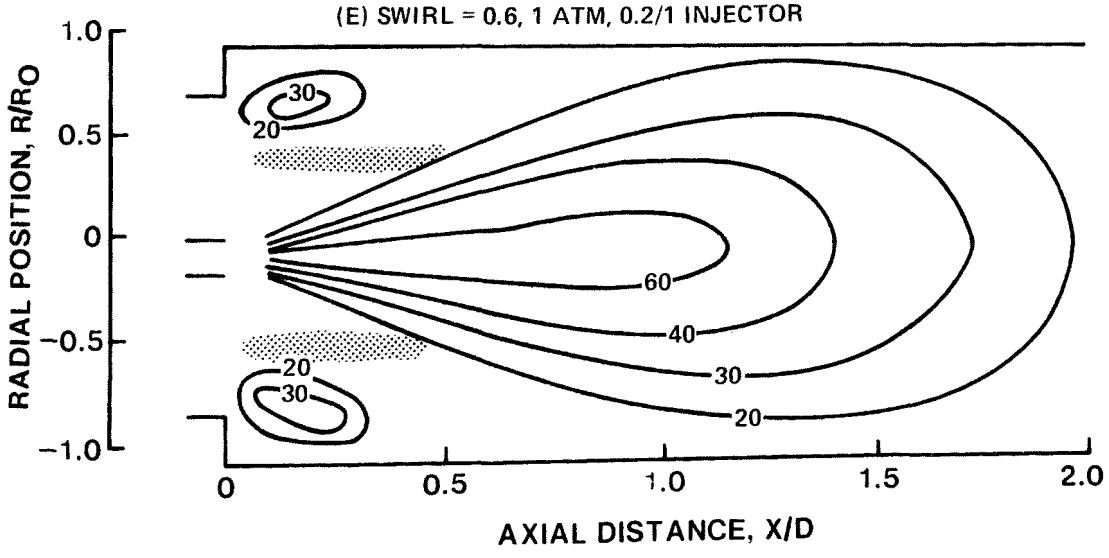

76-07-158-10

AXIAL MEAN AND RMS VELOCITY AND DIRECTIONAL INTERMITTENCY PROFILES

NO SWIRL, 3.8 ATM, $V_a/V_f = 21$

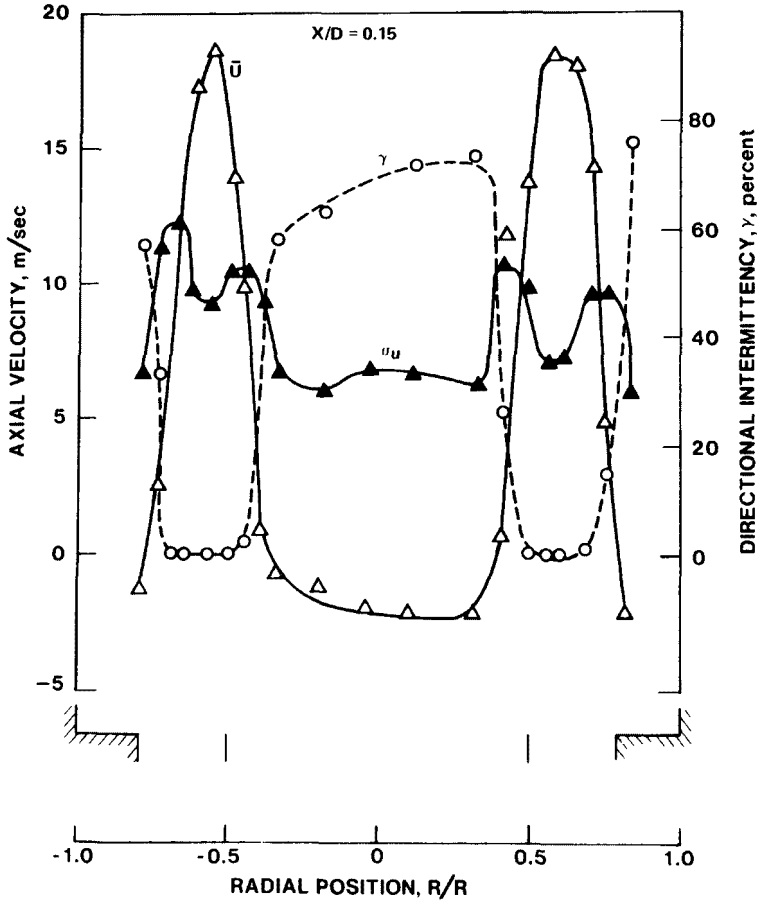

76−06−282−25

obtained at the edge of the fuel injector close to the exit plane. These instantaneous fuel jet direction changes give rise to the diverging rms velocity contours.

Tangential velocity fluctuation measurements at 3.8 atm are shown in Fig. 30. These data obtained at X/D = 1.48 show a sharp peak near the combustor centerline where the mean gradient is high. Contours of constant tangential rms velocity (Fig. 26) show that this peak becomes more pronounced as the flow proceeds downstream. This central rms velocity distribution can be directly related to the increase in directional intermittency and mean tangential velocity gradient induced by the transition from forced to Rankine vortex flow shown in Fig. 25.

The size, shape, recirculated mass flow and local turbulence levels associated with recirculation zones are important to flame stability and combustion intensity. High-speed motion pictures of the reacting flow field in the vicinity of the injection plane show that there are significant fluctuations in the flame structure and large-scale motions associated with flow reversal. These large-scale motions are associated with instantaneous movements of the recirculation zone location due to local imbalances between fluid entrained from and fluid deflected into the recirculation zone which are in turn related to the local velocity gradients, turbulence scales and recirculation zone size (Ref. 23).

Quantitative insight into this large-scale turbulent motion associated with flow recirculation can be obtained from velocity probability density distributions such as those shown in Fig. 31. These measurements, which can be obtained only with a velocimeter system with zero velocity frequency offset, show the unsteadiness of the flow field in the initial mixing region. For example, within the time-averaged recirculation zone (R/R_o = 0.35) there are a significant number of positive velocity occurrences (approximately 30 percent) which are the result of either instantaneous recirculation zone breakdown and/or extensive streamwise and lateral movement. These large-scale motions result in significant deviations from Gaussian turbulence. In the corner region (R/R_o = 0.9) approximately 25 percent of the instantaneous velocity occurrences are negative and again the velocity probability density distribution is skewed.

Defining directional intermittency (γ) at a given point as the fraction of the total observed velocity occurrences which are negative, contours of constant directional intermittency can be constructed. Such plots for the five test conditions are shown in Fig. 32. These data show that there are a significant number of negative velocity occurrences over most of the initial mixing region and that the

TANGENTIAL MEAN AND RMS VELOCITY AND DIRECTIONAL INTERMITTENCY PROFILES

SWIRL = 0.3, 3.8 ATM, V_a/V_f = 21

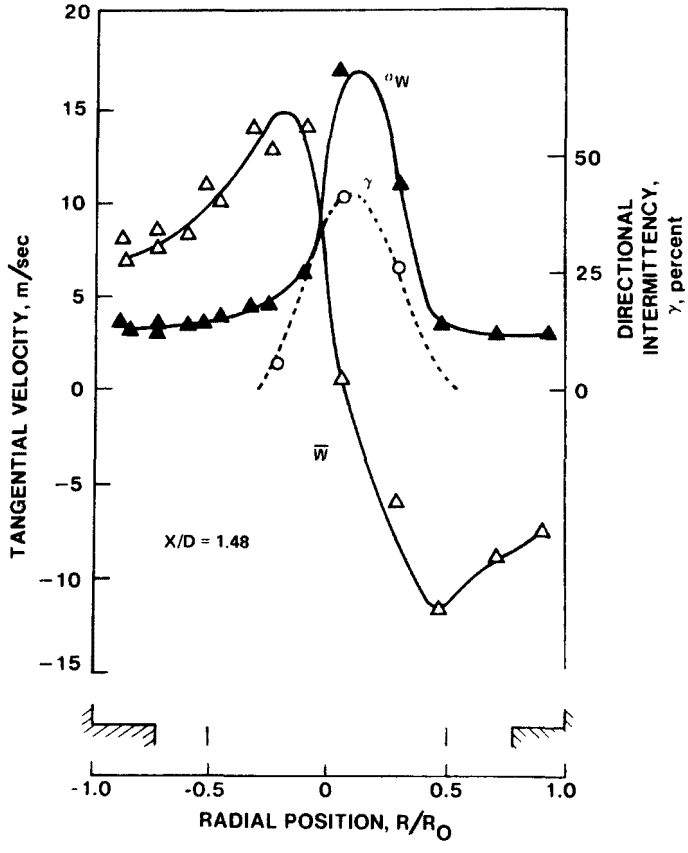

PROBABILITY DISTRIBUTION FUNCTIONS OF AXIAL VELOCITY

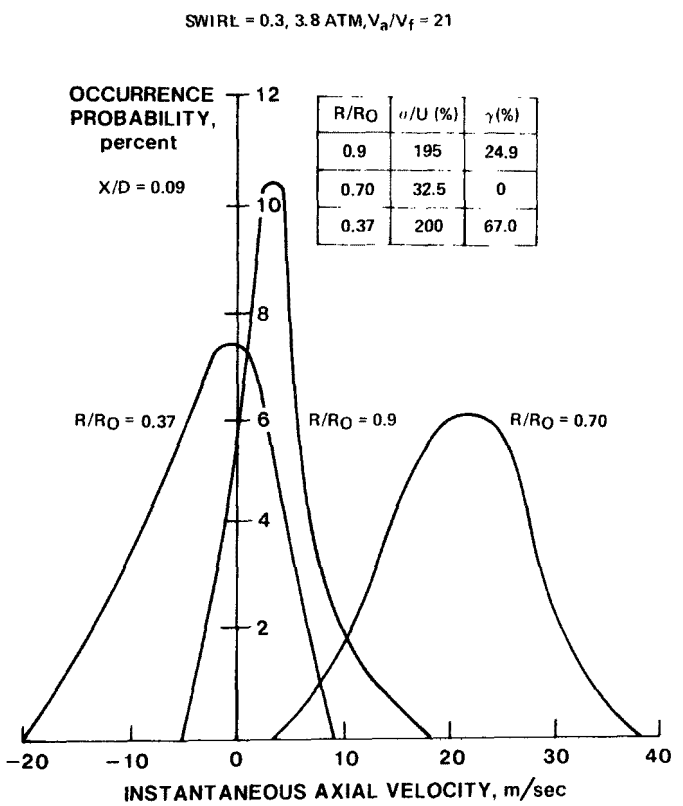

76-06-282-30

AXIAL DIRECTIONAL INTERMITTENCY DISTRIBUTIONS

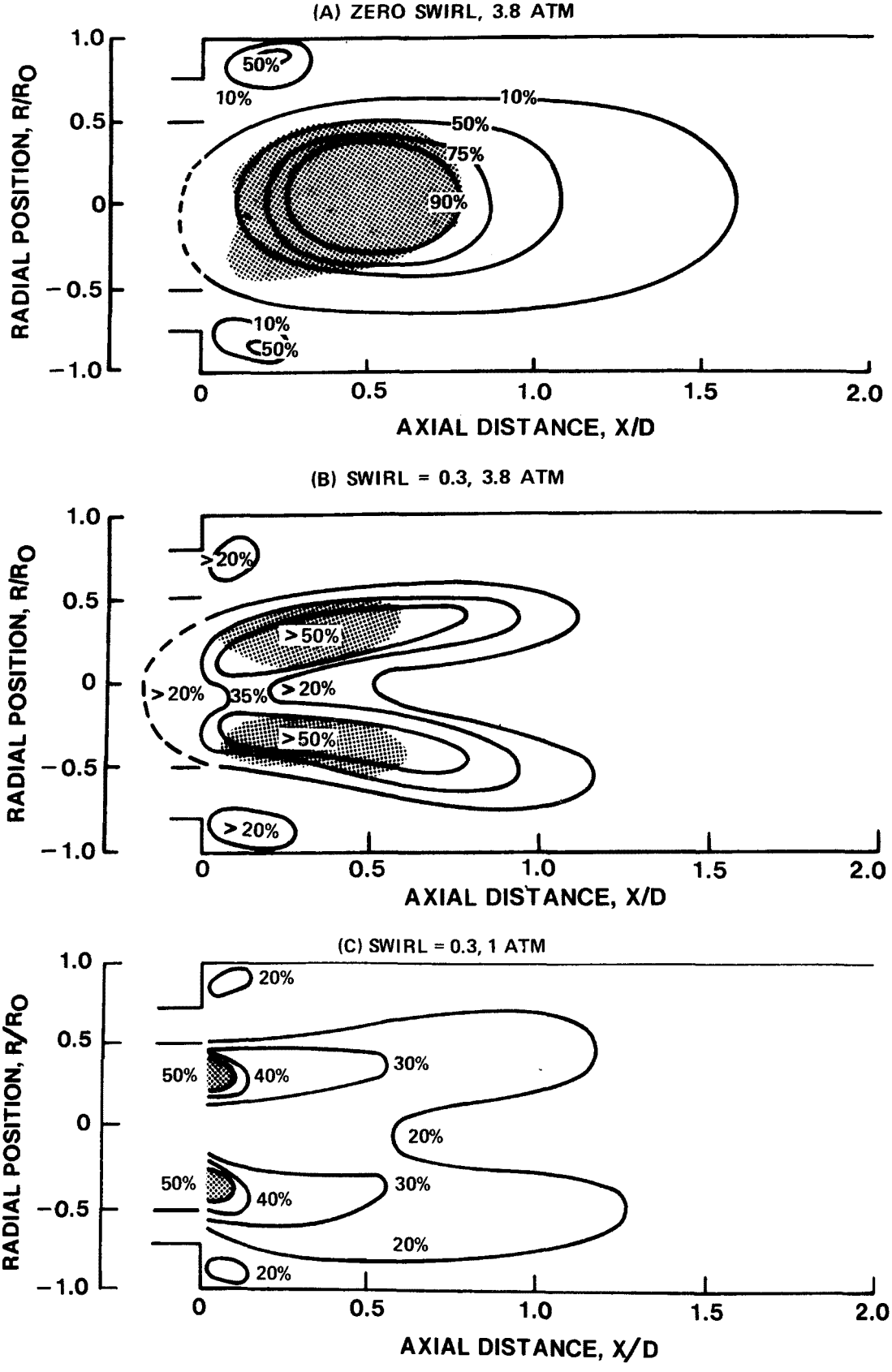

76-07-158-6

AXIAL DIRECTIONAL INTERMITTENCY DISTRIBUTIONS

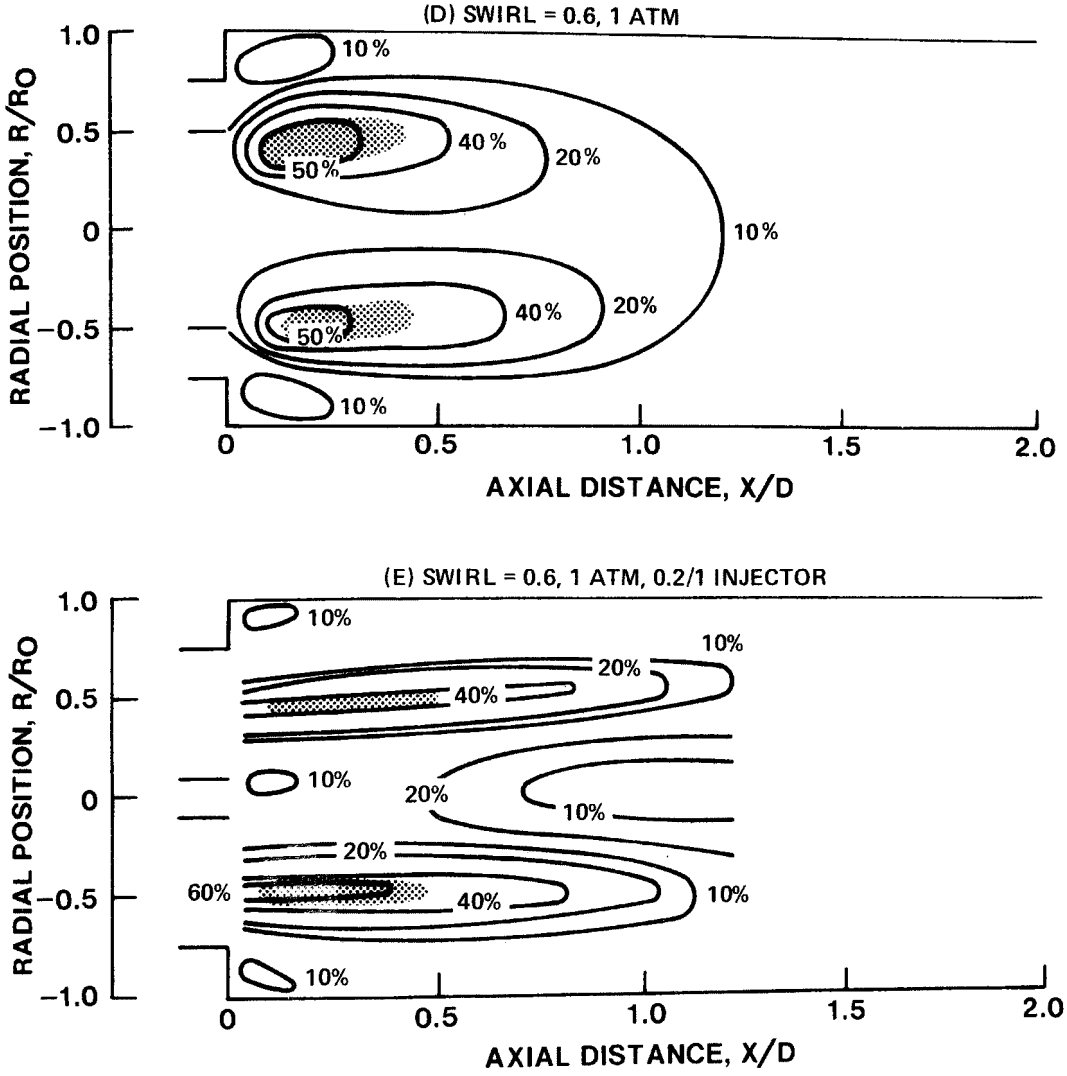

76-07-158-7

probability of reverse flow into the fuel port and in the region behind the backward facing step is high. Since the directional intermittency never exceeded 90 percent, it can also be concluded that there are significant spatial and temporal motions in the region of the time-averaged recirculation zone.

To obtain additional insight into the relative magnitudes of the small-scale and large-scale turbulent motions, consider the possible sources of the total velocity fluctuations (u'_T), namely, the small-scale turbulent fluctuations associated with forward and reverse flow (u' and u'_{REV}, respectively) and the additional large-scale source due to sign changes of mean velocity ($U-U_{REV}$) at the point in question.

Thus,

$$u'_T(x) = f\left[\alpha_x u'_{REV}, (1-\alpha_x)\, u', n_x\left(\bar{U}-\bar{U}_{REV}\right)\right] \tag{7}$$

where α_x is the percentage of time the mean flow is upstream and n_x is the frequency of mean flow reversal. Assuming similarity of character of the small-scale turbulence associated with forward and reverse flow, the instantaneous velocity (U) may be expressed as

$$\bar{U}=\bar{U} + u'+\tilde{u} \tag{8}$$

where $\tilde{u}$ represents the large-scale fluctuations. With the assumption that the small-scale and large-scale fluctuations are uncorrelated, i.e., $\overline{u'\tilde{u}} = 0$,

$$\sigma_T^2 = \overline{U^2} - \bar{U}^2 = \overline{u'^2} + \overline{\tilde{u}^2} \tag{9}$$

That is, the total mean square fluctuation level is the sum of the small and large-scale contributions. An indication of the relative contributions of the large-scale and small-scale fluctuations to the total rms velocity fluctuations may be obtained from Fig. 29. In this figure, which shows the radial profiles of the mean and rms velocities and directional intermittency, it is apparent that although the peak total rms velocity fluctuations occur in the regions of maximum mean velocity gradient, in the central and corner recirculation zones, where the mean velocity gradients are small, significant fluctuations are present. It is apparent that these fluctuations cannot be attributed solely to small-scale gradient transport and that they must be associated with the large-scale fluid motions. Two mechanisms for occurrence of the large fluctuations can be envisioned -- (1) large-scale motions of fluid through the

sample volume, as evidenced by high values of directional intermittency, and (2) large-scale convective transport of smaller-scale turbulence kinetic energy into the sample volume. It appears that these two mechanisms can account for as much as 50 percent of the total axial rms velocity fluctuations in the initial mixing regions.

Turbulent Shear Stress Measurements

At present time, efforts are being made at UTRC to develop numerical methods for predicting turbulent flow behavior. The rate of development of computational fluid dynamics, especially for combusting flow fields, is hampered by the present levels of understanding of the physics of turbulence and the structure of turbulent flows, which are required to model the turbulent correlations which result from time-averaging the Navier-Stokes equations.

Although significant progress has been made, the computation of turbulent flows is still only a practical proposition when the turbulent correlations ($\overline{u'w'}$ for example) which arise from the process of time-averaging the Navier-Stokes equations can be modeled by simple mixing length or turbulent kinetic energy assumptions. It is difficult to assess the potential of existing turbulence models due to the lack of turbulent structure information which could be used to assess the validity of present models or guide the formulation of improved models to account for turbulent nonequilibrium effects present in these combusting flow fields.

The feasibility of measuring the turbulence shear stress has been investigated in the present study. It is anticipated that more detailed higher order correlation measurements will prove useful in future turbulence model development. Measurements were made of the axial-tangential turbulent velocity correlation ($\overline{u'w'}$) at an axial distance of 0.65 cm from the injection plane (X/D = 0.05) for the case of 0.3 swirl at 3.8 atm. Velocity probability density measurements obtained at two different fringe orientations at R/R_o = 0.8 are shown in Fig. 33. The velocity components sensed in these two orientations are $1/\sqrt{2}$ ($u \pm w$). Thus, the difference between the two measured variances yields twice the turbulence shear stress, $\overline{u'w'}$. Figure 34 shows the measured turbulent shear stress correlation coefficient ($\overline{u'w'}/\sigma_u\sigma_w$) obtained at selected radial locations across the combustor. These data indicate that the maximum correlation coefficient is between 0.4 and 0.5, typical of values observed in the wall region of boundary layer flows, although there are substantial variations in the regions surveyed. These large variations suggest that detailed measurements will have to be made

FIG. 33

PROBABILITY DISTRIBUTION FUNCTIONS FOR SHEAR STRESS MEASUREMENTS

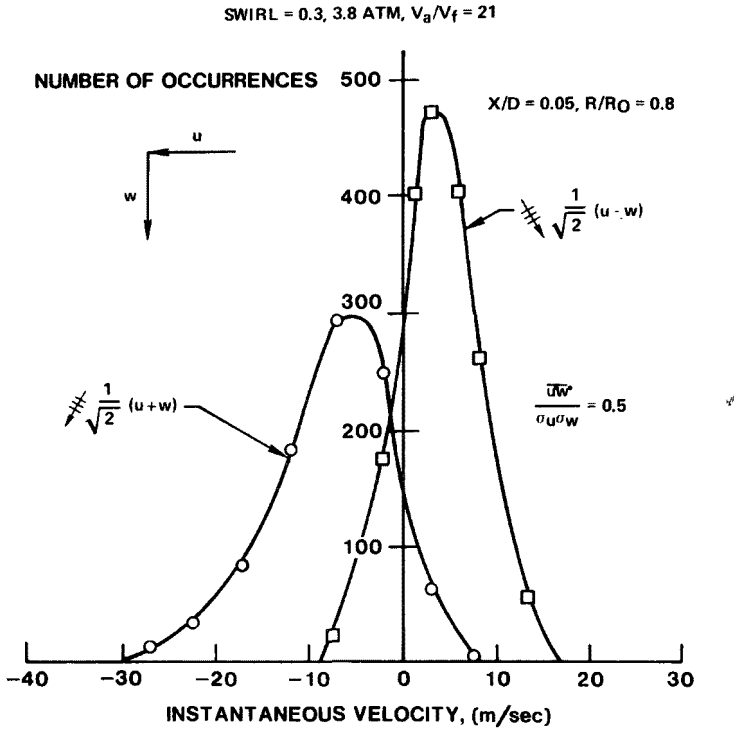

76−06−282−22

FIG. 34

AXIAL-TANGENTIAL VELOCITY CROSS CORRELATIONS

SWIRL - 0.3, 3.8 atm, V_a/V_f=21

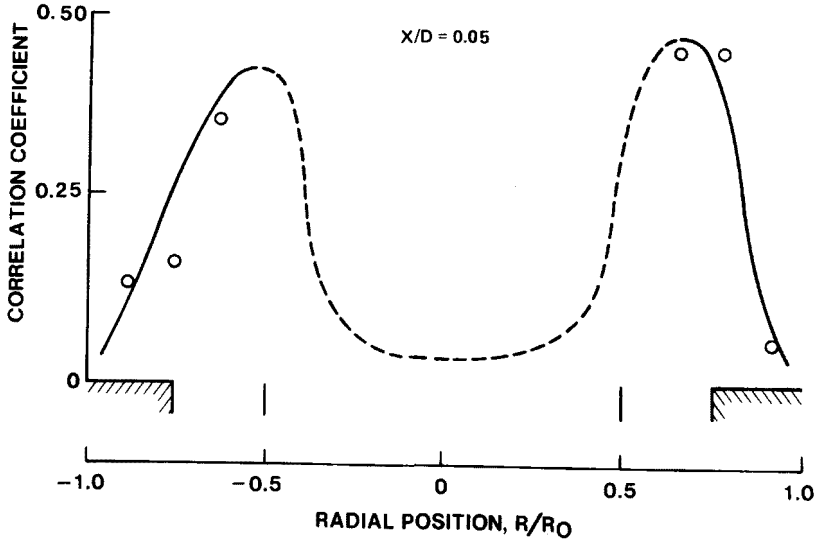

76−06−282−23

throughout the flow field before the adequacy of existing two-equation turbulence models can be assessed.

FUEL INJECTOR PROBING

The results of the present investigation and observations reported previously in Ref. 7 indicate that for several of the combustor configurations tested and, in particular, for flows without swirl there may be significant penetration of the recirculation zone into the fuel injector duct. Therefore, in order to determine the initial conditions for the combustor flow analysis, a radial traverse of the fuel jet was made within the injector to obtain the time-mean fuel velocity distribution upstream from the penetration region of the recirculation zone.

Measurements were made using a 0.95 cm diameter hemispherical-nose pitot probe (Fig. 7) and differential pressure transducers having an accuracy of 0.06 percent of the full scale range $\pm$ 0.03 atm. The results of a traverse made at a location approximately one injector diameter upstream of the injection station are shown in Fig. 35 and indicate a relatively flat velocity profile having a mean value of approximately 5 m/sec, which is in approximate agreement with the calculated value of 4 m/sec.

MEAN AXIAL VELOCITY DISTRIBUTION WITHIN FUEL INJECTOR I

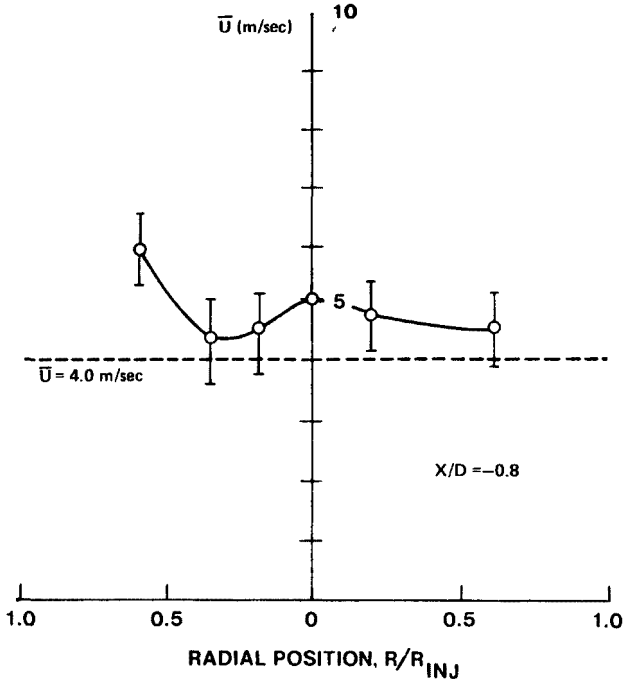

SECTION IV

DISCUSSION OF RESULTS

Variation of inlet air swirl, combustor pressure and air/fuel velocity ratio produces major changes in the time-mean flow field within the turbulent flame burner which significantly influence energy release and pollutant formation. Measurements in the initial mixing region in the burner indicate that for the case of zero swirl at 3.8 atm there is a large centrally-located time-average recirculation zone. With the introduction of swirl (S=0.3), a much smaller toroidal-shaped time-average recirculation zone is present. At 1 atm, increasing the swirl number from 0.3 to 0.6 results in an increase in the volume of the toroidal recirculation zone. Associated with these changes in the recirculation zone, are changes in the temperature and species concentration distributions in the initial regions of the burner. The temperature peaks in the nonswirling flow are broader and the maximum temperature is lower than in the swirling flow, suggesting a more diffuse combustion zone in the nonswirling flow. The radial species concentration gradients support this observation. Energy release rates, as evidenced by axial temperature gradients and by the hydrocarbon burn-out rate, are larger in the swirling flow. The higher temperatures associated with the swirling flow result in higher NO formation rates. Increasing the swirl number from 0.3 to 0.6 at 1 atmosphere results in an increased energy release rate, as evidenced by locally higher temperatures and increased hydrocarbon burn-out rates. The higher temperatures associated with the S=0.6 flow result in an increased NO formation in the initial regions of the flow.

A decrease in pressure from 3.8 to one atmosphere results in a significant decrease in NO emissions and a modest decrease in THC emissions for S=0.3. A major portion of this decrease may be attributed to a decrease in residence time. However, measurements in the initial regions of the flow show that the time-average flow field structure changes as combustor pressure is varied. Decreasing the pressure results in a substantial decrease in the recirculation zone volume and in the

energy release rate, as evidenced by the mean temperature distribution and lower hydrocarbon consumption rate. The combined effect of lower temperature and reduced combustor residence times result in lower NO formation at one atmosphere.

A decrease in air/fuel velocity ratio from 21 to 0.17, for an inlet air swirl number of 0.6 and atmospheric pressure, results in a reduction in NO emissions and an increase in THC emissions. This decrease produces a significant change in recirculation zone geometry and location with respect to the fuel injector, and a reduction in energy release rates and peak temperatures, resulting in lower NO formation rates.

There also are significant changes in the turbulent structure of the flow field with variations in inlet air swirl, combustor pressure and air/fuel velocity. In all of the flows investigated there appear to be substantial large-scale contributions to the total rms turbulent velocity field. In the initial mixing regions of these flows, the total rms velocity fluctuations can significantly exceed the local mean velocity. In the cases of high air/fuel velocities, the large-scale fluctuations are the result of low frequency movement of fluid in the central portion of the flow. Reverse movements produce bulges upstream which extend into the outer shear layer regions and result in rapid breakup and mixing as the fluid is convected downstream. Downstream movements create voids which draw outer shear layer fluid in towards the center of the combustor. This "pumping" action, which is indicated by the directional intermittency, is a function of the stability as well as the size of the recirculation zone.

These large-scale motions have significant effects on the species concentration, velocity fluctuations and chemical reaction rates. For example, the initial mixing region of the nonswirling flow is characterized by rapid apparent mixing of fuel and air and a relatively low energy release rate. However, it must be borne in mind that conventional time-average probe measurements provide no information on the scales at which the fuel, air and combustion products are being mixed. If fuel and air were well-mixed on a small scale, energy release rates, as evidenced by hydrocarbon burn-out rates and temperature should be large. But, in fact, the reverse is the case. This suggests that there are large-scale inhomogeneities in the flow and that the mixing has been accomplished by large eddies which have been generated by the pumping action of the recirculation zone. Such eddies, when convected past the sampling probe, would present the time-averaged appearance of a well-mixed flow although the scales involved actually result in locally inhomogeneous mixtures which tend to result in lower THC burn-out and overall energy release.

This hypothesis is qualitatively supported by both directional intermittency contours and the high-speed motion pictures which show substantial large-scale fluctuations in the zero swirl case.

The introduction of inlet air swirl tends to stabilize the recirculation zone, as evidenced by the directional intermittency data and the high-speed films. One would expect, therefore, a reduction in large-scale inhomogeneities in the initial mixing regions, thereby preserving the separation of the reactants for a greater axial distance. Thus, mixing should occur at a more clearly defined air/fuel interface. This smaller scale (high shear layer) mixing results in localized chemical reaction and produces locally high temperatures and NO formation rates at the air/fuel interface. Increased combustor pressure, at constant swirl number, also tends to increase recirculation zone stability, thereby reducing large-scale mixing. One would therefore anticipate increased segregation of the fuel and air streams and locally high energy release rates in the initial mixing region and, indeed, this is the case.

Changing the air/fuel velocity ratio from 21 to 0.17 for an inlet air swirl number of 0.6 at atmospheric pressure had a profound effect on the combustor flow field. The high-speed motion pictures and the total hydrocarbon contours indicate that the central fuel jet spreads very rapidly. This enhanced spreading rate is primarily due to the radial static pressure gradients induced by swirl and the large-scale interaction, i.e., entrainment of the fuel jet into the toroidal recirculation induced by the inlet air swirl vanes. This later unsteady interaction produces fuel jet motion about its time-averaged location, as evidenced by bi-modal fuel-velocity probability density distributions. Thus, in this case three mechanisms are responsible for rapid time-averaged fuel spreading rates.

Hence, it is felt that many of the changes in flow field structure observed in the present study may be related to the interaction between large-scale turbulent fluctuations, associated with the unsteadiness of the recirculating flow or the fuel jet, and small-scale fluctuations associated with shear-generated turbulence.

The large-scale fluctuations, discussed above, result in significant departures from Gaussian turbulence and isotropy in the initial regions of the burner. The intensity and inferred scale of the fluctuations in these regions suggest that existing turbulence models, which utilize local mean gradients, may not adequately represent turbulent transport in the combusting flows studied. Comparison of the experimental results obtained in the present investigation with predictions of the reacting flow field using the CRISTY computer code will serve to evaluate the

analytical procedures and turbulence models. Further evaluation of existing turbulence models may be obtained by making detailed measurements of the scale of turbulence and of turbulent shear stress and kinetic energy throughout the reacting flow field with a laser velocimeter.

SECTION V

RECOMMENDATIONS

The experimental investigations carried out under EPA Contracts 68-02-1092 and 68-02-1873 have shown that variations in inlet conditions, e.g., inlet air swirl, inlet geometry and fuel injection geometry, produce major changes in the mean flow field, including recirculation zone geometry and local fuel/air distributions, within a confined turbulent flame burner which result in subsequent changes in pollutant formation and destruction. In addition, it was found that turbulence significantly influenced mean flow field structure and pollutant formation. In the vicinity of the time-mean recirculation zones, the scale and intensity of the turbulent fluctuations were sufficiently large so as to suggest that turbulence models, which utilize local mean gradients, may not accurately represent turbulent transport in these regions of the combustor.

The present data base is inadequate to permit definitive correlations of mean flow field structure and pollutant emissions with burner inlet conditions. Such correlations would provide useful "rules-of-thumb" to the combustion designer in the selection of operating conditions to give maximum efficiency while minimizing pollutant emissions. In addition to obtaining the mean flow field structure, it is necessary to obtain information on the turbulent structure of the flow. The combined time-mean and turbulent flow field data will permit an assessment of the effects of turbulence on mean flow field structure to be made and will be useful in evaluation and development of turbulence models employed in analytical procedures for predicting reacting flows.

A logical extension of the present experimental effort would be a further investigation of the effects of burner inlet conditions and geometry on the mean and fluctuating flow field structure in a gaseous fueled axisymmetric turbulent diffusion flame burner and the subsequent effects on pollutant formation and destruction. Two major modifications in the combustor geometry employed in the present and previous studies

should be made. The structure of the highly confined flames investigated under Contracts 68-02-1092 and 68-02-1873 is significantly influenced by the close proximity of the combustor walls to the initial mixing and reaction zone, and the flames tend to be quite long. While the basic fluid dynamic and chemical phenomena occuring in these confined flames are the same as in practical combustion devices, the flame geometry differs considerably from that found in most industrial flames. To permit investigation of more realistic flame geometries, the ratio of combustor diameter to injector diameter should be increased to approximate ratios found in practical combustion equipment. As the second modification, the injection section would be altered to permit changes in fuel and air injector geometry and to provide an expanded range of inlet air swirl. Detailed measurements of the mean flow field, (velocity, temperature and species concentration), the turbulent structure of the flow (turbulent intensity and scale, shear stress and kinetic energy), pollutant emissions and heat transfer to the combustor walls would be measured as burner inlet conditions are varied. Changes in the mean flow field and subsequent variations in pollutant emissions would be correlated with changes in inlet conditions. Special emphasis should be placed on measurement of the inlet conditions (including mean and rms axial, tangential and radial velocities and mean temperature). State-of-the-art instrumentation should be employed, especially if required information on the turbulent structure of the flow is to be obtained. It is highly desirable to use optical diagnostic techniques whenever possible to avoid problems associated with probe techniques (flow disturbance, sample perturbation, ill-defined averaging) in turbulent structure of the flow can be measured using laser velocimetry.

Laser Raman scattering and laser fluorescence techniques for measurement of temperature and species concentration in practical combustion geometries are still in a developmental stage. However, as these techniques are refined, they should be incorporated into the experimental program. Until then, it still will be necessary to use probes to measure temperature, species concentration and the chemical composition of particulates.

Precise definition of the experimental program would be made following a comparison of results of the on-going combustor modeling effort (Ref. 12) with existing experimental data. A preliminary comparison of the experimental and analytical results indicate that more detailed information on the turbulent structure and inlet conditions are required to assist in development of analytical combustor models. Hence, the principal objectives of the proposed gaseous fuel tests would be:

(1) To provide an expanded set of test cases to be used to evaluate and develop both empirical and detailed analytical procedures for predicting pollutant emissions.

(2) To provide experimental data which can be used for assessment and development of turbulence models utilized in the above analytical proceures.

(3) To provide additional data for development of phenomenological correlations between pollutant emissions and burner inlet conditions.

A close coupling of the experimental program with the modeling effort is required if maximum benefit from both programs is to be derived.

APPENDIX A

LASER VELOCIMETER STATISTICAL ERRORS AND BIASING

Statistical confidence levels within stated error limits in the determination of both the mean and variance of any quantity with a Gaussian probability variation may be defined according to Ref. 24 as

$$\text{Error} = P\left(|\bar{x} - \beta| < K_\gamma \frac{S_x}{\sqrt{N}}\right) = \gamma_m \tag{10}$$

$$\text{Error} = P\left(|S_x^2 - \sigma^2|\right) < K_\gamma \sigma^2 \sqrt{\frac{2}{N-1}} = \gamma_T \tag{11}$$

where x is a random variable; N is the number of samples.

$$\bar{x} = \frac{1}{N}\left(\sum_{i=1}^{N} x_i\right) = \text{calculated mean} \tag{12}$$

$$S_x^2 = \frac{1}{N}\left[\sum_{i=1}^{N} (x_i - \bar{x})^2\right] = \text{calculated mean} \tag{13}$$

β is the true mean and σ^2 is the true variance.

For the particular case of the laser velocimeter measurements let us replace the random variable x by the measured Doppler frequency (f_D). Then the confidence level for the mean velocity determinations may be written

$$\frac{\left|\bar{f}_D - \beta_D\right|}{\bar{f}_D} < K_\gamma \frac{S_f}{\bar{f}_D} \frac{1}{\sqrt{N}} = \gamma_m \tag{14}$$

since

$$\frac{S_f}{\bar{f}_D} = \frac{\sqrt{\frac{1}{N}\left[\sum_{i=1}^{N}\left(f_i - \bar{f}_D\right)^2\right]}}{\bar{f}_D} \approx \frac{\sigma_u}{\bar{U}} \tag{15}$$

we see that

$$\frac{\left|\bar{f}_D - \beta_D\right|}{\bar{f}_D} < K_\gamma \left(\frac{\sigma_u}{\bar{U}}\right) \frac{1}{\sqrt{N}} \tag{16}$$

The confidence level for the standard deviation may be written as

$$\frac{\left|S_f^2 - \sigma_f^2\right|}{\sigma_f^2} \approx \frac{2\left|S_f - \sigma_f\right|}{\sigma_f} < K_\gamma \sqrt{\frac{2}{N-1}} = \gamma_T \tag{17}$$

Now since s_f and f_D are functions of the same random variable (f_D), the error in $\sigma_u/\bar{U}$ is the sum, not the square root of the sum of the squares of each error, i.e., the confidence level in $\sigma_u/\bar{U} = \gamma_M + \gamma_T$.

For normal distribution functions, confidence levels may be calculated using the following table.

γ	0.5	0.68	0.9	0.95	0.98	0.99
K_γ	0.675	1.00	1.6	1.96	2.33	2.57

For example: if at a particular location, the local turbulence level was 1 percent and 100 instantaneous velocities were measured, 50 percent of the mean measurements would be in error by less than 0.0675 percent of the true value. Whereas only 1 point in a hundred would be in error by more than 0.257 percent.

The velocity data presented in this report were obtained with seeded air flow. To evaluate biasing errors which might result from seeding only

the air stream, a limited number of axial velocity measurements were made using three seeding techniques -- (1) seeded air stream, (2) seeded fuel stream and (3) seeded fuel and air streams. These measurements were made immediately downstream from the large diameter fuel injector (x 10 = 0.16). It is in this initial mixing region, with high measured velocity fluctuations where the greatest probability of biasing errors exist. In these tests, the porous disk was removed from the fuel injector to permit seeding of the fuel stream. The mean axial velocities measured using the three different seeding techniques are shown in Fig. 36 for the combustor operating at atmospheric pressure with an inlet air swirl number of 0.3. These data show that there are no significant differences between the velocities measured using the different seeding techniques except in the outer regions of the flow where velocities measured with fuel seeding were low. Comparison of the probability distribution functions measured using the three seeding techniques, Fig. 37, shows that near the combustor center line the measured pdf does not depend on seeding technique. However, as expected, in the outer regions of the flow the pdf measured with fuel seeding differs from that obtained when both the fuel and air streams are seeded. These data indicate that for the present experiments, valid velocity data were obtained using air seeding.

COMPARISON OF MEAN AXIAL VELOCITY PROFILES MEASURED USING DIFFERENT SEED TECHNIQUES

SWIRL = 0.3, 1 ATM, V_a/V_f = 21

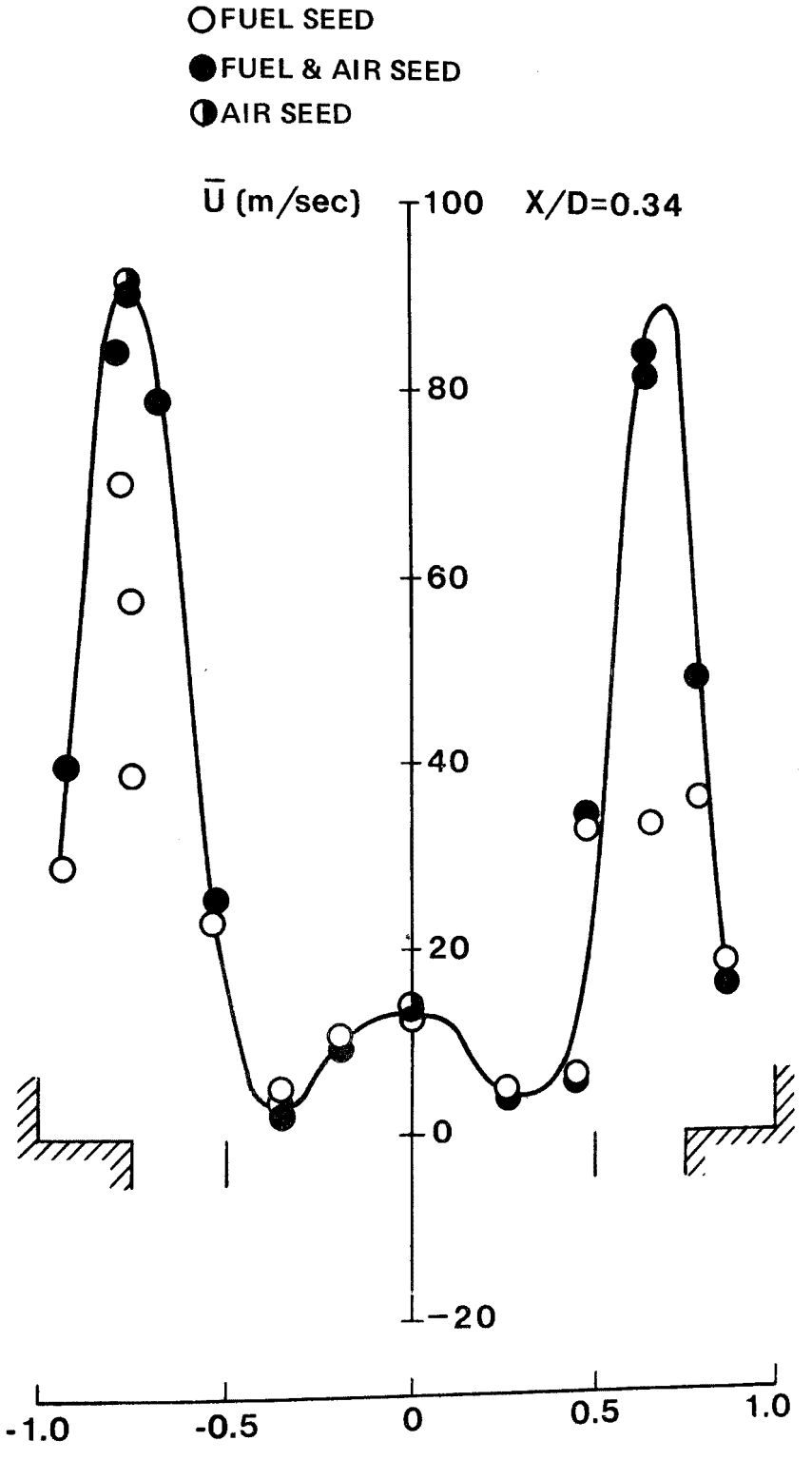

EFFECT OF SEEDING TECHNIQUE ON PROBABILITY DISTRIBUTION FUNCTIONS

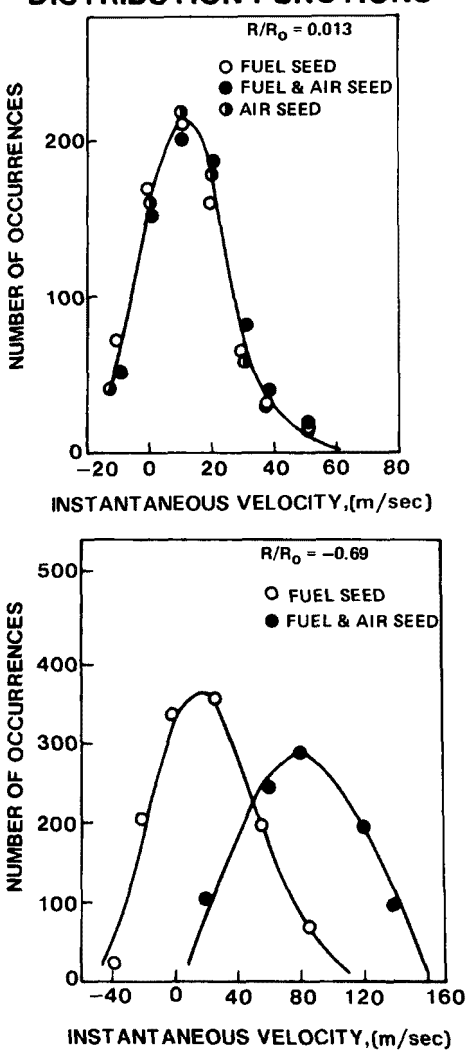

APPENDIX B

FUEL COMPOSITION

Table B-1. NATURAL GAS COMPOSITION

Species	Mole Percent			
	Trailer No. 1	No. 2	No. 3	Average
CH_4	96.14	97.1	96.5	96.58
C_2H_6	2.16	1.80	2.15	2.03
CO_2	0.65	0.56	0.55	0.59
C_3H_6, C_3H_8	0.21	0.15	0.29	0.22
O_2 + Ar	0.06	0.06	0.10	0.07
N_2	0.69	0.26	0.30	0.42
i - C_4H_{10}	0.05	0.03	0.07	0.05
n - C_4H_{10}	0.04	0.03	0.04	0.04

APPENDIX C

COMBUSTOR HEAT BALANCE

A thermal balance was performed on the combustion system for a typical operating condition to evaluate the magnitude of the heat transferred to the combustor walls and to provide a check on the accuracy of the exhaust gas temperature measurements. The heat transferred from the system was determined from measurements of the flowrate and the temperature rise of the cooling water. The results of the heat balance are summarized below:

Test No. 7	Natural Gas - Air
Swirl No. = 0.6	Air/Fuel Velocity Ratio = 0.18
P = 1 atm	Equivalence Ratio = 0.90
T_{air} = 750 ^{o}K	$\dot{m}_{air}$ = 0.137 kg/sec

$\underline{Q_{IN}}$

Air Heater:	15.9 kg cal/sec
Fuel:	88.69 kg cal/sec
	104.59 kg cal/sec

$\underline{Q_{OUT}}$

Combustion Products:	79.73 kg cal/sec
Cooling Water:	14.77 kg cal/sec
Unreacted Fuel:	2.23 kg cal/sec
	96.73 kg cal/sec

$$\frac{Q_{IN} - Q_{OUT}}{Q_{IN}} = .075$$

APPENDIX D

TEMPERATURE DISTRIBUTIONS: TABULATED DATA

Table D-1. TEMPERATURE DISTRIBUTIONS FOR TEST NO. 1

CH_4-Air
$\Phi = 0.91 \pm .01$
Pressure = 3.9 ± 0.1 atm

Inlet Air Swirl No. = 0
Inlet Air Temperature = 751 ± 8 °K
Air-Fuel Velocity Ratio = 20.7 ± 0.2

R/R_o	Temperature, °K				
	X/D=0.34	0.60	1.73	1.99	14.36
-0.75	922	1673	1889	2079	1888
-0.62	1011	1753	1815	1896	1900
-0.50	1305	1685	1744	1868	1935
-0.37	1371	1659	1722	1771	1985
-0.25	1282	1617	1653	1736	1935
-0.12	1237	1518	1631	1767	1980
0.00	1138	1399	1672	1861	1978
0.13	1060	1328	1811	1855	2095
0.25	993	1198	1923	1952	2106
0.38	1094	1255	2028	2101	2065
0.50	1205	1392	2006	1971	1995
0.63	1096	1733	1879	1781	1955
0.75	779	1446	1670	1528	1656
0.88	673	1002	1449	1244	1565
1.00	597	677	821	760	1056

Table D-2. TEMPERATURE DISTRIBUTIONS FOR TEST NO. 3

CH_4-Air
Φ = 0.91 ± .01
Pressure = 1.0 atm

Inlet Air Swirl No. = 0.3
Inlet Air Temperature = 743 ± 9 °K
Air-Fuel Velocity Ratio = 21.7 ± 0.5

R/R_o	Temperature, °K						
	X/D=0.34	0.60	1.99	3.38	4.77	13.50	14.95
-0.63	1416	1477	2034	2061	2102	---	1734
-0.55	---	---	---	2017	2069	1953	---
-0.50	1545	1502	1994	---	---	---	1815
-0.45	1541	---	---	1927	1958	2015	---
-0.37	1481	1565	1897	1850	1890	---	1837
-0.25	1425	1634	1845	1777	1828	2013	1852
-0.12	1416	1647	1830	1762	1808	1975	1840
0.00	1453	1626	1850	1798	1850	1960	1854
0.07	1479	---	---	1824	1870	---	---
0.12	1488	1618	1911	1850	1860	1975	1884
0.28	1473	1560	1950	1934	1939	2030	1880
0.38	1449	1490	1955	1993	2026	2061	1846
0.49	1359	1431	1901	1979	2018	2032	1768
0.58	---	---	---	1912	1925	1985	1679
0.63	1244	1300	1777	---	---	1925	---
0.69	---	---	---	1772	1741	---	---
0.75	1144	1160	1592	1625	1625	1760	1600
0.88	1029	1029	1446	1420	---	1620	1430
1.00	752	772	1075	---	1126	1500	1220

Table D-3. TEMPERATURE DISTRIBUTIONS FOR TEST NO. 4

CH_4-Air
Φ = 0.91 ± 0.01
Pressure = 3.7 ± 0.1 atm

Inlet Air Swirl No. = 0.3
Inlet air Temperature = 749 ± 7 °K
Air-Fuel Velocity Ratio = 20.5 ± 0.4

R/R_o	Temperature, °K				
	X/D=0.34	0.60	1.73	1.99	14.36
-0.63	1657	1703	2081	2133	1826
-0.50	1480	1559	2059	2096	1863
-0.37	1220	1454	1975	1950	1870
-0.25	1124	1373	1836	1821	1832
-0.12	1010	1276	1776	1747	1730
0.00	1015	1361	1774	1841	1764
0.13	1085	1468	1989	1978	1836
0.25	1235	1540	2105	2128	1888
0.38	1317	1582	2133	2189	1875
0.50	1230	1608	2116	2171	1827
0.63	1040	1538	1992	1993	1757
0.75	825	1168	1769	1783	1685
0.88	695	877	1510	1479	1626
1.00	626	618	975	935	1489

Table D-4. TEMPERATURE DISTRIBUTION FOR TEST NO. 6

CH_4-Air
ϕ = 0.91 ± .01
Pressure = 1.0 atm

Inlet Air Swirl No. = 0.6
Inlet Air Temperature = 750 ± 10 °K
Air-Fuel Velocity Ratio = 21.3 ± 0.5

R/R_o	Temperature, °K				
	X/D=0.34	0.60	1.73	1.99	14.36
-0.63	1624	1516	2233	2237	1920
-0.55	---	1591	---	---	1943
-0.50	1474	---	2181	2150	---
-0.45	---	1686	---	---	1984
-0.37	1244	1700	2046	2004	1980
-0.25	1089	1635	1935	1923	1915
-0.12	1024	1597	1933	1925	1835
0.00	1105	1615	2010	2013	1840
0.06	---	1622	---	---	1880
0.13	1341	1630	2146	2136	1925
0.25	1467	1600	2235	2203	1995
0.38	1537	1503	2240	2221	1997
0.50	1486	1352	2156	2168	1930
0.58	---	1227	---	---	1856
0.63	1341	---	1928	1974	---
0.70	---	1079	---	---	1762
0.75	1084	---	1578	1671	---
0.80	---	942	---	---	1691
0.88	862	810	1234	1336	1650
1.00	604	---	778	---	1490

Table D-5. TEMPERATURE DISTRIBUTION FOR TEST NO. 7

CH_4-Air
Φ = 0.91 ± 0.01
Pressure = 1.0 atm

Inlet Air Swirl No. = 0.6
Inlet Air Temperature = 746 ± 7 °K
Air-Fuel Velocity Ratio = 0.17 ± 0.01

R/R_o	Temperature, °K				
	X/D=0.76	1.01	2.15	2.41	14.77
-0.64	1610	1570	1874	1817	2050
-0.50	1326	1286	1750	1741	2085
-0.37	1193	1177	1616	1669	---
-0.25	1115	1149	1525	1604	1850
-0.12	1094	1149	1488	1588	1306
0.00	1147	1147	1516	1616	1230
0.13	1409	1187	1591	1718	1270
0.25	1667	1400	1689	1830	---
0.38	1666	1565	1797	2005	2135
0.50	1632	1566	1843	2055	2245
0.63	1429	1399	1637	1792	2020
0.75	1163	1135	1324	1451	1800
0.88	962	925	1086	1177	1615
1.00	652	620	662	700	1448

APPENDIX E

SPECIES CONCENTRATION DISTRIBUTIONS: TABULATED DATA

Table E-1. SPECIES CONCENTRATION DISTRIBUTIONS FOR TEST NO. 1

CH_4-Air
Φ = 0.91±0.01
Pressure = 3.9 ± 0.1 atm

Inlet Air Swirl No. = 0
Inlet Air Temperature = 751±8°K
Air-Fuel Velocity Ratio = 751±8°K

R/R_o	NO, ppm			
	X/D = 0.08	1.21	1.47	2.84
-0.85	1	41	90	198
-0.66	0	72	83	185
-0.44	7	55	53	115
-0.25	9	31	27	84
-0.04	20	33	19	110
0.16	11	83	54	166
0.38	8	133	108	235
0.58	1	135	120	240
0.80	0	59	69	158

R/R_o	NO_x, ppm			
	X/D = 0.08	1.21	1.47	2.84
-0.85	-	50	122	245
-0.66	2	104	142	-
-0.44	-	-	-	-
-0.25	-	-	-	-
-0.04	-	-	-	-
0.16	-	-	-	-
0.38	-	-	-	-
0.58	-	168	200	285
0.80	2	88	90	182

R/R_o	CO, Mole %			
	X/D = 0.08	1.21	1.47	2.84
-0.85	0.00	0.80	0.80	1.82
-0.66	0.00	2.90	2.86	6.15
-0.45	4.20	6.22	6.35	9.80
-0.25	3.50	8.40	8.20	11.3
-0.04	5.35	9.65	9.50	11.4
0.16	3.10	9.75	9.65	10.00
0.38	2.00	7.25	7.25	6.80
0.58	0.50	2.90	2.35	2.65
0.80	0.00	0.51	0.35	0.48

Table E-1. SPECIES CONCENTRATION DISTRIBUTIONS
(continued)

R/R_o	CO_2, Mole %			
	X/D = 0.08	1.21	1.47	2.84
-0.85	0.05	3.95	5.80	7.15
-0.66	0.05	5.30	6.70	6.75
-0.44	2.00	4.10	4.95	5.05
-0.25	1.80	3.48	3.50	4.40
-0.04	2.50	3.50	3.45	4.70
0.16	1.70	4.32	4.38	5.60
0.38	1.35	5.60	6.10	6.65
0.58	0.40	5.95	6.55	6.65
0.80	0.05	3.51	3.30	4.92

R/R_o	O_2, Mole %			
	X/D = 0.08	1.21	1.47	2.84
-0.85	18.0	12.9	10.1	6.40
-0.66	17.9	7.30	5.55	1.95
-0.44	1.82	4.40	3.79	1.05
-0.25	0.18	3.53	3.76	0.75
-0.04	0.19	2.50	2.76	0.35
0.16	0.11	1.43	1.67	0.53
0.38	0.13	2.30	1.72	1.95
0.58	14.4	6.60	6.55	6.50
0.80	20.2	14.3	14.7	12.3

R/R_o	THC, Mole %			
	X/D = 0.08	1.21	1.47	2.84
-0.85	0.041	2.05	0.50	0.79
-0.66	0.022	5.05	2.31	2.56
-0.44	>10.0	7.55	7.45	4.52
-0.25	>10.0	9.45	9.69	5.08
-0.04	>10.0	8.45	9.30	3.94
0.16	>10.0	5.85	6.18	2.94
0.38	>10.0	4.25	4.04	1.50
0.58	>10.0	2.75	0.97	0.51
0.80	0.011	1.85	0.19	0.10

Table E-2. SPECIES CONCENTRATION DISTRIBUTION FOR TEST NO. 3

CH_4-Air
$\Phi = 0.9 \pm 0.01$
Pressure = 1.0 atm

Inlet Air Swirl No. = 0.3
Inlet Air Temperature = 744±9°K
Air Fuel Velocity Ratio = 21.7±0.5

R/R_o	NO, ppm			
	X/D = 0.08	1.47	2.86	4.25
-0.85	1	15	27	45
-0.66	5	39	66	97
-0.46	5	70	102	121
-0.25	3	88	100	109
-0.04	3	87	87	100
0.17	7	85	93	101
0.37	14	73	103	125
0.57	10	42	79	107
0.80	1	17	27	47

R/R_o	NO_x ppm			
	X/D = 0.08	1.47	2.86	4.25
-0.85	18	43	57	82
-0.66	29	87	-	-
-0.46	-	-	-	-
-0.25	-	-	-	-
-0.04	-	-	-	-
0.17	-	-	-	-
0.37	-	-	-	-
0.57	35	78	133	172
0.80	13	47	69	84

R/R_o	CO, Mole %			
	X/D = 0.08	1.47	2.86	4.25
-0.85	0.607	0.94	0.60	0.70
-0.66	1.400	1.75	2.53	2.75
-0.46	2.150	3.40	5.65	7.00
-0.25	1.850	5.30	8.00	9.25
-0.04	1.600	6.40	8.79	9.80
0.17	2.340	5.70	8.66	9.60
0.37	3.025	4.20	7.08	7.80
0.57	1.810	1.82	2.85	2.51
0.80	0.680	0.92	0.72	0.68

Table E-2. SPECIES CONCENTRATION DISTRIBUTIONS
(continued)

R/R_o	CO_2, Mole %			
	X/D = 0.08	1.47	2.86	4.25
-0.85	1.85	4.62	5.56	6.18
-0.66	1.80	6.3	7.42	7.54
-0.46	2.05	7.15	7.10	6.71
-0.25	1.75	6.80	6.00	5.58
-0.04	1.55	6.17	5.45	5.10
0.17	1.87	6.58	5.63	5.27
0.37	2.85	7.04	6.69	6.27
0.57	2.90	6.44	7.42	7.90
0.80	1.30	4.79	5.79	6.33

R/R_o	O_2, Mole %			
	X/D = 0.08	1.47	2.86	4.25
-0.85	15.5	11.3	10.1	8.95
-0.66	14.0	7.10	5.37	3.75
-0.46	5.40	3.35	1.51	1.05
-0.25	3.05	1.45	0.57	0.50
-0.04	1.80	1.00	0.38	0.43
0.17	2.03	1.25	0.42	0.47
0.37	2.65	2.65	1.03	0.77
0.57	11.6	6.60	4.06	3.37
0.80	16.5	10.8	8.50	8.66

R/R_o	THC, Mole %			
	X/D = 0.08	1.47	2.86	4.25
-0.85	1.66	1.73	0.57	0.27
-0.66	6.00	2.50	0.95	0.55
-0.46	>10.0	4.60	2.45	1.80
-0.25	>10.0	7.40	4.60	3.10
-0.04	>10.0	9.50	6.35	4.28
0.17	>10.0	7.80	5.75	4.00
0.37	>10.0	6.00	3.55	2.35
0.57	8.31	2.80	1.31	0.54
0.80	2.23	1.64	0.55	0.18

Table E-3. SPECIES CONCENTRATION DISTRIBUTIONS FOR TEST NO. 4

CH_4-Air
Φ = 0.91 ± 0.01
Pressure = 3.7±0.01 atm

Inlet Air Swirl No. = 0.3
Inlet Air Temperature = 749 ± 7°K
Air-Fuel Velocity Ratio = 20.5±0.4

	NO, ppm			
R/R_o	X/D = 0.08	1.21	1.47	2.60
-0.85	0	28	53	125
-0.66	2	86	110	280
-0.45	8	123	119	327
-0.26	7	116	130	205
-0.04	10	71	69	65
0.16	6	88	93	93
0.38	4	140	152	305
0.58	0	138	131	292
0.80	0	53	55	165

	NO_x, ppm			
R/R_o	X/D = 0.08	1.21	1.47	2.60
-0.85	4	66	89	138
-0.66	5	90	133	-
-0.45	-	-	-	-
-0.26	-	-	-	-
-0.04	-	-	-	-
0.16	-	-	-	-
0.38	-	-	-	-
0.58	4	-	-	305
0.80	2	58	-	196

	CO, mole %			
R/R_o	X/D = 0.08	1.21	1.47	2.60
-0.85	0.00	0.9	1.17	1.8
-0.66	0.28	3.3	4.02	5.1
-0.45	3.58	8.6	8.55	8.0
-0.25	1.70	11.4	10.8	10.3
-0.04	1.86	12.0	11.8	13.2
0.16	1.10	11.9	11.5	13.0
0.38	1.23	10.3	10.2	10.6
0.58	0.19	6.2	6.41	6.8
0.80	0.00	1.5	1.78	2.2

Table E-3. SPECIES CONCENTRATION DISTRIBUTIONS
(continued)

R/R_o	CO_2, mole %			
	X/D = 0.08	1.21	1.47	2.60
-0.85	0.00	3.1	4.11	5.6
-0.66	0.01	5.1	5.48	7.2
-0.45	1.82	5.3	5.16	7.1
-0.25	1.35	4.8	4.90	5.6
-0.04	1.35	4.2	4.09	4.1
0.17	1.07	4.5	4.46	4.4
0.38	1.08	5.5	5.39	6.4
0.58	0.10	5.9	5.90	7.0
0.80	0.04	3.9	4.26	6.1

R/R_o	O_2, mole %			
	X/D = 0.08	1.21	1.47	2.60
-0.85	20.8	14.5	11.7	8.6
-0.66	19.4	7.0	6.0	2.5
-0.45	1.3	2.3	1.0	0.6
-0.26	0.4	0.6	0.3	0.1
-0.04	0.1	0.2	0.1	0.1
0.17	0	0.2	0.1	0.1
0.38	0.4	0.2	0.2	0.3
0.58	8.3	3.2	2.8	1.5
0.80	20.4	11.2	10.3	7.6

R/R_o	THC, mole %			
	X/D = 0.08	1.21	1.47	2.60
-0.86	0.04	2.74	2.05	0.86
-0.66	3.09	4.58	3.92	0.62
-0.45	> 10.0	4.55	3.99	0.68
-0.26	> 10.0	4.55	3.46	1.69
-0.03	> 10.0	7.51	6.76	4.32
0.16	> 10.0	6.00	4.95	3.24
0.38	> 10.0	3.43	2.78	0.71
0.58	6.73	3.84	3.61	0.44
0.80	0.05	4.44	3.67	0.30

Table E-4. SPECIES CONCENTRATION DISTRIBUTIONS FOR TEST NO. 6

CH_4-Air
Φ = 0.91 ± 0.01
Pressure = 1.0 atm

Inlet Air Swirl No. = 0.6
Inlet Air Temperature = 750±10°K
Air-Velocity Ratio = 21.3±0.5

R/R_o	NO, ppm			
	X/D = 0.08	1.21	1.47	2.86
-0.85	2	3	6	30
-0.66	3	17	29	84
-0.45	-	62	72	125
-0.35	22	-	90	-
-0.25	-	89	92	123
-0.04	21	86	80	96
0.17	-	88	89	102
0.27	19	-	92	-
0.38	-	80	89	117
0.48	15	-	71	-
0.58	6	34	47	10
0.67	2	-	20	-
0.75	2	-	-	-
0.81	1	7	5	50

R/R_o	NO_x, ppm			
	X/D = 0.08	1.21	1.47	2.86
-0.85	9	17	28	72
-0.66	15	42	-	123
-0.45	-	-	-	-
-0.35	-	-	-	-
-0.25	-	-	-	-
-0.04	-	-	-	-
0.17	-	-	-	-
0.27	-	-	-	-
0.38	-	-	-	-
0.48	-	-	-	-
0.58	-	70	87	-
0.67	-	-	54	-
0.75	7	28	-	-
0.81	-	-	29	-

Table E-4. SPECIES CONCENTRATION DISTRIBUTIONS
(continued)

R/R_o	CO, Mole %			
	X/D = 0.08	1.21	1.47	2.86
-0.85	0.04	1.29	1.44	2.25
-0.66	0.69	2.91	2.87	3.59
-0.45	-	5.52	6.05	6.24
-0.35	3.33	-	7.47	-
-0.25	-	8.34	9.00	9.26
-0.04	3.16	9.82	10.7	10.87
0.17	-	9.23	10.0	9.17
0.27	2.86	-	8.94	-
0.38	-	6.58	7.57	8.34
0.48	2.92	-	5.92	-
0.58	1.46	4.08	4.54	4.06
0.67	0.48	-	3.20	-
0.81	-	1.58	1.60	2.26

R/R_o	CO_2, Mole %			
	X/D = 0.08	1.21	1.47	2.86
-0.85	0.06	2.31	2.66	5.34
-0.66	1.27	5.26	5.82	7.42
-0.45	-	7.22	7.12	7.44
-0.35	2.35	-	6.75	-
-0.25	-	6.65	6.26	6.24
-0.04	2.16	5.68	5.50	5.58
0.17	-	6.10	5.90	5.73
0.27	2.10	-	6.24	-
0.38	-	7.08	6.88	6.63
0.48	2.42	-	7.05	-
0.58	1.36	6.24	6.66	7.98
0.67	0.44	-	5.01	-
0.81	0.05	2.80	3.00	6.49

Table E-4. SPECIES CONCENTRATION DISTRIBUTIONS
(continued)

R/R_o	O_2, Mole %			
	X/D = 0.08	1.21	1.47	2.86
-0.85	19.8	13.2	13.2	8.50
-0.66	16.4	7.80	6.80	3.58
-0.45	-	2.10	1.65	0.89
-0.35	0.2	-	0.75	0.20
-0.25	-	0.37	0.30	-
-0.04	0.2	0.08	0.09	0.07
0.17	-	6.10	0.10	0.0
0.27	0.4	-	0.32	-
0.38	-	7.08	0.70	0.39
0.48	2.5	-	1.85	-
0.58	9.7	5.01	4.10	2.20
0.67	16.2	-	7.60	-
0.81	20.6	14.00	12.6	6.75

R/R_o	THC, Mole %			
	X/D = 0.08	1.21	1.47	2.86
-0.85	-	5.71	4.75	1.83
-0.66	7.47	3.83	2.40	0.66
-0.45	>10.0	2.55	1.99	-
-0.35	>10.0	-	-	0.67
-0.25	>10.0	3.64	2.62	1.09
-0.04	>10.0	3.14	2.86	1.46
0.17	>10.0	2.95	2.71	1.42
0.38	>10.0	2.16	1.84	1.18
0.48	>10.0	-	-	-
0.58	>10.0	2.52	1.94	0.46
0.69	>10.0	-	2.87	-
0.81	1.04	4.80	4.12	1.00

Table E-5. SPECIES CONCENTRATION DISTRIBUTIONS FOR TEST NO. 7

CH_4-Air
$\Phi = 0.91 \pm 0.01$
Pressure = 1.0 atm

Inlet Air Swirl No. = 0.6
Inlet Air Temperature = $746 \pm 7°K$
Air-Fuel Velocity Ratio = 0.17 ± 0.01

R/R_o	NO, ppm			
	X/D=0.24	0.50	1.63	1.89
-0.85	2	3	4	4
-0.66	34	21	32	33
-0.45	68	48	48	48
-0.25	55	16	42	45
-0.04	0	0	39	46
0.17	0	4	41	46
0.38	55	37	46	48
0.58	67	23	39	36
0.80	16	5	6	5

R/R_o	NO_x, ppm			
	X/D=0.24	0.50	1.63	1.89
-0.85	12	16	27	26
-0.66	89	58	-	-
-0.45	-	-	-	-
-0.25	-	-	-	-
-0.04	-	-	-	-
0.17	-	-	-	-
0.38	-	-	-	-
0.58	-	-	-	-
0.80	40	21	38	31

R/R_o	CO, mole%			
	X/D=0.24	0.50	1.63	1.89
-0.85	0.45	0.24	0.56	0.53
-0.66	2.60	0.70	5.69	6.10
-0.45	7.08	6.05	6.95	7.40
-0.25	6.72	4.58	6.37	7.20
-0.04	0.46	1.92	6.30	7.22
0.17	1.45	2.61	6.46	7.22
0.38	6.84	5.36	6.97	7.34
0.58	6.29	4.63	6.34	6.33
0.80	0.45	0.27	0.84	0.63

Table E-5. SPECIES CONCENTRATION DISTRIBUTIONS
(continued)

R/R_o	CO_2, mole%			
	X/D=0.24	0.50	1.63	1.89
-0.85	0.94	16.1	2.30	2.11
-0.66	6.66	4.48	5.59	5.67
-0.45	5.53	5.66	4.71	4.81
-0.25	4.76	3.95	4.31	4.53
-0.04	1.44	2.47	4.20	4.63
0.17	2.49	2.83	4.24	4.64
0.38	4.94	4.45	4.54	4.92
0.58	6.58	5.97	5.53	5.81
0.80	3.01	1.59	3.03	2.63

R/R_o	O_2, mole%			
	X/D=0.24	0.50	1.63	1.89
-0.85	18.7	18.1	15.8	16.3
-0.66	6.00	2.37	2.84	2.39
-0.45	0.62	1.35	1.23	1.01
-0.25	0.97	2.67	1.48	1.14
-0.04	3.06	3.10	1.53	1.13
0.17	3.18	2.95	1.44	1.14
0.38	0.90	1.70	1.20	1.03
0.58	1.06	5.00	2.04	2.60
0.80	14.8	17.5	14.3	15.2

R/R_o	THC, mole%			
	X/D=0.24	0.50	1.63	1.89
-0.85	0.06	0.05	0.64	4.40
-0.66	0.66	0.20	0.82	7.65
-0.45	>10.0	>10.0	>10.0	>10.0
-0.25	>10.0	>10.0	>10.0	>10.0
-0.04	>10.0	>10.0	>10.0	>10.0
0.17	>10.0	>10.0	>10.0	>10.0
0.38	>10.0	>10.0	>10.0	>10.0
0.58	4.28	5.60	9.32	8.15
0.80	0.02	0.06	8.00	4.35

APPENDIX F

MEANS AND RMS VELOCITY DISTRIBUTIONS: TABULATED DATA

Table F-1. AXIAL VELOCITY DISTRIBUTIONS (M/SEC) FOR TEST NO. 1

CH_4-Air
Φ = 0.91±0.01
Pressure = 3.9±0.1 atm

Inlet Air Swirl = 0
Inlet Air Temperature = 751±8°K
Air/Fuel Velocity Ratio = 20.7±0.2

X/D = 0.052

R/R_0	$\bar{U}$	$\sqrt{\overline{u'^2}}$
-0.917	4.30	5.2
-0.788	18.6	6.0
-0.667	21.1	4.1
-0.542	15.0	6.4
-0.371	0.07	2.9
-0.204	1.90	2.5
-0.038	2.86	2.8
0.146	3.43	2.5
0.354	3.30	2.8
0.563	20.7	4.4
0.708	18.7	5.9

X/D = 0.146

R/R_0	$\bar{U}$	$\sqrt{\overline{u'^2}}$
-0.875	-1.4	3.3
-0.813	2.5	5.6
-0.750	14.7	6.1
-0.688	17.2	4.8
-0.625	18.5	4.6
-0.542	13.9	5.3
-0.492	9.9	5.2
-0.433	1.9	4.6
-0.375	-0.7	3.3
-0.204	-1.2	3.0
-0.038	-1.9	3.4
0.125	-2.1	3.3
0.350	-2.3	3.1
0.458	1.8	9.0
0.458	0.6	5.3
0.554	13.8	4.9

Table F-1. AXIAL VELOCITY DISTRIBUTIONS (M/SEC)
(continued)

X/D = 0.146

R/R_0	$\bar{U}$	$\sqrt{\overline{u'^2}}$
0.625	18.5	3.5
0.704	18.0	3.6
0.771	14.2	4.8
0.833	4.9	4.8
0.908	-2.1	3.0

X/D = 0.187

R/R_0	$\bar{U}$	$\sqrt{\overline{u'^2}}$
-0.917	14.4	4.5
-0.792	16.9	3.9
-0.667	12.6	4.7
-0.538	5.0	5.0
-0.417	-1.4	4.6
-0.292	-4.4	3.8
-0.158	-5.2	3.7
-0.017	-6.0	3.8
0.125	-5.7	3.7
0.250	-5.6	3.5
0.375	-4.2	3.9
0.500	1.9	5.3
0.625	10.6	4.7
0.750	16.2	3.8
0.875	16.3	3.6

Table F-1. AXIAL VELOCITY DISTRIBUTIONS (M/SEC)
(continued)

X/D = 1.58

R/R_0	$\bar{U}$	$\sqrt{\overline{u'^2}}$
-0.917	13.5	3.7
-0.788	14.9	3.1
-0.667	14.1	3.1
-0.542	13.1	3.6
-0.417	12.3	3.5
-0.292	10.8	3.3
-0.163	10.2	3.0
-0.042	10.6	3.3
0.083	10.4	3.1
0.208	10.4	3.0
0.338	12.3	3.4
0.463	12.0	3.5
0.588	13.0	3.2
0.708	13.0	2.6
0.838	12.9	2.7
0.942	12.3	2.7

X/D = 1.79

R/R_0	$\bar{U}$	$\sqrt{\overline{u'^2}}$
-0.913	14.5	3.5
-0.771	15.9	2.8
-0.625	15.7	2.8
-0.463	14.3	3.1
-0.296	13.2	2.9
-0.125	12.4	3.0
0.046	12.8	3.0
0.208	12.6	3.2
0.375	13.6	3.6
0.546	14.6	3.3
0.713	14.9	2.5
0.875	14.3	2.4

Table F-2. AXIAL VELOCITY DISTRIBUTIONS (M/SEC) FOR TEST NO. 3

CH_4-Air
Φ = 0.91±0.01
Pressure = 1.0 atm

Inlet Air Swirl No. = 0.3
Inlet Air Temperature = 744 ± 9°K
Air/Fuel Velocity Ratio = 21.7±0.5

X/D = 0.052

R/R_0	$\bar{U}$	$\sqrt{\overline{u'^2}}$
-0.917	6.2	7.2
-0.792	36.9	19.7
-0.733	61.6	20.7
-0.679	70.2	17.2
-0.663	68.2	25.0
-0.600	59.3	22.0
-0.542	27.6	24.5
-0.413	-3.6	13.9
-0.267	1.4	11.9
-0.125	5.9	10.2
0.000	10.3	24.0
0.167	5.2	11.1
0.375	-1.8	12.1
0.500	18.6	24.3
0.558	58.9	26.8
0.704	85.1	19.1
0.708	87.5	17.9
0.833	39.6	28.6
0.917	5.8	7.7

Table F-2. AXIAL VELOCITY DISTRIBUTIONS (M/SEC)
(Continued)

X/D = 0.128

R/R_0	$\bar{U}$	$\sqrt{\overline{u'^2}}$
-0.917	30.5	30.3
-0.913	30.0	23.4
-0.763	101.	49.5
-0.741	44.3	36.7
-0.671	84.4	58.7
-0.583	15.3	33.9
-0.579	46.0	44.8
-0.400	5.3	22.0
-0.229	11.9	21.7
0.042	18.7	21.9
0.167	13.9	22.6
0.254	4.1	25.7
0.421	24.1	44.3
0.588	94.8	63.4
0.588	107.	60.5
0.663	102.	54.8
0.758	49.4	32.8
0.833	13.0	22.5

X/D = 0.486

R/R_0	$\bar{U}$	$\sqrt{\overline{u'^2}}$
-0.929	42.1	31.6
-0.875	62.4	41.6
-0.833	80.7	49.6
-0.833	87.5	55.7
-0.788	85.4	55.3
-0.767	87.5	55.7
-0.708	86.4	69.0
-0.667	66.1	62.3
-0.588	48.6	52.7
-0.583	49.7	51.1
-0.354	24.1	40.9
-0.158	36.2	39.3
0.042	42.2	36.4

Table F-2. AXIAL VELOCITY DISTRIBUTIONS (M/SEC)
(Continued)

X/D = 0.486 (Cont'd)

R/R_0	$\bar{U}$	$\sqrt{\overline{u'^2}}$
0.254	27.8	40.1
0.458	45.9	49.5
0.567	45.6	59.1
0.667	91.0	64.2
0.729	83.1	54.0
0.846	61.3	41.4
0.850	54.2	40.7

X/D = 0.519

R/R_0	$\bar{U}$	$\sqrt{\overline{u'^2}}$
-0.871	59.0	26.2
-0.746	61.8	25.3
-0.688	64.4	25.8
-0.596	58.4	24.3
-0.446	56.5	27.6
-0.279	51.7	36.3
-0.113	62.8	43.1
0.054	72.4	44.5
0.142	64.8	41.9
0.146	67.0	25.7
0.263	54.6	34.7
0.471	63.1	26.8
0.638	59.8	26.7
0.808	59.8	27.9
0.858	63.7	27.7

Table F-2. AXIAL VELOCITY DISTRIBUTIONS (M/SEC)
(Continued)

X/D = 1.88

R/R_0	$\bar{U}$	$\sqrt{\overline{u'^2}}$
-0.871	57.1	28.0
-0.704	67.0	29.4
-0.546	62.8	27.1
-0.375	53.8	30.0
-0.208	56.5	33.0
-0.041	69.9	45.6
0.004	77.6	44.7
0.004	75.0	43.0
0.142	54.0	40.4
0.296	45.3	32.9
0.471	50.8	27.8
0.633	53.6	26.5
0.800	55.6	27.5
0.867	56.9	29.8

X/D = 3.00

R/R_0	$\bar{U}$	$\sqrt{\overline{u'^2}}$
-0.875	60.0	24.4
-0.838	68.0	30.5
-0.746	71.6	30.9
-0.596	70.4	29.5
-0.458	67.0	32.2
-0.267	70.1	36.5
-0.108	68.6	36.9
0.038	68.3	41.4
0.350	68.0	35.0
0.521	73.2	31.7
0.517	67.9	27.7
0.671	68.9	26.2

Table F-3. AXIAL VELOCITY DISTRIBUTIONS (M/SEC) FOR TEST NO. 4

CH_4-Air
$\Phi = 0.91 \pm 0.01$
Pressure = 3.7±0.1 atm

Inlet Air Swirl = 0.3
Inlet Air Temperature = 749±7°K
Air/Fuel Velocity Ratio = 20.5±0.4

X/D = 0.052

R/R_0	$\bar{U}$	$\sqrt{\overline{u'^2}}$
-0.938	0.7	3.6
-0.813	5.2	4.6
-0.683	14.9	5.8
-0.542	8.3	6.2
-0.408	-1.1	4.5
-0.271	0.2	4.1
0.042	3.6	3.0
0.458	1.0	4.3

X/D = 0.093

R/R_0	$\bar{U}$	$\sqrt{\overline{u'^2}}$
-0.892	2.1	4.1
-0.779	16.6	6.8
-0.683	19.8	6.4
-0.585	13.3	8.1
-0.471	7.8	10.7
-0.371	-2.4	4.8
-0.167	0.8	3.9
0.038	1.0	3.8
0.250	0.3	4.3
0.346	-1.9	4.6
0.458	5.0	7.6
0.458	4.8	7.4
0.563	18.1	5.6
0.667	21.6	5.2
0.771	14.5	6.8
0.833	7.1	8.1

Table F-3. AXIAL VELOCITY DISTRIBUTIONS (M/SEC)
(Continued)

X/D = 0.291

R/R_0	$\bar{U}$	$\sqrt{\overline{u'^2}}$
-0.879	11.0	6.6
-0.708	19.2	6.2
-0.617	13.8	7.7
-0.538	3.9	7.4
-0.458	-0.8	5.7
-0.375	-2.9	5.5
-0.167	0.9	5.5
0.038	2.1	4.8
0.167	-2.6	5.3
0.458	0.4	6.2
0.562	9.8	7.0
0.667	17.0	6.1
0.771	18.3	5.0
0.858	12.6	5.9
0.900	6.4	6.7
1.021	18.1	6.3

X/D = 0.550

R/R_0	$\bar{U}$	$\sqrt{\overline{u'^2}}$
-0.913	14.0	8.3
-0.879	17.2	5.6
-0.792	18.0	6.2
-0.750	15.6	6.5
-0.695	11.9	6.7
-0.600	10.2	8.7
-0.583	5.2	6.9
-0.488	0.03	5.7
-0.413	5.9	9.2
-0.333	-1.4	8.0
-0.250	2.6	8.4
-0.083	4.6	6.9
0.083	4.3	5.3
0.188	2.0	6.7
0.346	-0.8	6.0
0.463	-2.0	4.3

Table F-3. AXIAL VELOCITY DISTRIBUTIONS (M/SEC)
(Continued)

X/D = 0.550 (Cont'd)

R/R_0	$\bar{U}$	$\sqrt{\overline{u'^2}}$
0.570	1.8	5.4
0.667	7.0	5.5
0.713	10.4	5.8
0.767	13.2	5.3
0.838	16.3	5.1
0.942	17.5	4.0

X/D = 1.48

R/R_0	$\bar{U}$	$\sqrt{\overline{u'^2}}$
-0.888	17.1	3.8
-0.792	16.2	3.9
-0.688	15.3	4.1
-0.579	14.4	3.9
-0.458	13.6	4.3
-0.333	13.4	4.4
-0.208	13.4	4.7
-0.079	15.9	6.2
0.046	15.9	6.0
0.167	14.3	4.7
0.304	13.9	4.0
0.417	14.3	4.0
0.567	16.1	4.3
0.675	17.9	4.0
0.792	18.8	3.7

X/D = 3.00

R/R_0	$\bar{U}$	$\sqrt{\overline{u'^2}}$
-0.913	15.1	3.3
-0.788	17.2	3.0
-0.621	17.8	3.4
-0.367	18.7	4.1
-0.163	18.7	5.1
0.046	20.3	5.8
0.250	18.9	4.4
0.458	18.4	3.6
0.667	17.7	3.8
0.775	17.3	3.7

Table F-4. AXIAL VELOCITY DISTRIBUTIONS (M/SEC) FOR TEST NO. 6

CH_4-Air
Φ = 0.91±0.01
Pressure = 1 atm

Inlet Air Swirl = 0.6
Inlet Air Temperature = 750±10°K
Air/Fuel Velocity Ratio = 21.3±0.5

X/D = 0.160

R/R_0	$\bar{U}$	$\sqrt{\overline{u'^2}}$
-0.913	37.8	25.6
-0.867	67.9	29.0
-0.792	83.8	34.5
-0.729	76.5	34.4
-0.688	45.7	47.0
-0.600	20.7	39.4
-0.479	-5.4	19.6
-0.371	0.6	19.3
-0.250	5.5	17.0
-0.075	14.1	15.2
0.088	14.2	15.8
0.250	6.0	18.1
0.417	-3.1	18.8
0.588	0.06	31.5
0.671	15.0	36.3
0.750	57.2	44.5
0.813	68.0	36.3
0.879	77.7	39.8
0.962	58.7	31.2

Table F-4. AXIAL VELOCITY DISTRIBUTIONS (M/SEC)
(continued)

X/D = 0.405

R/R_0	$\bar{U}$	$\sqrt{\overline{u'^2}}$
-0.892	46.5	18.3
-0.892	73.4	27.8
-0.833	63.4	29.4
-0.792	49.4	22.7
-0.754	49.0	28.3
-0.675	23.3	28.0
-0.575	8.6	25.1
-0.458	3.5	25.3
-0.313	3.3	26.8
-0.167	14.5	24.3
0.042	21.6	22.3
0.250	14.7	20.6
0.458	2.5	24.6
0.667	21.4	30.3
0.771	39.6	32.6
0.875	66.4	30.5
0.946	72.5	28.2

X/D = 1.55

R/R_0	$\bar{U}$	$\sqrt{\overline{u'^2}}$
-0.87	60.1	16.2
-0.746	57.4	15.3
-0.625	50.1	15.7
-0.475	42.0	19.0
-0.367	35.6	20.0
-0.242	44.0	24.6
-0.100	59.2	31.5
0.033	57.5	31.0
0.150	49.9	30.3
0.275	37.6	23.5
0.395	36.1	18.8
0.525	41.1	16.6
0.667	47.2	14.2
0.775	56.5	15.4
0.871	66.2	16.8
0.904	66.5	18.0

Table F-4. AXIAL VELOCITY DISTRIBUTIONS (M/SEC)
(continued)

X/D = 1.75

R/R_0	$\bar{U}$	$\sqrt{\overline{u'^2}}$
-0.892	59.2	21.2
-0.792	62.1	15.1
-0.754	63.6	15.0
-0.688	57.4	13.6
-0.583	53.9	14.4
-0.467	48.3	17.7
-0.375	45.3	19.8
-0.267	39.0	24.0
-0.167	43.6	28.4
0.058	42.1	31.0
0.042	29.7	34.2
0.146	33.3	27.6
0.250	29.1	27.0
0.333	35.3	24.1
0.467	45.6	20.5
0.558	50.2	16.8
0.667	58.2	15.9
0.771	62.3	15.0
0.879	67.1	17.4

Table F-5. AXIAL VELOCITY DISTRIBUTIONS (M/SEC) FOR TEST NO. 7

CH_4 = Air
Φ = 0.91 ± 0.01
Pressure = 1 atm

Inlet Air Swirl = 0.6
Inlet Air Temperature = 746 ± 7°K
Air/Fuel Velocity Ratio = 0.17 ± 0.01

X/D = 0.052 R/R_0	$\bar{U}$	$\sqrt{u'^2}$
- 0.954	4.6	18.1
- 0.950	8.1	17.2
- 0.917	19.9	19.5
- 0.825	26.6	14.0
- 0.813	49.3	24.2
- 0.750	85.0	34.8
- 0.688	61.7	34.5
- 0.583	15.7	24.5
- 0.488	-0.9	22.2
- 0.329	10.0	17.2
- 0.204	24.4	17.8
- 0.075	38.4	25.1
- 0.025	98.1	73.0
0.017	87.5	86.5
0.046	56.2	67.5
0.175	34.8	12.9
0.292	19.8	12.6
0.417	2.5	12.3
0.479	-1.9	13.3
0.571	8.9	22.9
0.646	53.9	29.0
0.713	89.2	31.4
0.846	64.1	30.0
0.963	10.8	18.3

Tabe F-5. AXIAL VELOCITY DISTRIBUTIONS (M/SEC)
(continued)

$\frac{X/D = 0.615}{R/R_0}$	$\bar{U}$	$\sqrt{u'^2}$
- 0.879	82.7	20.8
- 0.750	49.9	21.8
- 0.617	19.5	20.1
- 0.500	5.0	21.8
- 0.354	13.5	37.2
- 0.217	37.9	50.7
- 0.083	75.5	65.7
0.050	92.3	66.6
0.196	69.8	63.3
0.338	28.2	48.3
0.483	0.90	26.2
0.633	7.7	19.5
0.779	40.2	20.1
0.917	71.8	19.1
1.000	79.8	23.8

$\frac{X/D = 1.97}{R/R_0}$	$\bar{U}$	$\sqrt{u'^2}$
-0.908	61.3	11.7
-0.791	51.4	11.6
-0.671	43.6	11.2
-0.538	40.5	15.6
-0.413	38.7	15.1
-0.288	43.5	16.7
-0.167	50.9	17.1
0.042	58.9	17.2
0.083	59.4	17.1
0.217	53.6	15.7
0.338	46.9	15.6
0.458	42.2	16.1
0.592	44.6	14.0
0.667	48.2	12.3
0.708	55.3	13.6
0.829	60.2	14.8
0.925	65.7	10.1

Table F-6. TANGENTIAL VELOCITY DISTRIBUTIONS (M/SEC) FOR TEST NO. 3

CH_4 = Air
Φ = 0.91 ± 0.01
Pressure = 1 atm

Inlet Air Swirl = 0.3
Inlet Air Temperature = 744 ± 9°K
Air/Fuel Velocity Ratio = 21.7 ± 0.5

$\frac{X/D = 0.128}{R/R_0}$	$\bar{W}$	$\sqrt{\omega'^2}$
- 0.900	52.1	22.0
- 0.788	52.8	23.7
- 0.679	47.0	29.6
- 0.542	26.0	21.1
- 0.325	12.7	17.2
0.000	1.9	16.5
0.000	3.9	14.9
0.350	-27.2	21.8
0.563	-54.6	30.5
0.663	-56.0	28.2
0.771	-44.6	19.3
0.833	-42.0	19.1

$\frac{X/D = 0.486}{R/R_0}$	$\bar{W}$	$\sqrt{\omega'^2}$
- 0.938	56.4	24.9
- 0.850	59.8	25.8
- 0.767	67.9	29.9
- 0.675	71.1	30.1
- 0.579	68.1	29.9
- 0.354	58.9	26.4
- 0.167	44.5	28.4
- 0.167	37.7	28.8
0.038	-10.2	-19.9
0.041	- 1.0	-27.7
0.296	54.9	28.0
0.738	65.4	27.5
0.858	57.6	26.5
0.913	57.3	26.0

Table F-6. TANGENTIAL VELOCITY DISTRIBUTIONS (M/SEC)
(Continued)

$\frac{X/D = 1.60}{R/R_0}$	$\bar{W}$	$\sqrt{\omega'^2}$
- 0.867	54.5	19.3
- 0.717	60.3	18.3
- 0.583	64.5	19.9
- 0.438	65.6	19.9
- 0.271	65.0	23.6
- 0.083	41.2	35.7
- 0.079	41.7	37.7
0.025	4.9	36.7
0.104	-45.4	37.0
0.229	-63.5	27.8
0.471	-66.4	17.9
0.683	-64.8	20.0
0.791	-61.5	18.3

$\frac{X/D = 1.88}{R/R_0}$	$\bar{W}$	$\sqrt{\omega'^2}$
0.867	96.9	44.8
0.792	64.4	18.7
0.708	69.7	18.8
0.542	68.4	20.1
0.421	66.4	20.5
0.250	58.7	22.9
0.088	39.8	32.3
0.000	28.4	33.8
0.017	23.7	33.5
0.083	-63.9	22.2
0.146	-67.3	24.6
0.200	-73.2	24.2
0.354	-71.5	17.8
0.533	-69.6	18.1
0.675	-66.5	16.7
0.804	-69.9	19.1

Table F-7. TANGENTIAL VELOCITY DISTRIBUTIONS (M/SEC) FOR TEST NO. 4

CH_4 = Air
Φ = 0.91 ± 0.01
Pressure = 3.7 ± 0.1 atm

Inlet Air Swirl = 0.3
Inlet Air Temperature = 749 ± 7°K
Air/Fuel Velocity Ratio = 20.5 ± 0.4

$\frac{X/D = 0.291}{R/R_0}$	$\overline{W}$	$\sqrt{\overline{w'^2}}$
- 0.885	5.9	4.6
- 0.783	8.7	4.6
- 0.688	9.5	4.5
- 0.579	7.2	4.8
- 0.463	4.8	4.3
- 0.267	4.4	4.1
0.017	0.8	3.5
0.254	-4.9	3.6
0.458	-6.6	3.3
0.663	-7.8	3.8
0.817	-9.6	3.0
0.904	-8.9	3.0

Table F-7. TANGENTIAL VELOCITY DISTRIBUTIONS (M/SEC)
(Continued)

$\frac{X/D = 0.550}{R/R_0}$	$\overline{W}$	$\sqrt{\overline{\omega'^2}}$
- 0.896	8.9	4.1
- 0.792	9.0	4.1
- 0.667	8.0	4.7
- 0.583	8.4	4.3
- 0.492	9.5	4.4
- 0.325	10.2	4.6
- 0.163	7.8	4.7
- 0.071	3.7	5.1
0.021	1.3	5.2
0.213	- 4.6	4.7
0.383	- 6.2	4.2
0.508	- 5.6	4.1
0.575	- 4.7	4.1
0.625	- 4.1	3.9
0.688	- 3.3	3.8
0.750	- 4.4	4.1
0.833	- 5.6	3.5
0.875	- 6.6	3.5
0.900	- 6.2	3.1
0.979	- 4.2	3.7

$\frac{X/D = 1.48}{R/R_0}$	$\overline{W}$	$\sqrt{\overline{\omega'^2}}$
- 0.892	8.0	3.4
- 0.875	6.6	3.2
- 0.750	8.7	3.2
- 0.745	7.3	3.4
- 0.613	8.3	3.4
- 0.538	10.8	3.6
- 0.475	10.2	3.8
- 0.329	14.0	4.4
- 0.267	12.7	4.3
- 0.121	14.0	6.2
0.042	0.6	18.1
0.296	- 6.1	11.3
0.475	-10.6	3.4
0.712	- 8.9	3.0
0.917	- 7.6	3.3

Table F-8. TANGENTIAL VELOCITY DISTRIBUTIONS (M/SEC) FOR TEST NO. 6

CH_4 = Air
Φ = 0.91 ± 0.01
Pressure = 1 atm

Inlet Air Swirl = 0.6
Inlet Air Temperature = 750 ± 10°K
Air/Fuel Velocity Ratio = 21.3 ± 0.5

$\frac{X/D = 0.162}{R/R_0}$	$\overline{W}$	$\sqrt{\overline{w'^2}}$
- 0.917	57.6	21.2
- 0.808	60.8	23.5
- 0.708	48.5	20.1
- 0.583	38.6	17.1
- 0.458	34.0	15.4
- 0.329	26.7	15.8
- 0.171	19.8	17.3
0.000	14.9	22.0
0.000	9.0	25.2
0.021	-6.1	27.9
0.171	-27.3	22.5
0.333	-43.9	21.0
0.500	-46.3	17.9
0.633	-47.5	18.2
0.750	-54.0	20.4
0.875	-65.5	24.4
0.942	-53.5	26.3

Table F-8. TANGENTIAL VELOCITY DISTRIBUTIONS (M/SEC)
(continued)

$\frac{X/D = 0.405}{R/R_0}$	$\overline{W}$	$\sqrt{\overline{\omega'^2}}$
0.891	66.0	24.2
0.791	63.5	21.0
0.687	60.2	22.0
0.583	57.9	17.9
0.375	63.6	19.8
0.275	65.0	17.0
0.158	50.1	25.4
0.083	35.5	22.7
0.016	8.2	26.7
0.029	17.4	22.4
0.145	-47.2	22.2
0.250	-60.2	20.5
0.345	-66.2	19.1
0.458	-64.2	18.9
0.562	-63.7	21.8
0.666	-62.1	24.0
0.750	-56.2	23.9
0.875	-66.0	22.8
0.916	-63.8	21.2

Table F-8. TANGENTIAL VELOCITY DISTRIBUTIONS (M/SEC)
(continued)

X/D = 1.55 R/R_0	$\bar{W}$	$\sqrt{\overline{\omega'^2}}$
-0.875	64.8	13.0
-0.725	68.1	13.8
-0.621	76.4	16.8
-0.500	80.8	16.8
-0.367	88.7	16.6
-0.217	88.7	17.1
-0.083	50.5	32.4
0.000	14.3	32.4
0.021	21.6	31.6
0.088	-20.2	25.0
0.150	-68.2	26.3
0.213	-81.8	21.7
0.392	-84.5	16.7
0.563	-76.0	16.2
0.708	-68.8	15.5
0.771	-66.6	15.8
0.883	-67.9	19.0

X/D = 1.75 R/R_0	$\bar{W}$	$\sqrt{\overline{\omega'^2}}$
-0.900	55.9	15.1
-0.788	66.1	14.7
-0.688	65.3	16.3
-0.583	72.9	17.2
-0.371	82.3	17.2
-0.167	56.0	23.3
0.042	7.3	32.5
0.046	-38.7	23.3
0.250	-74.9	19.1
0.463	-79.8	17.4
0.563	-70.9	16.8
0.667	-65.8	13.8
0.771	-63.2	13.3

Table F-9. TANGENTIAL VELOCITY DISTRIBUTIONS (M/SEC) FOR TEST NO. 7

CH_4 = Air
Φ = 0.91 ± 0.01
Pressure = 1 atm

Inlet Air Swirl = 0.6
Inlet Air Temperature = 746 ± 7°K
Air/Fuel Velocity Ratio = 0.17 ± 0.01

$\frac{X/D = 0.052}{R/R_0}$	$\bar{W}$	$\sqrt{\overline{w'^2}}$
-0.958	63.5	27.0
-0.833	63.8	27.9
-0.708	65.6	29.3
-0.583	53.9	20.6
-0.458	64.8	15.2
-0.329	71.5	22.9
-0.204	73.7	26.3
-0.079	79.7	31.8
0.171	-75.7	22.8
0.292	-67.4	17.2
0.417	-64.3	13.6
0.667	-89.9	17.4
0.708	-101.8	24.0
0.708	-103.8	21.7
0.833	-87.1	22.9
0.833	-100.5	23.7
0.958	-60.3	14.7
0.958	-60.1	14.2

$\frac{X/D = 0.615}{R/R_0}$	$\bar{W}$	$\sqrt{\overline{w'^2}}$
-0.895	56.9	15.1
-0.745	63.4	13.6
-0.620	66.3	17.0
-0.479	69.1	16.1
-0.333	63.4	24.4
-0.187	42.5	31.8
-0.041	12.6	37.5
-0.037	27.0	38.1
0.087	-14.0	38.4
0.125	-35.7	35.8
0.254	-45.5	35.2
0.375	-54.6	29.0

Tabe F-9. TANGENTIAL VELOCITY DISTRIBUTIONS (M/SEC)
(continued)

$\frac{X/D = 1.97}{R/R_0}$	$\bar{W}$	$\sqrt{\overline{\omega'^2}}$
- 0.871	59.8	7.3
- 0.750	63.4	8.2
- 0.620	67.5	9.8
- 0.500	70.9	11.3
- 0.375	66.3	15.1
- 0.250	57.0	17.8
- 0.121	29.3	19.5
0.017	2.2	17.9
0.021	8.0	20.3
0.146	-17.3	17.2
0.288	-32.6	15.6
0.417	-51.1	14.9
0.546	-62.0	14.0
0.667	-64.5	13.8
0.792	-62.1	8.6
0.875	-49.6	9.6
0.938	-57.1	12.6

Table F-10. RADIAL VELOCITY DISTRIBUTIONS (M/SEC) FOR TEST NO. 3

CH_4 = Air
Φ = 0.90
Pressure = 1 atm

Inlet Air Swirl = 0.3
Inlet Air Temperature = 748°K
Air/Fuel Velocity Ratio = 21.4

R/R_0	$\bar{V}$	$\sqrt{\overline{v'^2}}$
-0.373	5.8	16.6
-0.373	3.8	14.5
-0.342	2.4	--
-0.290	2.0	13.8
-0.207	0.9	11.3
-0.124	-0.8	14.1
-0.041	-1.5	10.9
0.041	-3.8	11.3
0.166	-5.1	10.5
0.290	-6.9	11.2
0.415	-10.1	13.3
0.498	-9.4	14.4

PUBLICATIONS

The following publications have been produced as a result of the research program described in this report:

Owen, F. K. Laser Velocimeter Measurements of a Confined Turbulent Diffusion Flame Burner. AIAA Paper 76-33 presented at the AIAA 14th Aerospace Sciences Meeting, Washington, D.C., January 26-28, 1976.

Owen, F. K., L. J. Spadaccini and C. T. Bowman. Pollutant Formation and Energy Release in Confined Turbulent Diffusion Flames, to be presented at the 16th Symposium (International) on Combustion, Boston, August 15-20, 1976.

REFERENCES

1. Heap, M. P., T. M. Lowes and R. Walmsley. The Effect of Burner Parameters on Nitric Oxide Formation in Natural Gas and Pulverized Fuel Flames. Paper presented at First American Flame Days Meeting, Chicago, Illinois, September 1972. p. 78.

2. Heap, M. P., T. M. Lowes and R. Walmsley. Emission of Nitric Oxide from Large Turbulent Diffusion Flames. Fourteenth Symposium (International) on Combustion. Pittsburgh, The Combustion Institute, 1973, pp. 883-895.

3. Shoffstall, D. R. and D. H. Larson. Aerodynamic Control of Nitrogen Oxides and Other Pollutants from Fossil Fuel Combustion. Environmental Protection Agency, Research Triangle Park, N. C., Publication Number 650/2-73-033a.

4. Shoffstall, D. R. Burner Design Criteria for Control of Pollutant Emissions from Natural Gas Flames. Paper presented at Symposium on Stationary Source Combustion, Atlanta, GA., September 1975.

5. Mellor, A. M., R. D. Anderson, R. A. Altenkirch and J. H. Tuttle. Emissions From and Within an Allison J-33 Combustor. Comb. Sci. Technol.6: 169-176, 1972.

6. Jones, R. E. and J. Grobman. Design and Evaluation of Combustors for Reducing Aircraft Engine Pollution. Atmospheric Pollution by Aircraft Engines, AGARD Document CP-125, April 1973.

7. Bowman, C. T. and L. S. Cohen. Influence of Aerodynamic Phenomena on Pollutant Formation in Combustion. Environmental Protection Agency, Research Triangle Park, N. C., Publication Number 650/2-75-061a, July 1975. p. 159.

REFERENCES (Cont'd)

8. Spalding, D. B. Mathematical Models of Continuous Combustion. In: Emissions from Continuous Combustion Systems, Cornelius W. and W. G. Agnew (eds.), New York, Plenum Press, p. 3-18, 1972.

9. Anasoulis, R. F. and H. McDonald. A Study of Combustor Flow Computations and Comparison with Experiment. Environmental Protection Agency, Research Triangle Park, N.C., Publication Number 650/2-73-045, p. 94, December 1973.

10. Bray, K. N. C. and J. B. Moss. A Unified Statistical Model of the Premixed Turbulent Flame. University of Southampton, Southampton, England. Report No. 335, p. 64, November 1974.

11. Caretto, L. S. Mathematical Modeling of Pollutant Formation. Prog. Energy Combust. Sci. 1: 47-71, 1976.

12. Buggeln, R. C. and H. McDonald. Work in Progress.

13. Kerr, N. M. and D. Fraser. Swirl. Part I: Effect on Axisymmetrical Turbulent Jets. J. Inst. Fuel 38: 519-538, 1965.

14. Bowman, C. T. Probe Measurements in Combustion - A Synopsis. Progress in Astronautics and Aeronautics (to be published).

15. Bilger, R. Probe Measurements in Turbulent Combustion. Progress in Astronautics and Aeronautics (to be published).

16. Tuttle, J. H., R. A. Shisler and A. M. Mellor. Nitrogen Dioxide Formation in Gas Turbine Engines: Measurements and Measurement Methods. Combust. Sci. Technol. 9:261-271, 1975.

17. Bennett, J. C. Use of Five-Hole Pneumatic Probes in Unsteady Flows. Progress in Astronautics and Aeronautics (to be published).

18. Becker, H. A., H. C. Hottel and G. C. Williams. On the Light-Scatter Technique for the Study of Turbulence and Mixing. J. Fluid Mech. 30:259-284, 1967.

19. Anon. Procedure for the Continuous Sampling and Measurement of Gaseous Emissions from Aircraft Turbine Engines. Aerospace Recommended Practice 1256, SAE, p. 16, 1971.

20. Owen, F. K. Laser Velocimeter Measurements in Free and Confined Coaxial Jets with Recirculation. United Technologies Research Center (Presented at 13th AIAA Aerospace Sciences Meeting. Pasadena, CA, January 20-22, 1975) p. 10.

21. Schefer, R. W., R. D. Matthews, N. P. Cernansky and R. F. Sawyer. Measurement of NO and NO_2 in Combustion Systems. University of California. (Presented at the Western States Section/Combustion Institute Meeting, El Segundo, October 1973) p. 18.

22. Cernansky, N. P. and R. F. Sawyer. NO and NO_2 Formation in a Turbulent Hydrocarbon/Air Diffusion Flame. Fifteenth Symposium (International) on Combustion. Pittsburgh, The Combustion Institute, pp. 1039-1050, 1975.

23. Owen, F. K. Laser Velocimeter Measurements of a Confined Turbulent Diffusion Flame Burner. United Technologies Research Center. (Presented at the 14th AIAA Aerospace Sciences Meeting. Washington, D.C., January 26-28, 1976) p. 10.

24. Lindgren, B. W. and G. W. McElrath. Introduction to Probability and Statistics, New York, Macmillan, p. 165, 1959.

NOMENCLATURE

a = defined by Eq. (5)

d = outer diameter of air annulus, cm

d_h = inner diameter of air annulus, cm

D = Combustor diameter = 0.122 m

D_p = particle diameter,

f = frequency, Hz

f_D = Doppler frequency, Hz

f_o = offset frequency, Hz

K = Cunningham constant ≈ 1.8

K_Y = defined by Eq. (10)

ℓ = mean free path, cm

L = height of air annulus, cm

m = V_a/V_f = air/fuel velocity ratio

$\dot{M}$ = mass flow rate, kg/sec

n_x = frequency of mean flow reversal, Eq. (7)

N = total number of samples

P = error as defined by Eqs. (10) and (11)

NOMENCLATURE (CONT'D)

R = radius, m

R_o = combustor radius = 0.0612 m

S = swirl number as defined by Eq. (1)

S_x = calculated variance in the variable x, Eq. (11)

T = temperature, °K

u_p = rms particle velocity, m/sec

$\bar{U}$ = mean axial velocity, m/sec

U_c = convective velocity, m/sec

U_i = instantaneous axial velocity, m/sec

u' = axial velocity fluctuation, m/sec

$\tilde{u}$ = large-scale axial velocity fluctuation, m/sec, Eq. (8)

V_a = bulk mean air velocity, m/sec

V_f = bulk mean fuel velocity, m/sec

$\bar{W}$ = mean tangential gas velocity, m/sec

w' = tangential velocity fluctuation, m/sec

x = random variable

X = axial distance, m

Z = d_h/d

α_x = percentage of time mean flow is reversed, Eq. (7)

β = true mean of the variable x, Eq. (10)

γ = directional intermittency

γ_m = error in the mean, Eq. (10)

γ_T = error in the variance, Eq. (11)

η = swirl vane angle, deg

θ = angle, deg

λ = wavelength, m

μ = viscosity, gm/cm-sec

ρ_p = particle density, gm/cc

σ = rms velocity, m/sec

Φ = overall fuel-air equivalence ratio = $(\dot{m}_{fuel}/\dot{m}_{air})/(\dot{m}_{fuel}/\dot{m}_{air})_{stoich.}$

TECHNICAL REPORT DATA
(Please read Instructions on the reverse before completing)

1. REPORT NO.	2.	3. RECIPIENT'S ACCESSION NO.
EPA-600/2-76-247a		

4. TITLE AND SUBTITLE	5. REPORT DATE
INFLUENCE OF AERODYNAMIC PHENOMENA ON POLLUTANT FORMATION IN COMBUSTION (Phase I. Gaseous Fuels)	September 1976
	6. PERFORMING ORGANIZATION CODE
7. AUTHOR(S) L. J. Spadaccini, F. K. Owen, and C. T. Bowman	8. PERFORMING ORGANIZATION REPORT NO.
9. PERFORMING ORGANIZATION NAME AND ADDRESS United Technology Research Center 400 Main Street East Hartford, Connecticut 06108	10. PROGRAM ELEMENT NO. 1AB014; ROAP 21BCC-014
	11. CONTRACT/GRANT NO. 68-02-1873
12. SPONSORING AGENCY NAME AND ADDRESS EPA, Office of Research and Development Industrial Environmental Research Laboratory Research Triangle Park, NC 27711	13. TYPE OF REPORT AND PERIOD COVERED Phase Final; 4/75-5/76
	14. SPONSORING AGENCY CODE EPA-ORD

15. SUPPLEMENTARY NOTES IERL-RTP project officer for this report is W. S. Lanier, Mail Drop 65, 919/549-8411 Ext 2432.

16. ABSTRACT The report gives results of an experimental investigation of the effects of the interaction between fluid dynamics and chemistry on pollutant formation and destruction in a natural-gas-fired, turbulent diffusion flame burner. The investigation determined the effects of inlet air swirl, combustor pressure, and air/fuel velocity ratio on the time-mean and fluctuating flow field, using probing and optical techniques. Changes in flow field structure were correlated with changes in pollutant emissions from the furnace. The investigation also showed that varying these parameters produces major changes in the time-mean flow field within the burner which significantly influence pollutant formation. It was also discovered that there are substantial large-scale contributions to the total rms turbulent velocity field. These large scale fluctuations result in significant departures from Guassian turbulence and isotopy in the initial mixing regions of the burner and have pronounced effects on mixing, chemical reaction, and pollutant formation.

17. KEY WORDS AND DOCUMENT ANALYSIS

a. DESCRIPTORS		b. IDENTIFIERS/OPEN ENDED TERMS	c. COSATI Field/Group	
Pollution	Aerodynamics	Pollution Control	13B	20D
Natural Gas	Turbulence	Stationary Sources	21D	
Combustion	Swirling	Gaseous Fuels	21B	07A, 13H
Furnaces	Speed Indicators	Laser Velocimetry	13A	14B
Nitrogen Oxides			07B	
Lasers			20E	

18. DISTRIBUTION STATEMENT	19. SECURITY CLASS *(This Report)*	21. NO. OF PAGES
Unlimited	Unclassified	150
	20. SECURITY CLASS *(This page)*	22. PRICE
	Unclassified	

EPA Form 2220-1 (9-73)